2007

Sediment transport on a river-dominated shallow water shelf: Atchafalaya Bay region, Louisiana

Renee T. Bellotte
Louisiana State University and Agricultural and Mechanical College

SEDIMENT TRANSPORT ON A RIVER-DOMINATED SHALLOW WATER SHELF: ATCHAFALAYA BAY REGION, LOUISIANA

A Thesis

Submitted to the Graduate Faculty of the
Louisiana State University and
Agricultural and Mechanical College
in partial fulfillment of the
requirements for the degree of
Master of Natural Sciences

in

The Interdepartmental Program in Natural Sciences

by
Renee T. Bellotte
B.S. Louisiana State University, 2001
August 2007

ACKNOWLEDGEMENTS

I extend my deepest gratitude to Dr. Nan Walker for investing her time and energy for a non-traditional student, which required an extra measure of flexibility. Dr. Walker was attentive to my questions, imparting her knowledge and experience, and quick to respond with guidance at every occasion. I am also grateful to Dr. Oscar Huh, founder of the Earth Scan Laboratory, who took me seriously when I requested he teach me remote sensing theory as independent study. Dr. Huh got me started on this remarkable journey, and even lent me his personal copy of "The Incomplete Guide to the Art of Discovery" by Jack E. Oliver. I want to thank Dr. Gregory Stone for sharing his expertise in sediment transport and allowing me access to the WAVCIS station data and to participate on field trips to study coastal morphodynamics. Dr. Shih Hsu provided me a foundation in the processes of coastal meteorology and encouraged me with different perspectives on how to approach this study.

Thanks to DeWitt Breaux for fine-tuning my ERDAS Imagine skills. Padmanava Dash taught me how to process sea-water samples: we spent many hours filtering, combusting and weighing, while engaging in invigorating conversation about our research projects and life in general. Ron Stanford and Bill Gibson of the LSU Field Support Group provided logistics, information and documentation on maintenance and procedures for the WAVCIS station. Dr. Xiongping Zhang and Yixin "Peter" Luo are to be thanked for their gracious support in acquiring WAVCIS data which could not be obtained through the website. I must thank Shreekanth Balasubramanian for technical assistance and Dr. Lawrence Kiage for inspiration.

I am grateful to my parents for having the good sense to raise me near the ocean, where the first signs of approaching storms were the seagulls seeking shelter in the fields near our home. To Jeanette Mendoza, my best friend, thank you for your prayers and encouragement.

TABLE OF CONTENTS

LIST OF TABLES

LIST OF FIGURES

ABSTRACT

Cold front passage impacts on sediment transport on the inner continental shelf near Atchafalaya Bay were studied, combining satellite imagery and in-situ meteorological and oceanographic measurements. An empirical model relating atmospherically corrected MODIS imagery reflectance to surface measurements of suspended sediment concentration was developed and successfully applied to the coastal waters. An equation for predicting total suspended sediment from Nephelometric Turbidity Units was also applied to the water column at 1, 2, and 3 meters from the seabed. Five case study weeks were selected to examine the dynamics of pre-frontal and post-front forcing mechanisms on sediment transport in a fine-grained sediment environment, with the major objective to determine whether changes in surface sediment concentration revealed characteristics of sediment transport in the vertical structure of the water column.

Remote-sensing data showed that great spatial variation occurred in the surface mud-plume during pre-frontal, post-front and inter-frontal conditions. Southeasterly winds confined the plume nearer shore and often within the bays during pre-frontal conditions. Post-frontal northwesterly and northerly winds increased plume area by 3 to 4 times, extending past the 10 meter isobath and reversing the dominant transport direction from westward to southeastward. A comparison of the surface sediment concentrations at WAVCIS station CSI-3 (seaward of Marsh Island) to simultaneous maxima elsewhere in the mud-plume revealed that the main plume sediment concentrations were often an order of magnitude greater south of the Atchafalaya River mouth.

The presence or absence of the plume over the CSI-3 site was not indicative of the level of sediment flux throughout the water column at CSI-3. High rates of surface and upper water

column sediment transport were primarily in response to strong currents from wind-forcing. In contrast, the dynamics of near-bottom transport at CSI-3 showed high rates of sediment flux in the post-front period attributed to high sediment concentrations. Total suspended sediment in the bottom meter sustained peaks which were 2 – 10 times that of the surface and mid-depth concentrations, reaching maxima of 1,100 mg/l due to resuspension and/or the advection of fluid mud from the Chenier Plain coast.

CHAPTER 1 INTRODUCTION

1.1 Overview and Justification

In recent years, much attention has been given to the rapid loss of Louisiana wetlands and the existing and potential consequences to the physical landscape, wildlife habitats and economic interests such as fishing, transportation and energy resources / infrastructure. Scientists sounded the alarm decades ago, and government agencies are finally heeding the call, especially with the impacts of recent hurricanes which took advantage of compromised coastal areas with devastating effects to the human population in coastal and low-lying inland areas. In order to more effectively manage our coastal resources, purposeful collection and analysis of time series data is vital for geomorphic and ecological investigation. Understanding the impacts of sediment concentration on water quality, benthic and phytoplankton productivity, and pollution transport in the coastal zone is critical to the process.

Louisiana coastal systems are complex and therefore require examination on various scales, both spatially and temporally, to accurately measure and fully evaluate the dynamic interactions of ocean, atmosphere and coastal landmasses. The process of attaining an in-depth comprehension of open ocean waters and of sandy environments, like those of Louisiana's front-line defense barrier islands and the areas along the northern Gulf of Mexico east of the Mississippi River delta, is well underway. However, Louisiana's muddy coastal environments, with sediment loads comprised primarily of terrigenous silts, clays and a near-bottom fluid mud layer, have only more recently come under closer scrutiny. Specifically, this environment's response to successive winter storms within a season, as well as the cumulative effects over years on the Louisiana coastline deserves further study. The entrainment, suspension and depositional

characteristics of this sediment type differ significantly to those of sandy nearshore environments (Woodroffe, 2002; Kemp, 1986).

Although the coast of Louisiana is considered a low energy environment (microtidal range < 0.5 meters), exchanges of sediment between the foreshore, shoreface and inner continental shelf occur due to seasonal changes (such as river flooding), anthropogenic activity and meteorological events. Drastic and sudden changes resulting from hurricanes often draw more attention than the less obvious changes due to winter storms. "Although the waves and currents during cold fronts are weaker than during extratropical and tropical cyclones, they occur more frequently and can be as important for the evolution of low energy coasts in the Gulf of Mexico" (Keen, 2002). The frequency of cold air outbreaks in the Gulf of Mexico is between 20-30 events for the period October to April. With a return frequency of 4 - 7 days, there is little recovery time in comparison to more severe occurrences such as hurricanes.

1.2 Approach and Scope

This study focused on understanding the coastal processes in the river-dominated Atchafalaya Bay region which are associated with winter frontal passages and cold-air outbreaks. Satellite remote sensing was combined with meteorological and oceanographic in-situ measurements to investigate and quantify sediment concentrations and fluxes throughout the water column on the inner shelf seaward of Atchafalaya Bay. Validation of surface sediment transport from satellite imagery was accomplished by analysis of the sediment plume; verification was obtained through the collection of sea-surface water samples. In-situ measurements of current direction, current velocity, water levels, and optical backscatter at a Wave-Current-Surge Information System (WAVCIS) station in the Gulf of Mexico provided an

effective means to characterize variations in sediment concentration and sediment flux within the water column.

The vertical scope began with the surface plume from river outflow, and progressed down through the water column in depth to gain understanding of the variability of ocean currents and wind forcing on sediment flux and resuspension in this fine-grained sedimentary environment. The horizontal scope included input from the Atchafalaya River affecting West Cote Blanche Bay, East Cote Blanche Bay, Atchafalaya Bay, and Fourleague Bay, then extended seaward across the inner continental shelf (Figure 1.1).

The study specifically analyzed the cold front processes that altered the typical sediment transport patterns from "non-storm" condition winter days. Cold fronts, with their changes in wind speed and direction, have significant impacts on sediment transport in shallow water. In fluid mud layers, viscosity is higher than for sandy areas due to fine-grain sediment's cohesive properties. By selecting a data-rich station (WAVCIS CSI-3) near the coast in less than 10 meters water depth, it was possible to evaluate the passage of each front on the shallow waters at three vertical levels. Wind speed, direction and duration at 10 meters height, and significant wave height were analyzed to evaluate variations in sediment concentration and fluxes in the vertical and over time due to the various phases of passing winter storms.

1.3 Hypothesis, Key Questions and Objectives

What happens to the fine-grained sediment load which is flushed beyond the bayhead deltas, or to bottom sediments which are resuspended by strong southeasterly winds preceding a cold front? Are they carried cross-shelf to be deposited in deeper waters by strong northerly winds? Does alongshore transport supercede frontal passage dynamics and maintain westward flow toward the Chenier Plain coast? Will tracking a surface sediment plume by satellite reveal

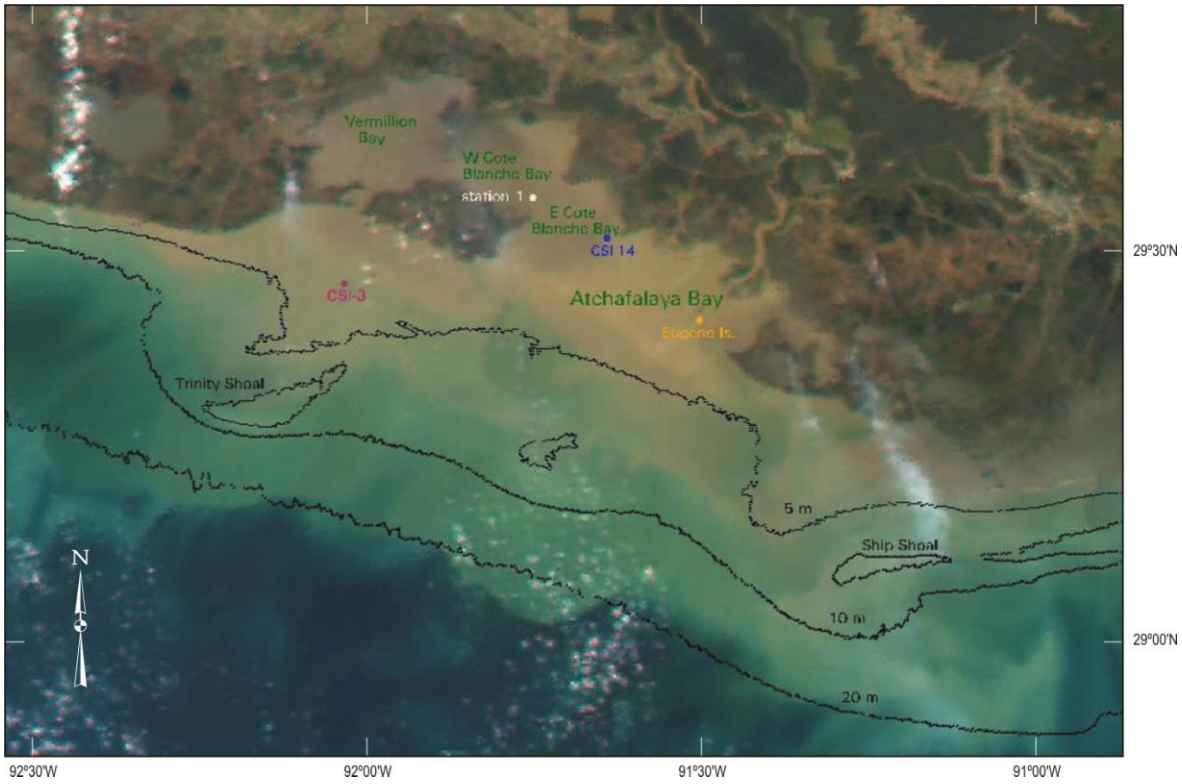

Figure 1.1 Study area. Annotated with location of WAVCIS CSI-3 and CSI-14 stations, "station 1", Eugene Island station, and bathymetry and shoal contours..

characteristics of sediment flux throughout the water column? Can the process of river discharge sediment delivery to the inner shelf be distinguished from resuspension?

Besides sediment load and wind influence, many processes contribute to sediment flux, such as: variations in river discharge, wave dynamics, fetch length, and astronomical tides. Detection of sediment concentration changes and transport with remote sensing is influenced by atmospheric scattering as well as absorption of the light in the water column by Colored Dissolved Organic Matter (CDOM) from the decay process of phytoplankton or plants.

My hypothesis is that spatial and temporal changes in surface sediment concentrations are direct indicators of the characteristics of sediment resuspension and transport throughout the water column on the inner continental shelf. With a multitude of hydrodynamic and geomorphic processes as a backdrop, this study focused on the following objectives:

1) to develop and test an empirical model to estimate suspended sediment concentration (SSC) in the surface plume of the Atchafalaya Bay Complex and on the nearby Louisiana inner shelf using atmospherically corrected MODIS reflectance values,
2) to apply the Nephelometric Turbidity Unit (NTU) to Suspended Sediment Concentration (SSC) conversion model previously developed by Walker (2001) for the bays to the inner continental shelf water column, and to compare this data with the new MODIS imagery reflectance to SSC model,
3) to couple remote sensing with meteorological and water column observations in order to investigate and quantify sediment delivery, resuspension and transport responses to cold front passages at several levels in the water column.

The completion of these objectives provided a more comprehensive perspective on the variations of sediment flux at CSI-3. This unique approach enabled the examination of

the forces which dominate each level of the water column and drive sediment transport to be more readily identified. Qualitatively, the relationships of sediment resuspension and transport between the various water depths and the limits thereof were distinguished. Sediment transport was quantified at three depths and comparisons were made with satellite derived data to test the hypothesis.

CHAPTER 2 LITERATURE REVIEW

2.1 Historical Framework of the Northern Gulf of Mexico

The coastal zone is the interface between marine and non-marine environments. Since the major controls on sedimentation are eustacy, tectonism and sediment supply (Winker, 1991), it is incumbent upon us to probe the geologic past of the region to better understand its current status.

During the Pliocene epoch (to 5.5 m.y. B.P.) the shelf edge prograded rapidly into the northern Gulf of Mexico (GOM) as revealed by shifting of the positions of sediment depocenters subsequently further offshore (Woodbury et al, 1973). The Quaternary record (to 1 m.y. B. P.) revealed that during periods of lower sea level, the northern GOM basin margin was seaward of its current position. Therefore, sediment loads bypassed the low-gradient shelf (as it exists today), and deposition occurred at the continental slope, as evidenced by entrenched river valleys buried on the continental shelf as well as shelf margin deltas. In the late Pleistocene, barred embayments were present between delta headlands. During the Holocene epoch (to 11,000 y. B.P.) rising sea level caused headlands to retreat and barrier island progradation. Some of the modern day open bays are actually re-occupied Pleistocene barred embayments.

Tectonism, the deformation of the lithosphere in the GOM, is manifest in multiple ways with compaction and isostatic loading as prominent contributors to subsidence rates. Along the Louisiana coast, mud accumulations in the Mississippi complex have created subsidence rates up to 40 mm/yr (Winker, 1991). Subsidence also is attributable to salt withdrawal and movement of growth faults on the shelf margin and continental slope. Hydroistostasy, the vertical movement between continents and ocean basins due to loading and unloading of ocean basins in changing global sea level, also influences tectonism, although to a lesser magnitude in this region.

2.2 Mississippi River Diversion by the Atchafalaya River

The Mississippi River supplies ~500 million tons of sediment to the GOM basin annually (Winker, 1991). During lower sea level, it was a fast flowing, sediment laden river which occupied many shallow channels. As sea level rose, meandering began on the low slope of the alluvial valley near the river mouth and then developed upstream. As sea level approached its present level, new courses arose which have shorter paths to the ocean basin and thereby a gradient advantage. River diversions occurred when actively migrating meander loops encountered a tributary stream in an adjacent flood basin. In this case, avulsion occurred through a short stream ("Old River") which followed a portion of an ancient Mississippi River meander loop (Figure 2.1). As the Atchafalaya enlarged its course, partially attributable to the scouring of the faster moving Red River (Figure 2.1), water discharge and sediment load were being captured from both the Red River and the Mississippi River. During the 1950's and 1960's the Old River Control Structure was built by the Army Corp of Engineers to regulate the Atchafalaya's draw from the Mississippi; to maintain the status quo, approximately 30% of water discharge and 50% of suspended sediment load (Mossa and Roberts, 1990; Moeller et al, 1993), thereby preventing the Mississippi River delta's demise via delta switching. It is crucial to maintain the Mississippi River as a navigation channel which supports vital shipping ports in both New Orleans and Baton Rouge.

The Atchafalaya River water discharge rates for 1950 – 1985 were: the maximum ~22,653 $m^3 s^{-1}$, the mean ~7,079 $m^3 s^{-1}$, and the minimum ~ 800 $m^3 s^{-1}$ (Mossa, 1990). For the water year 2004-05, the Atchafalaya River mean water discharge was 7,306 $m^3 s^{-1}$ and the mean sediment discharge was 141,000 tons/d, to the shallow continental shelf of central Louisiana (nwis.waterdata.usgs.gov).

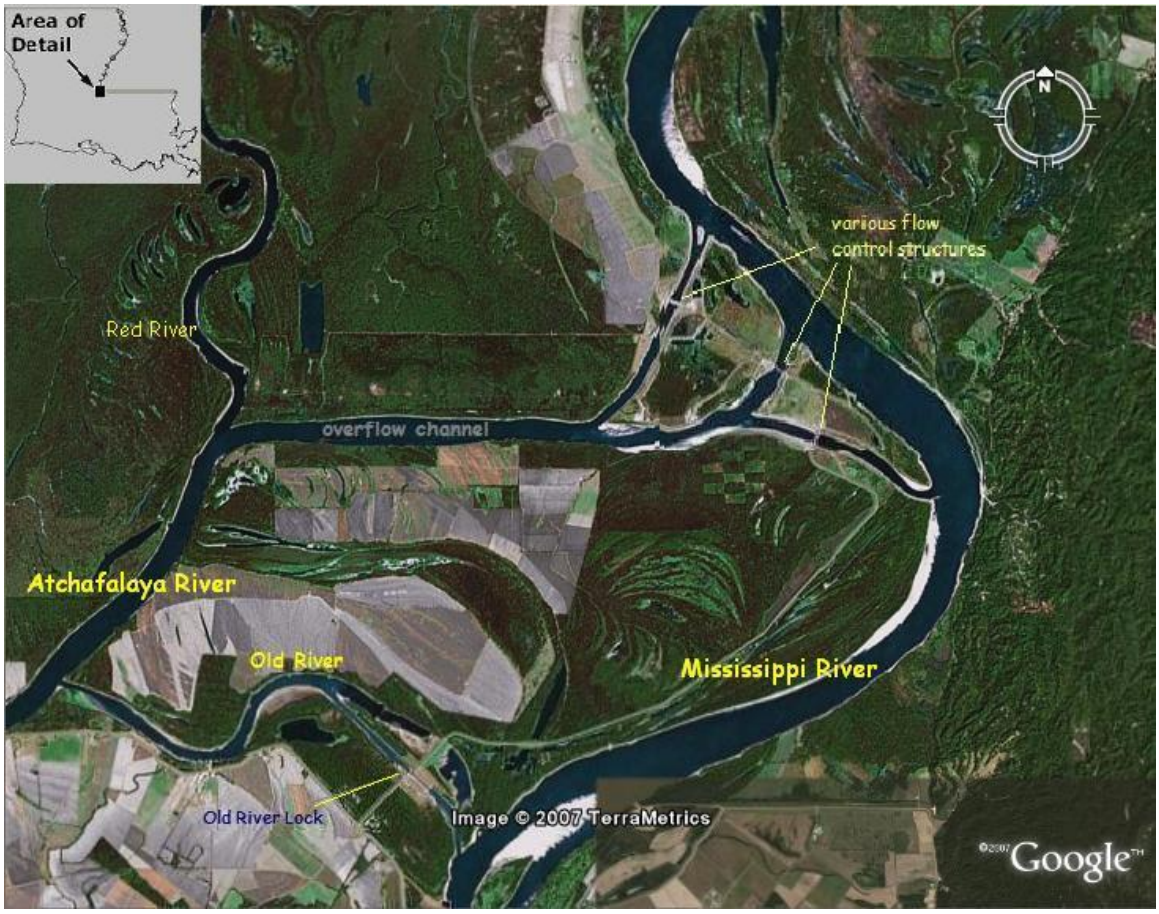

Figure 2.1 Stream capture location of Mississippi River flow by the Atchafalaya River and placement of Old River Control Structures. Source: Google Earth ™ mapping service/© 2007 TerraMetrics. Annotations by author.

2.3 The Atchafalaya Basin and the Delta Building Cycle

The Atchafalaya Basin is characterized by heavily forested flood basins in the northern reaches which give way to grass covered marshlands toward the coast. The most extensive area, the backswamp, is continually flooded and supports woody vegetation (Tye and Coleman, 1989). Sediment deposition in the backswamp is primarily in the form of overbank flooding of channels with fine grained silty clay. Once the alluvial plain is established, the delta cycle begins. The delta cycle spans 1000 to 2000 years including both a regressive, river dominated (building) phase and a transgressive, marine dominated (deteriorating) phase (Roberts, 1997).

2.3.1 The Regressive Phase of the Delta Cycle

In the first phase, interdistributary basin aggradation is the result of fluvially dominated lacustrine delta building, whereby inland lakes along the rivers' path are eventually filled with layers of sediment. Here, sediment deposits are very fine-grained silty sands with intraclasts and/or laminations of organic backswamp materials. Overlying the lacustrine deposits are the finest grained clay prodelta sediments, forming a widespread platform over which the coarser grained deltaic deposits prograde into the lake. Distributary mouth sand bars develop, delta lobes weld together and aquatic vegetation takes root in the channel bed, acting as a sediment catch; eventually the distributary channel may be abandoned. Subsequent cycles of lacustrine filling can occur due to subsidence in the alluvial plain or from a downstream marine delta undergoing delta lobe switching. The process also repeats in subsequent lakes along the river's path to the sea. Early records from maps originating from explorations in the second half of the 16th century showed the Atchafalaya River as a Mississippi River tributary (Fisk, 1952). Until the 1900's, Atchafalaya River diversion was sporadic; evidence of sediment bypassing the basin and being

deposited at the coast did not appear until the 1950's. This demonstrates that alluvial basin filling can take centuries (Roberts, 1997).

A second type of delta development continues the river dominated regressive phase and is marked by bayhead delta building at the coast. Currently, the Atchafalaya River complex is engaged in progressive bay-head delta building at two locations, the Atchafalaya River mouth (AR) and the Wax Lake outlet (WLO) (Figure 2.2).

The first signs of sedimentation along the coast were mud flat accretion on the eastern Chenier Plain: oyster reef burial and mud accumulation atop the sand beaches such as the resort area Cheniere au Tigre, just west of Marsh Island. In 1973, an abnormally high flood (exceeding 900,000 cfs) scoured coarse grained materials from the lower Atchafalaya River and established the sand rich lobes of the subaerial bayhead deltas (Roberts et al, 1997). The next two years exhibited continued growth due to the average annual sediment load having doubled with high water conditions. In 1988, the Wax Lake Outlet Weir was installed which unexpectedly directed more flow to the eastern AR delta at the expense of the western WLO delta, resulting in a 10-12% decrease in annual sediment output into the bay from the WLO. In 1994, the weir was removed; as of that time the deltas comprised ~ 153 km^2 of new land above the -0.6 datum (AR=101.5 km^2 and WLO=51.1 km^2) (Roberts et al, 1997). While the WLO delta was still undergoing channel elongation, channel bifurcation and delta sand bar formation, the more "geologically mature" AR delta was already demonstrating channel abandonment and delta lobe fusion. Since that time, the Atchafalaya bayhead delta's progress has been influenced by human activity (such as dredging) in close proximity, more so than the Wax Lake delta, which is evolving with minimal human intervention.

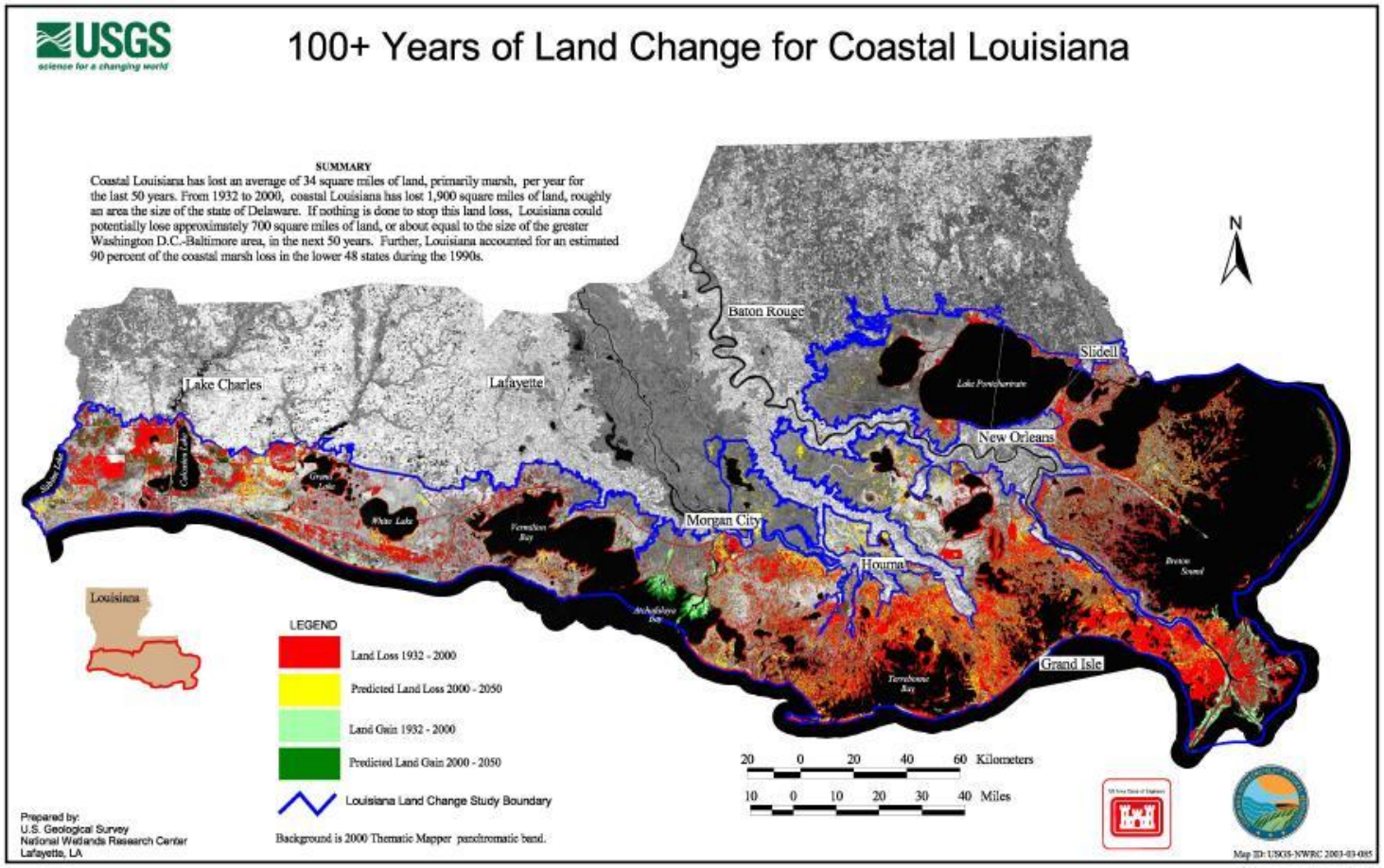

Figure 2.2 USGS 100+ Years of Land Change for Coastal Louisiana. Source: (http://www.lacoast.gov/maps/2003landloss/landloss11X17.pdf).

Sediment input to the Atchafalaya Bay is seasonal with the greatest loads in the winter and early spring and less in the summer and fall (Mossa and Roberts, 1990). Sand transport has a linear increase with water discharge while finer silt and clay sized particles do not. During the low water portion of the flood cycle these sediments are "stored" in the channel. However, suspension concentrations for fine-grained silts and clays supplied primarily from the Red River (mean 42%, maximum 70% of Atchafalaya suspended sediment load) increase sharply from erosive action as water flow increases in the **lower** river discharge ranges, leveling off with moderate flows and finally tapering off as water discharge increases (Mossa, 1990; Roberts et al 1997). While sand still deposits to build the AR delta, finer grained silts and clays bypass the delta and are deposited on the inner continental shelf. This process has resulted in layers of cohesive fluid mud bottom deposits on the shelf and/or transport from dominant westward alongshore currents. The size, extent and concentration of the sediment plume varies with the water and sediment load discharges, averaging 4400 km^2 associated with high river discharge (>5666 $m^3 s^{-1}$) (Walker and Hammack, 2000).

A third type of delta development (still within the regressive phase) occurs when continued increases in sediment flux cause the bayhead delta to prograde across the continental shelf (shelf delta). The Atchafalaya and Wax Lake deltas have not yet reached this last stage of river dominated delta building.

2.3.2 The Transgressive Phase of the Delta Cycle

The transgressive marine dominated phase begins when decreasing hydraulic efficiency prevents extension of the delta building process. This phase is characterized by subsidence, overbank flooding on the delta lobes and crevasse splays. The lobes are weakened by marine processes overtaking them due to relative sea level change. Final stages are evidenced by the

appearance of barrier islands, spits and island arc formations. Storm conditions cause overwash, and eventually the submarine shoals are remnants of a completed delta cycle.

2.4 Circulation on the Continental Shelf and the Bay Complex

2.4.1 Current Responses to Seasonal Changes in Wind Stress on the Continental Shelf

The Louisiana coastline from 90° W to 94° W is basically concave shaped along an east-west orientation. The shelf is wide (150-200 km) and relatively shallow, with the shelf break in depths of 75-100 meters (Cochrane and Kelly, 1986).

Cochrane and Kelly (1986) studied wind stress and current response along the Louisiana-Texas coastline, and found that for much of the western Louisiana coastline and into Texas, the alongshore component of the current is coherent with the alongshore component of wind stress for both surface and bottom layers. For much of the year, easterly winds create a "downcoast" westerly alongshore current. Wind stress parallel to the coast also produces transport normal to the coast (Ekman transport: convergence or divergence). Due to the coastal boundary to the north, upwelling occurs with westerly winds and downwelling occurs with easterly winds. To compensate for cross-shelf transport in the surface layer, an "adjustment drift" in the bottom layer occurs, and is deflected to the right by the Coriolis force (Cochrane and Kelly, 1986).

Alongshore easterly winds which dominate in autumn, winter and early spring, also drive a 40-90 cm s^{-1} surface current from south of the Mississippi delta, creating exchange of river and shelf waters from the Louisiana/Mississippi/Alabama shelf to the Louisiana/Texas shelf (Walker, 2005a).

2.4.2 Salinity: Seasonal Variability on the Continental Shelf

In the Atchafalaya Bay region and along the inner continental shelf, river discharge plays a bigger role than either precipitation or evaporation in salinity distributions. Typically, the river

peaks in April, and salinity along the coast reaches a minimum in May. Murray (1998) vertically profiled a buoyant low salinity (< 24 psu) plume in April 1992, which was 8-10 meters in depth and extended out to 35 km from the coast. This hypopycnal flow was trapped above an 8-10 meter thick layer of high salinity GOM water. Although there was some variability in the seaward extent and vertical depth of the low salinity plume, this pattern repeated the following spring. Murray also described the low salinity coastal plume in April 1992 which began at the Atchafalaya River mouth (~ 16 psu) and extended 500 km westward, running quasi-parallel with the coast (~ 26-27 psu). Salinity along the Louisiana-Texas coastline increased toward the west and south, due to downcoast advection from both the Mississippi and Atchafalaya River discharge. In October 1992, when Atchafalaya River discharge was low (~4,400 m^3 s^{-1}), Murray compared the autumn downcoast regime's salinity profiles to the spring pattern. Surface salinity observations delineated a well-developed coastal plume with ambient coastal waters (29 to 33 psu) converging on the plume outflow which resulted in extensive mixing beginning inside the Atchafalaya Bay (~21-28 psu) and continued along the length of the downcoast plume to 410 km downstream. The high salinity water (34 psu) normally underlying the buoyant surface water was confined to the inshore near the source of the river water, while the outer edge of the coastal plume was truncated by a high speed, southwestward flowing jet. While the Atchafalaya River water pushed the 29 psu outflow to 37 km offshore near the source (similar to spring conditions), gradual downstream mixing of the plume with ambient coastal waters pushed the outcropping closer to shore: to 25 km, then 8 km, from the coastline. Strong winds and low discharge in the autumn and winter seasons enhanced vertical mixing and reduced stratification. The salinity distribution of the alongshore progression confirms the downcoast currents which prevail for much of the year.

2.4.3 Coastal and Inner Shelf Geostrophic Flow and the Shelf-break Countercurrent

Cochrane and Kelly (1986) also used measurements of temperature and salinity to compute monthly mean time-averaged geopotential anomalies, (after Montgomery, 1941 and Csanady, 1979) which provided a picture of coastal geostrophic flow. Near-bottom flows close to the coast deviated from geostrophy, due to upwelling and downwelling. Mapping upper layer geopotential anomalies revealed the persistence from September to May of an elongated cyclonic gyre: circulation was westward along the coast at the inner limb of the gyre (the "coastal jet"), seaward on the southwest end of the cyclone, toward the east along the outer shelf/shelf-break ("countercurrent") and finally shoreward on the eastern end of the cyclone. Although the center of the gyre migrated along the coast seasonally, its influence extended from 91° W to 95° W, regardless of the position of the center of the gyre. While the cyclone disappeared and was replaced by anticyclonic flow during the summer, it was re-established in August or September. This finding, a downcoast flow along the inner limb of the gyre for most of the year, is consistent with the wind stress results and with low salinity brackish waters progressing seasonally downcoast.

Relatively shallow depths (where the heat storage capacity is less) mean that the sensible and latent heat loss with the onset of autumn/winter cooling is rapid. The waters on the continental shelf respond to cold continental air masses with strong winds, which cause the water column to become well-mixed even to depths of 100 meters (or the entire column in shallower depths (Nowlin and Parker, 1974). During fall and winter, surface drifters released on the LATEX shelf in 15-25 meter depths moved westward in close proximity to, or toward, the inner shelf sea-surface temperature (SST) front with an average speed of 20 cm s^{-1}, marking the edge of the cool coastal water band. Likewise, drifters deployed in deeper waters also moved westward, also approaching the SST front near the 20 meter isobath (Walker, 2005b).

2.4.4 Upcoast Current Reversal and Loop Current Eddy (LCE) Entrainment

Variation from the dominant downcoast alongshore current occurs for 4 to 6 weeks in the summer as an upcoast current reversal in response to persistent onshore southerly and southwesterly winds (Walker, 2005b). Cochrane and Kelly (1986) noted the absence of a downcoast coastal jet along the coast during summer due to the deterioration of the cyclonic gyre.

Murray (1998) found that the summer regime consisted of a low salinity outflow (12 - 20 psu) which was confined tightly to the inshore (to 20 km) as a shallow 5 m thick buoyant plume; further seaward, an intermediate mixing zone (20-30 psu) about 40-50 km in width and 13 m deep; and finally a homogeneous, weakly stratified, high salinity water mass (31-36 psu) flowed upcoast. Murray interpreted the intermediate mixing zone to be 'old' coastal plume water that had been previously advected downcoast prior to the onset of the summer upcoast regime. East of the Atchafalaya Bay, Murray found the upper layer was comprised of water (23-34 psu) with relatively level isohalines down to a depth of 14 m. Beneath the buoyant plume was a quasi-homogeneous high salinity, undiluted (35-36 psu) layer which encroached to within 10 km of the shoreline.

Monthly mean velocity stream function fields for the summer months derived from moored current meters by Cho et al (1998), support upcoast current reversal, sometimes initiated by June each year and generally well established by July. There was little, if any, cross-shelf flow indicated during this period, upcoast flow dominated both the inner and outer continental shelf. The return to a pattern of downcoast flow over the inner shelf typically occurred by the end of August. Interannual variability of a given months' stream function field showed a strong

correlation of the timing of current reversal (or the subsequent return to downcoast flow) with along-shelf wind variability.

There was a time lag between wind reversals and current reversal, yet the development of the upcoast flow regime was not solely the result of wind-forcing; alongshore sea-surface slopes were also a controlling factor (Murray, 1998; Walker 2005). The upcoast current reversal in depths of up to 50 meters reached maximum speeds of ~ 46 cm s^{-1} with a mean of ~ 24 cm s^{-1} in June 1994 (Walker 2005). Individual periods of current reversal lasted as long as a month.

A numerical simulation using the Navy Coastal Ocean Model (NCOM) by Morey et al (2003), suggested that while the buoyant, low salinity, weakly stratified river water is trapped at the coast by alongshore flow during the autumn/winter regime, it formed a strongly stratified, freshwater "cap" over portions of the LATEX shelf waters in summer. This is also supported by the salinity maps of Cochrane and Kelly (1986) and vertical salinity profiles of Murray (1998).

Temporarily interruptions in the dominant downcoast flow regime can also occur in response to cold front passage in winter. Strong westerly and northwesterly winds cause current deceleration and flow reversals on the order of one to several days (Walker, 2005b).

The circulation pattern of the Gulf of Mexico is strongly influenced by the intrusion of the Loop Current (LC) and the anticyclones called Loop Current Eddies (LCE) which separate from the LC flow at intervals of 6 to 11 months (Wiseman and Sturges, 1999; Sturges and Leben, 2000). These eddies can initiate cross-shelf flow into deeper water, exporting low salinity river discharge across and away from the continental shelf, more commonly in winter than in summer . Some entrainment does occur in summer along the Mexican coastline where the shelf narrows and decaying LCE's can penetrate closer to shore. Morey also described a weak summer transport of freshwater eastward on to the Mississippi/Alabama/Florida (MAFLA) shelf.

2.4.5 Circulation in the Bay Complex

The Atchafalaya Bay complex consists of 5 interconnected bays (Vermilion, West Cote Blanche, East Cote Blanche, Atchafalaya and Fourleague) totaling ~ 1,500 km^2 area (Walker, 2001). The Atchafalaya River discharge has varied from 60 to over 500 x 10^3 cfs (1,700 to over 14,158 $m^3 s^{-1}$) throughout the last five years, as a plot from the U.S. Army Corps of Engineers, Water Control Section's recent data shows (Figure 2.3).

The river's flow is first discharged into the wide and shallow (1 to 2 meters) bay where it is subject to tidal and wind mixing. Much of the discharge is subsequently expelled into the GOM through a 45 km wide passage between March Island and Point Au Fer (Murray et al, 1998).

Walker and Hammack (2000) found that during northerly wind events the salinity values in the bays reached minimums of 2-4 psu, especially when in tandem with rainfall events, local flooding and high river discharge. This is in contrast to maxima of 20 psu resulting from tidal inflows during water level adjustments *after* frontal passage (Walker, 2001). Higher salinity water is advected from the inner shelf, often through Southwest Pass (>25m depth) to the west of Marsh Island. Salinity values have an inverse relationship with river discharge, with fluctuations of + - 15 psu in West and East Cote Blanche Bays (Walker, 2001).

2.5 Influences on a Coastal Shallow Water Muddy Environment

2.5.1 Meteorological Impacts - Cold Front Cycle Impacts on Sediment Concentration

The Gulf of Mexico is dominated by particular weather types during the autumn and winter seasons (Muller and Wax (Louisiana Office of State Climatology), 1977; Hsu 1999). In the fall, the atmospheric circulation pattern is designated as "Continental High", typified by polar or arctic outbreaks with northerly or northwesterly winds and cooler drier air prevailing over a

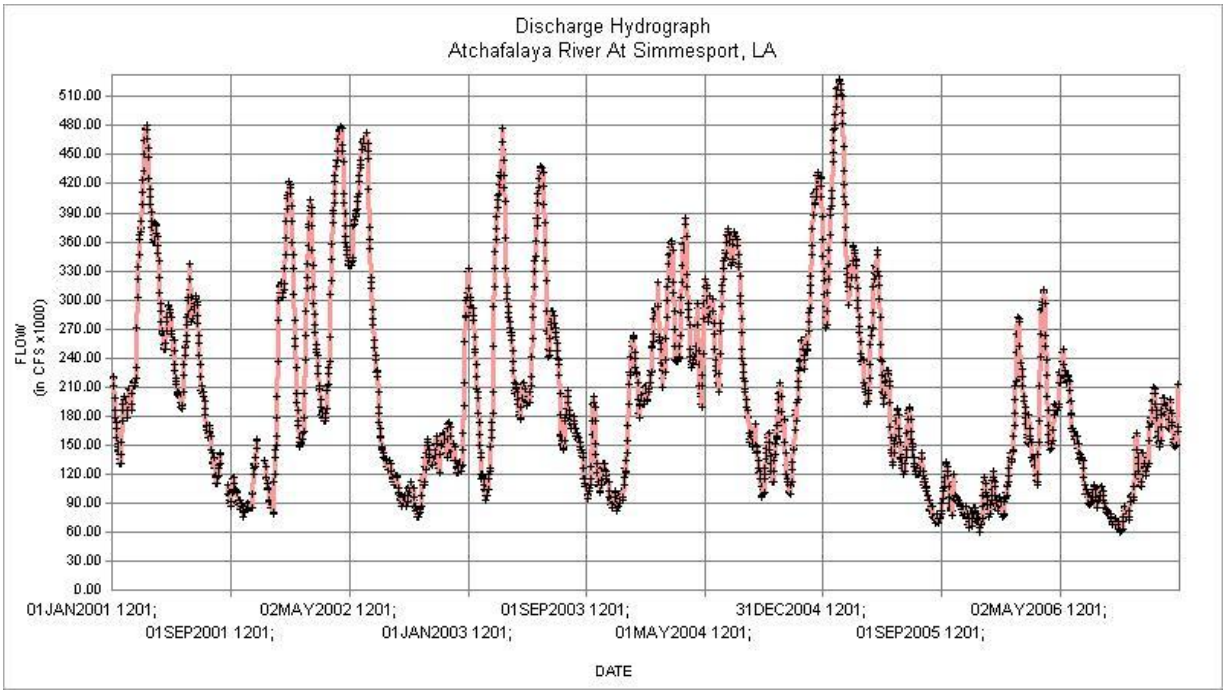

Figure 2.3 Interannual variability of Atchafalaya River Discharge from 2001 to 2005. Source: http://www.mvn.usace.army.mil/eng/Edhd/Wcontrol/opfiles/094492.asp

large section of the GOM. In winter, “Frontal Overrunning” is the more common pattern, with cloudy, rainy conditions persisting as cold fronts became stationary along the Gulf coast or the northern or central GOM.

Hsu (1999) found that over the GOM as a whole, wind speeds are ~ 6 m s^{-1}, with higher wind speeds in winter. In the near-shore areas, lighter wind speeds were encountered due to the sheltering effects of nearby land. Hsu also noted the influence exerted by the Bermuda high-pressure system on wind direction in the GOM: more easterly wind over the eastern GOM and more southeasterly wind over the western GOM. In examining the ocean current, wave generation and Ekman pumping relating to upwelling in the GOM, Hsu notes that for a given wind speed, the momentum flux is higher within the bay system than in the open GOM. Hsu inferred from geostrophic vorticity of local wind patterns that upwelling was more active in the southern LATEX shelf than in the northern LATEX shelf.

A cold front represents a boundary zone between continental polar air moving south/southeast overtaking warmer maritime air masses which move north. These cold fronts also have a general west to east flow component. Spatial and temporal changes in wind speed and direction, and barometric pressure occur; and the intensity and forward velocity of the front controls the duration of wind forcing on the coastal system (Roberts et al, 1989).
During the pre-frontal (non-frontal) phase a warm, humid atmospheric condition exists, with generally falling barometric pressure (Moeller et al, 1993). Winds blow from the south or southeast, attaining wind speeds of 10-13 ms^{-1} for several hours duration at a time. The long fetch causes water level set-up against the coast, with corresponding wave action increases causing resuspension of bottom sediments in the shallow nearshore. Water level within the bay

complex can elevate as much as 0.9 meters (Perez et al, 2000) with waters carrying suspended cohesive silts and clays which inundate coastal marshes.

As the front approaches, barometric pressure drops suddenly and short-lived, intense squalls may create intense rainfall. The frontal passage phase has strong and variable winds and a sharp wind direction shift from southerly to westerly (Moeller et al, 1993).

Once the front has advanced across the coast, the post-frontal phase (or cold air outbreak (CAO)) is characterized by: a further clockwise rotation in wind direction to northwesterly, northerly, or northeasterly, a dramatic rise in barometric pressure, a drop (-10°C or greater) in air temperature, and a decrease in humidity. These changes cause a water level set-down (Kemp et al, 1980; Walker and Hammack, 2000) which generally ranges from 0.5 to 1 meter in nearshore waters. Resuspension is enhanced with falling water levels during periods of strong winds. Since the plume aligns with the bottom bathymetry, it is plausible that resuspension contributes significantly to the sediment plume on the inner shelf.

As winds with a northerly component persist, seaward flow from the bays ensues in the surface waters, with the sediment laden plume being pushed offshore to the continental shelf. Walker and Hammack (2000) estimated that of the sediment plume detectable in satellite imagery, 20 to 25% was from discharge flushed onto the shelf and 75 to 80% was from resuspension and transport of inner shelf bottom sediments. As the winds relax, the sediment particles fall out of suspension onto the subaqueous bottom. They are available for the next resuspension by wind or wave event or for alongshore westward transport toward the Chenier Plain coast.

2.5.2 River Discharge Variation Concurrent with Cold Front Passage: Impacts on SSC

Changes in SSC during cold front passage also vary in response to river discharge rates. Walker and Hammack (2000) noted that at low river stage, highest sediment concentrations were caused by wind-wave resuspension in shallow areas; winds from different directions would move the region of maximum resuspension. Water level responses were maximized when wind effect are in phase with the astronomical tide (Walker and Hammack, 2000; Moeller et al, 1993).

Water discharge rates demonstrated a linear relationship to plume sediment concentrations (Walker, 2005a). During both high and low river discharge, the size of the Atchafalaya plume was maximized by northwest winds. However, the increased size of plume did not necessarily correspond with increased SSC (Walker, 2000).

2.5.3 Frontal Passage Effects on Bay Complex and Inner Shelf Sediment Transport

Water level set-up in the pre-frontal phase of a winter cold front causes inflow from the coastal ocean into the bay complex (Wiseman and Inoue, 1993; Walker, 2001). Chuang and Wiseman (1983) attributed the strong water level response to cross-shelf wind forcing in the Atchafalaya Bay to the shallow depths of the inner shelf, where increased bottom resistance (r) in shallow waters caused preferential response to cross-shelf transport over alongshore transport, especially in northerly, high wind speed events.

During northwest and north wind events, much of the water in the western bays is driven out of the system through the wide openings to the inner shelf at East Cote Blanche Bay and Atchafalaya Bay. Ebb flow, directed by Ekman transport during westerly winds along this east-west linear coast, is enhanced by a favorable gravity gradient as Gulf waters recede (Perez et al, 2000). After cold front passage, a rebound flow restores water levels through Southwest Pass and East Cote Blanche Bay (Walker and Hammack, 2000).

Moeller et al (1996) used a MODIS Airborne Simulator (MAS) to collect imagery over the bay complex during clear, dry, post-frontal conditions with surface winds of 5 ms^{-1} from the east-northeast (ENE). This imagery was used to generate water motion/velocity vectors from time series georeferenced data. Suspended sediment concentration estimates were acquired from atmospherically corrected reflectance values and verified against in situ water samples. Combining SSC values with water motion vectors produced the sediment transport values. On this post-frontal day, dominant water flows in the eastern region moved seaward from the Atchafalaya Bay due to strong northerly winds and river discharge. In the western bays, a strong westward current flowed into East Cote Blanche Bay and beyond, as the system sought to re-establish equilibrium with the higher water level gradient on the shelf. Despite winds ENE, there was some circulation into, and back out of, Fourleague Bay. Comparing water motion with sediment transport, it became clear that high water motion velocity does not imply high sediment transport. Moeller et al (1996) found that the maximum SSC on this day was located in a region of high water motion velocity at the southwest side of Atchafalaya Bay, most likely attributable to enhanced resuspension. Local transport patterns on this particular post-frontal day indicated net positive sediment flux to East Cote Blanche Bay and Fourleague Bay, as well as to the shelf of the Gulf of Mexico. Perez et al (2000) recorded total suspended sediment concentrations of 600 – 1527 mg l^{-1} due to northerly or northwesterly winds forcing flow from the Atchafalaya River into Fourleague Bay, and from resuspension within the bay. Walker and Hammack (2000) estimated the average sediment transport onto the shelf (based on SSC at 200 mg l^{-1} throughout the water column) to be 400,000 metric tons per winter storm.

Moeller et al (1996) estimated total sediment transport from the Atchafalaya River mouth on January 24, 2005 at 9612 kg/s. They also estimated total sediment volume for the high

turbidity zone of the Atchafalaya Bay southwest of the river mouth, assuming TSS at 200 mg/l, area at 20 km * 20 km * 1 m depth, at 80,000,000 kg with variations due to heavy precipitation (local or upstream), or seasonal flooding. They reasoned that at this estimated transport rate from the river mouth, the time required for replacement of the sediment load in the bay is on the order of a few hours.

2.6 Sediment Transport Westward to the Chenier Plain

Sediment cores and water column measurements of salinity and SSC are useful tools for understanding the seasonal variability of deposition and the reworking of sediments by hydrodynamics in context with the decadal accumulation patterns in which they occur. Seasonal flood deposits from the Atchafalaya River accumulated at a rate 2 to 6 times that of the long term sedimentation rate at inshore sites (<10 meters depth) on the inner continental shelf (Allison et al, 2000). In contrast, offshore sites at ~20 meters water depth showed decreased short term accumulation rates in comparison to long term rates, suggesting a more seasonally balanced sediment supply and that these sites are the recipients of sediments from resuspension at inshore shallow water high energy sites. Thickness of sediment deposits on the inner shelf were several centimeters and thickness decreased with distance offshore. Seasonally, a series of cold front passages which are characterized by resuspension of up to several centimeters of the seabed on the inner shelf, gave way to the period of maximum deposition by flooding.

Allison et al (2000) found that sediment input from the Mississippi discharge near the Atchafalaya region is minimal, as evidenced by a core taken updrift (east) from the Atchafalaya River (T1) which exhibited no correlation with discharge and no long term accumulation. This core showed millimeter scale interlamination, low porosity and an absence of ^{137}Cs (an anthropogenic tracer with a half life of 30 years), which indicated that this is a relict sedimentary

environment with no modern accumulation. The core taken offshore from the Chenier Plain outside the 10 meter isobath (WH1) demonstrated a near complete homogenization of primary structures from bioturbation by soft-bodied infauna, which indicated low sedimentation rates. Core MI6, taken inshore (< 10 meters depth) seaward of Marsh Island, showed minimal bioturbation and primary stratification on a millimeter to centimeter scale, indicating high sedimentation rates. This station, and WH6 (no core shown) were downdrift of the strong westward coastal current which dispersed Atchafalaya sediment within the 10 meter isobath.

Allison et al (2000) also used water column measurements of salinity, temperature and SSC from cross-shore transects at the Chenier Plain and seaward of Marsh Island to map the suspended sediment field and document hydrography under varying river discharge and wave energy conditions. Transect profiles at Marsh Island showed strong temporal and spatial variability in the low salinity, turbid plumes. October 1997 was a period of low discharge and low wave energy with surface salinities of 30-34 psu. March 1998 and March 1999 were high discharge periods and had high wave energy due to cold front passages. Although October 1997 and March 1999 varied in the amount of freshwater present, they both showed a highly stratified upper water column. In March and April of 1998, the water column was well-mixed close to shore due to high energy waves. Seaward of the 30 meter isobath however, stratification was stronger for both salinity and SSC. The sediment plume was confined close to shore even when the low salinity plume extended to 50 km.

Examination of a time series of cross-shore transect profiles at the Chenier Plain revealed that conditions in the water column were subject to rapid change, especially during the passage of cold fronts. The distributions of salinity and SSC responded to wind conditions in a matter of hours. Allison et al (2000) described the change in the water column with the onset of increasing

winds as evolving from a stratified water column (salinity, density and SSC) to one of a well mixed and vertically homogenous water column in 12 hours time. Within 2 hours of the wind speed decreasing, suspended sediments settled quickly and formed a cohesive fluid mud suspension layer (25,000 mg l^{-1}) at 20cm above the seabed. It is suggested, considering that a correlation with a salinity indicator was lacking, that waves and currents combined were contributing to resuspension. Kineke et al (2006) found evidence in one cold front event, both the development of a suspension layer (SSC > 10g L^{-1}) in the lower 0.1 m of the water column occurred just prior to the wind shift from SE to NW, and the formation of fluid mud just after the wind shift. Kineke et al (2006) also noted that during the post-frontal period, currents were offshore for z > 1.0 m from the bottom and weakly onshore for z < 1.0 m from the bottom. Although the onshore velocity was low, the flow reversal in the lower meter was also in the region of highest SSC, making it important for transport. This current pattern also indicates a component of upwelling which was induced by post-frontal winds.

Sediment fluxes during low energy conditions were to the west toward the Chenier Plain at (17 g s^{-1} m^{-1}) and onshore (3 g s^{-1} m^{-1}); an order of magnitude greater during the pre-frontal phase, strongly westward and onshore, with most of the flux occurring in the bottom meter of the water column. During the frontal passage, sediment flux was also westward and essentially zero cross-shelf, before the wind shift to NW or N became established. Post-frontal conditions were still an order of magnitude greater than low energy conditions, to the east (110 g s^{-1} m^{-1}) and onshore (32 g s^{-1} m^{-1}) (Kineke et al, 2006).

Huh et al (2001) described the process by which the mud stream from the Atchafalaya sediment plume washed onshore, converted from fluid mud sheets to a consolidated cracked mud sheet to firm polygon clay “cobbles” during the drying process from cold northerly winds and

solar desiccation. These recent deposits are accreting over relict mud flat zones that alternate with shore-parallel 1to 3 meter ridges of coarser sands and shells that form the Chenier Plain. This conversion of the eastern Chenier Plain from a transgressive shell-sand ridge phase to a prograding mud flat phase is building seaward at ~ 50 meters per year. Huh et al (2001) confirmed earlier findings that the progradation of the coast was found over the eastern section of the Chenier Plain only, while the western portion was subject to coastal retreat, as is much of the Louisiana coastline.

Draut et al (2005) studied the western extent of the sediment accumulation using sedimentary, geochemical and shallow acoustic data from shore-perpendicular transects and cores on the inner shelf seaward of the Chenier Plain. Shallow acoustic data from the easternmost (~ 92.1°W) transect (T1) revealed bedding that dipped gently seaward showing active sedimentation. The core taken from this transect (OF) exhibited a thin layer of poorly consolidated mud atop a thick 1.5 meter layer of uniform, black mud with some bioturbation and small shell fragments. Bioturbation in the presence of relatively high accumulation rates here suggested rapid and episodic deposition (from storms and cold fronts), separated by intervals of slower accumulation and biogenic reworking.

Moving westward to 92.55°W, shallow acoustic data along transect (T11) revealed broadly concave sea-floor geometry, lacking the sigmoidal cliniforms found to the east. The core taken here (OC) exhibited a 0.2 meter layer of soft mud over a layer of uniform, black mud 0.5 meter thick. It was inferred that the homogenous, poorly consolidated mud from this core was also recently derived distal sediment from the Atchafalaya River.

The westernmost transect (T19) near the center of the Chenier Plain ~92.9°W, was also broadly concave in geometry, and the Core (OMLb) exhibited a series of thin layers ~ 0.1 each

(from the top down) of hard mud with small shells, stiff clay with millimeter-scale laminations, and sand/shells. Below these was a ~0.7 m layer of stiff clay with occasional small shells with millimeter-scale planar bedding. A lack of ^{137}Cs in this core implies relict sediment that had not been exposed to the water column in the last 100 years.

Draut et al (2005) concluded that the subaqueous Atchafalaya delta, which was 2.5 meters thick just seaward of Point au Fer, thinned westward to ~ 1.5 meters in Core (OF) and reached its westward limit near 92.5°W at 0.74 meter thick in Core (OC). The sand-shell layers that underlie the sediments from these cores also compared favorably with the shell-hash facies found south of the Atchafalaya River mouth. Draut et al (2005) further concluded that after the Atchafalaya Bay is filled, sediment will bypass the present Atchafalaya Bay depocenter and increased deposition will occur seaward of the Point au Fer reef. This will increase the amount of sediment available for westward transport and sedimentation will increase on the central Chenier Plain. The Atchafalaya Bay will not be filled in the next 40 years as put forth by Wells et al (1984), due to interference of natural distributary growth by the Old River Control structure and other anthropogenic effects in the drainage basin (Draut et al, 2005), as well as the effects of cold front passages which flush sediment from the bays (Walker and Hammack, 2000).

2.7 Wave Dissipation in Fluid Mud Environment

Until recently, little was known about the differences in the hydrodynamics between sandy sea beds and muddy bottoms. Studies on wave dissipation in mud environments were historically based on the "long wave paradigm" (LWP) which was sufficient for sandy environments; the assumption was that dissipation resulted solely from direct wave-bottom interaction, and that only long wave motion reached deep enough into the water column to encounter bottom friction. However, sediment resuspension, flocculation and settling to form a

near-bottom fluid-mud layer changes the properties of the water column, thereby changing its responses to and interactions with waves.

Sheremet and Stone (2003) compared the effects of cold front passage over two ocean-meteorological stations in the GOM. They bore similarities in location: about 150 km apart, in water depth < 10 m, they were subject to the same wind conditions from passing fronts, had similar low slope shelf gradient, and were subject to identical tidal and offshore wave influences. The critical difference is that the CSI-3 station was situated in a mud-dominated zone of fine grained sediments (particle size 2-6 μm) and the CSI-5 station was situated in a sheet of quartzitic sands with a mean particle size of 0.1 mm.

Using a frequency threshold: with short wave, high frequency "sea" > 0.2 Hz and long wave, low frequency "swell" < 0.2 Hz, Sheremet and Stone (2003) monitored wave evolution and found that while advanced models such as SWAN (Booij et al, 1999) accurately reproduced long wave propagation at sandy sites, they failed to correctly describe short wave characteristics at the CSI-3 muddy site, even when adjusted for increased bottom friction. Model performance (with CSI-3 run as a sandy site) indicated that short wave dissipation was *not* the result of other mechanisms, such as wave breaking or refractive scattering.

During the prefrontal and frontal phase of winter storms, wave heights increased at similar rates at both sites, but decayed faster and to lower values at CSI-3 (Sheremet and Stone, 2003: Roberts et al, 2005). The energy distribution at CSI-5 demonstrated a continuous increase to a pronounced peak in the low-frequency band and then decreased likewise in the course of the frontal passage and post frontal cold air outbreak. Low frequency wave energy dominated during the course of the storm at CSI-5. In contrast, low-frequency waves at CSI-3 were considerably less intense. High-frequency waves grew at similar rates at both stations, yet CSI-3 did not attain

the energy levels compared with CSI-5 at the peak of the storm. High frequency waves dissipated more quickly at CSI-3 as wind forcing weakened in the wake of the frontal passage.

The presence of resuspended sediments and the formation of a fluid mud layer above the sea bed is a significant contributor to damping wave energy. Kineke et al (2006) stated "The inner shelf is less turbulent because of wave attenuation, but turbulent enough to prevent deposition and maintain a high-concentration bottom layer (fluid mud)." Rather than viewing mud-induced wave dissipation and wave-induced sediment resuspension as discrete processes, these hydronamic and sedimentary processes should be approached as a coupled system which induces a positive feedback loop.

2.8 Remote Sensing of Suspended Sediments

2.8.1 Solar Radiance

With the arrival of satellite technology, it became possible to quantify sediment in both fresh and marine waters on greater spatial and temporal scales. Satellite imagery provides a means to examine the optical properties of the water's constituents with "a large-scale synoptic view of the highly dynamic coastal environment" (Miller et al, 2005), albeit for the water body's surface layer only. Sensors on satellite platforms measure signals which are returned from solar radiation on/into the water body, across various frequencies in the electromagnetic spectrum, each wavelength revealing different aspects of the composition of the water medium.

Solar radiation is measured as radiant flux (Φ), that is, the time rate of flow of radiant energy, with radiant intensity (I) the measure of radiant flux per unit solid angle in a specified direction, and radiance (L) at a point in space being the radiant flux at that point, in a given direction per unit solid angle, per unit area, at right angles to the direction of propagation.

Radiance is a function of direction of the zenith angle (θ), between the beam of light and the upward vertical, and the azimuth angle (φ) between the vertical plane incorporating the beam of light and the vertical plane of the satellite view, measured clockwise relative to North.

2.8.2 Radiance, Reflectance and Atmospheric Correction

Radiance is commonly written as $L(\theta, \varphi)$ and is expressed in watts (W) or (quanta s^{-1}) m^{-2} $steradian^{-1}$. The total radiance arriving at the sensor is

$$L = L_r + L_a + L_g + tL_w \quad (2.1)$$

where L_r is molecular scattering in the atmosphere (Rayleigh scattering), L_a is aerosol scattering from dust, smoke, and haze in the atmosphere (Mie scattering), L_g is sun glint reflected from the water surface, and tL_w is the water leaving radiance transmitted by the atmosphere, including photons which are introduced from adjacent regions into the field of view (Gordon, 1978; Moeller et al, 1993; Kirk, 1994). The goal is to remove photons which have not penetrated the sea surface, and consequently do not reveal any information about the subsurface conditions. Irradiance (E) is the radiant flux per unit area of a surface, with the irradiance reflectance (R) given as

$$R = E_u / E_d \quad (2.2)$$

that is, the ratio of upward irradiance (E_u) to downward irradiance (E_d) at a given point in the field.

The radiance reflectance (R_{rs}) is that which is measured by the satellite, but is subject to attenuation from the atmosphere, given by the equation

$$R_{rs} = L_u / E_d \quad (2.3)$$

that is, the ratio of upwelling water leaving radiance from just below the sea surface (L_u) to downward irradiance (E_d). Once the atmospheric affects are removed, the remaining water

leaving radiance is expressed as irradiance (or subsurface) reflectance (*R*) (Robinson, 1985) and a regression can be performed against in-situ samples of SSC.

In one method to perform aerosol and sunglint atmospheric correction, Gordon et al (1983) took advantage of the fact that water absorbs light most strongly in the near infrared region of the electromagnetic spectrum. Hence, essentially all radiance measured at this end of the spectrum can be attributed to scattering within the atmosphere (Kirk, 1994). Subtracting the data values of the near infrared pixels of a satellite image from the corresponding pixels in the visible range of the image will reduce the atmospherically scattered signal to the sensor. This method is most effective for the more homogeneous open ocean waters which are not influenced by the presence of terrigenous materials.

A second method to reduce Rayleigh, aerosol and sunglint atmospheric effects is the dark pixel correction method. It reasons that the darkest pixel in the image will have an equal contribution of scattering from atmosphere as all the other pixels, but it must have the smallest contribution from scattering within the water (Kirk, 1994). In other words, the darkest pixel is assumed to be "clear water" and the signal received is assumed to be attributed solely to atmospheric scattering. Hence, this dark pixel value is subtracted from all other pixels to remove atmospheric interference. Once again, this method is most effective when there is a dark water pixel with a relatively low data value, when atmospheric conditions in the entire image are relatively constant, and the water in the scene is homogenous and Case I open ocean. However, this method can be used in the study of Case II waters, if care is taken that selection of the dark water pixel is made as close to the same longitude of the turbid area of interest as possible, but over open waters and outside the sediment plume (Walker and Hammack, 2000).

Stumpf (1992) developed a technique which combined the two methods described above. First, corrections for changes in downwelling irradiance and transmission based on the Rayleigh optical depth and the gaseous optical depth are made in the red and near-infrared channels. Secondly, the near-infrared channel reflectances are subtracted from the red channel reflectances (creating a new image) to remove aerosol and sunglint effects. Lastly, the dark pixel of this new image is identified near the area of interest, and this pixel value is subtracted from the entire image. The method was used successfully by Stumpf in nearby Mobile Bay and by Walker (1996) in the Mississippi River plume , but fails (in step two) in the Atchafalaya region, due to the assumption that in the near-infrared water reflectance is zero, when in these high turbidity waters, such not the case. Adaptation of the method by Walker and Hammack (2000) affected a solution by removing step two; however, images with spatial variability of either aerosols or sunglint in/near the area of interest can not be utilized.

2.8.3 Inherent and Apparent Optical Properties: Light in the Aquatic Medium

Photons from the sun, each with a unique wavelength (λ) and frequency (f), which enter a water body, are either absorbed or scattered. Inherent optical properties (IOP) such as the absorption coefficient (a) and the scattering coefficient (b) depend only on the substances in the aquatic medium and not on the geometric structure of the light field within the water (Kirk, 1994). On the other hand, apparent optical properties (AOP) such as reflectance (R), and vertical attenuation coefficients (downward irradiance (K_d) and upward irradiance (K_u)) are dependent on both the constituents of the water medium and the light field in which they are measured, i.e. depth, sun angle, sky conditions, and shadowing.

Water reflectance is affected by both the absorption coefficient (a) and the scattering coefficient (b) of its components. Scattering is further identified by the direction of scatter, either

forward (b_f), or backscatter (b_b). In turbid waters, backscattering from sediment is much greater than backscattering from water (Stumpf and Pennock, 1989). Backscattering from sediments increases reflectance at all wavelengths while absorption from yellow substances (Colored Dissolved Organic Matter CDOM), chlorophyll *a*, and phytoplankton decreases reflectance, most notably in the lower blue-green wavelengths. However, "very low absorption does not in itself lead to a high reflectance, since there must be scatterers present" (Robinson, 1985).

Most of the upward irradiance flux originates in backscattering, thus, we can expect reflectance to be approximately proportional to the backscattering coefficient (b_b) for the water mass under consideration (Kirk, 1994). Applying the same logic, reflectance varies inversely with the absorption coefficient (a). Mathematical modeling (Monte Carlo calculations) of the underwater light field provided a simplified version of the radiative transfer theory which produced these equations:

1) that for irradiance reflectance at the sea surface

$$R = f\ b_b / (a + b_b) \tag{2.4}$$

where f is a variable dependent on solar zenith angle, the optical properties of seawater and the wavelength of light (Morel and Gentili, 1991; D'Sa and Miller, 2005), and

2) that for radiance reflectance from just below the sea surface

$$R_{rs} = 0.083\ b_b / a \tag{2.5}$$

(Kirk, 1994), both of which show the relationships between the inherent and apparent optical properties.

2.8.4 Remote Sensing of Turbid Waters

In turbid waters, suspended sediment is the optically dominant constituent, with backscattering increasing at all wavelengths. Overall, the spectral shape does not change much

due to increases in sediment load, making a model relating SSC to reflectance possible. Sea-truth verification by water samples being filtered and weighed for volume measurement and for distinguishing between organic and inorganic particulate matter is still integral to the process. Walker and Hammack (2000) studied the Atchafalaya Bay and found that when TSS exceeded 10 mg l^{-1}, inorganics comprised at least 80% of the suspended sediment concentration. Regardless of alterations to the signal by sediment grain size across all wavelengths, and due the absorption by organic and inorganic pigments in the blue-green end of the spectrum, the red and near infrared spectral bands are preferred for examining sediments in turbid water (Stumpf and Pennock, 1989; Kirk, 1994). Kirk (1994) also noted the need for locality-specific algorithms for SSC in turbid waters, since local variations in phytoplankton content and the spectral distribution of the light reflected by suspended inorganic particulate matter varies with the absorption properties determined by the chemical nature of the sediments themselves.

Miller et al (2005) conducted a study to examine the coupling between bottom sediment resuspension and the surface expression of that resuspension with remotely sensed imagery over Lake Ponchartrain, Louisiana. Although this environment differs from a fresh water river discharging into the coastal ocean (the lake has limited freshwater inflow and small tidal influence and is a relatively confined water body), similarities to the Atchafalaya region exist in sediment type, water depth, and the fact that it has a large surface area (1645 km^2) dominated by wind-driven resuspension and circulation. To model resuspension: bathymetry, wind speed and direction, and estimates of fetch were input; images were generated for all parameters such as critical wind speed (U_c), resuspension potential (*RP*) and resuspension intensity (*RI*) for use in comparison/verification to actual MODIS imagery during several cold front passages. The model

showed that for winds from the northeast, significant resuspension occurs with wind speeds over 4 m s^{-1}.

MODIS imagery was atmospherically corrected with the dark pixel method, georeferenced and masked for land and clouds. Miller et al (2005) noted that differences in sediment distribution between two images in a time series can be derived by subtracting one image's reflectance values from the other to examine horizontal changes in SSC, but that the changes may be due to transport (advection) in or out of the area or from localized resuspension. The model output was graphically formatted and integrated with imagery to analyze sediment dynamics.

There was a high correlation between resuspension intensity (*RI*) and MODIS reflectance values, with a curvilinear relationship. MODIS reflectance (band 1; red) increased linearly with *RI* increases until a maximum value was reached (reflectance ~ 0.04) and then reflectance plateaued. Miller et al (2005) proposed that this upper limit may be due to maximum loading of bottom sediments in the lake's water depth, since a previous study (Miller and McKee, 2004) reported that the dynamic range of the MODIS band 1 was sufficient to detect much higher reflectance (from high SSC) in turbid coastal waters.

There was good agreement in resuspension potential (*RP*) and MODIS imagery in that the patterns and orientation of the gradients in total suspended matter (TSM) were aligned with the axis of wind direction, and that magnitudes were commensurate with wind speed. However, one cold front demonstrated higher actual TSM values than what was predicted. A review of the wind speed data prior to image acquisition revealed that wind speeds were elevated for 6 hours (averaging over 6 m s^{-1}) so that complete settling of the sediments has not yet occurred. Miller et

al (2005) noted the need to perform complete analysis of all available data and the incorporation of additional techniques such as radiochemical tracers to examine bottom sediment dynamics.

CHAPTER 3 RESEARCH DATA AND METHODOLOGY

3.1 Suspended Sediment Concentration Empirical Modeling

3.1.1 Satellite Image Processing and Analysis for Model Development

This study utilized imagery from two satellites, Aqua and Terra of NASA's Earth Observing System. Data from Terra has been archived since 2000 and from Aqua since 2003; both are available from NASA's Goddard Space Flight Center's LAADS website (http://ladsweb.nascom.nasa.gov/index.html) in compressed .hdf format. The sensor on both satellites, the Moderate Resolution Imaging Spectroradiometer (MODIS) has a swath width of 2330 kilometers, wide enough to cover the entire Gulf of Mexico. Flown at 705 km altitude, MODIS instruments are in sun-synchronous, near-polar, near-circular orbits with a 10:30 am local time (Terra) descending pass and a 1:30 pm local time (Aqua) ascending pass each day. On board calibration is extensive for verification of spatial, spectral and radiometric measurements; they are tested against pre- and post-launch ground based references.

Individual days' swaths from the LSU Earth Scan Laboratory archives (http://www.esl.lsu.edu/imagery/modis/web/modis_archive.php) were visually assessed for cloud-free conditions over the Gulf of Mexico in conjunction with in situ sea-truth collection times (within +- 2 hours of image GMT). Samples collected outside this window may not be representative of the conditions at the time the image was made. For the year 2001, only Terra images were available. For 2002 and 2003, both Terra and Aqua images were evaluated. In cases where both a Terra and Aqua image were available, selection was based on a combination of 1) clear sky; 2) image time agreement with sea water sampling; and 3) the greater number of sample matches available. The images analyzed for Suspended Sediment Concentration (SSC)

modeling are listed in Table 3.1, with two images (May 20 and May 21, 2001) having been eliminated due to cloudiness.

Table 3.1 SSC Model Development - Sample Collections Match with Images

Sampling Date	Julian Day	Sample GMT	Terra Image GMT	Aqua Image GMT	select sample times between	possible stations
20010321	080	1500 to 1814	1650		1450 to 1850	AR1 to FLB15
20010522	142	1314 to 1826	1705		1505 to 1905	C10 to C25
20021123	327	1745 to 2152	~~1620~~	1925	1725 to 2125	AR1 to R28
20031030	303	1630 to 2115	~~1635~~	1945	1745 to 2145	20 to AR1

For each swath selected, the following were downloaded:

- MODIS Level 1B Calibrated Radiances 1KM, HKM, and QKM
- MODIS Level 1A Geolocation.

The QKM file contains channel 1 (0.62 - 0.67 μm) and channel 2 near infrared (0.84 - 0.87 μm) both at 250 meter spatial resolution. The HKM file contains channel 3 (0.46 - 0.48 μm) and channel 4 (0.55 - 0.57 μm) at 500 meter spatial resolution.

The HKM file contains also channels 5 through 7 at 500 meter resolution and channels 8 through 36, at 1000 meter spatial resolution. Although these channels are not specifically utilized for sediment concentration analysis, the HKM and Geolocation files are input along with the QKM and 1KM files to perform atmospheric correction and sun/sensor geometry corrections.

Jacques Descloitres of NASA's MODIS Rapid Response Project developed a MODIS Corrected Reflectance algorithm to correct molecular path (Rayleigh) scattering, remove the gross effects of sun and sensor geometry by adjusting for solar zenith and azimuth angles, and convert radiance values to output reflectance values (Gumley et al, 2003). This program was run on each day's set of images.

Next, the HDF-EOS to GIS Format Conversion Tool (HEG), developed by NASA's Earth Observing System (EOS) Core System Project Office, was used to reformat and re-project channels 1, 2 in the QKM, and 3, 4 in the HKM to output individual layer GEOTIFF (.tif) files and subset each to only the Atchafalaya Bay region (ULX -92.72 W, ULY 29.98 N, LRX -90.57 W, LRY 27.79 N). These files were then imported into ERDAS Imagine and saved as image (.img) files for subsequent processing.

Visible channels 1, 4 and 3 were layer stacked in ERDAS Imagine (Interpreter function) and assigned color guns red, green and blue (RGB) respectively, to enhance the images to "true color" which reveals the optical color properties of water masses. Band 1 was automatically interpolated from 250 meters to 500 meters in this process, reducing its spatial resolution. These multispectral images were used only for 1) visual assessment of cloud cover, 2) evaluating proximity to frontal boundary areas, cloud shadows or land masses and 3) presentation purposes. Station overlay files Arc Coverage (.ovr) and Symbology (.evs) were created from exact latitude and longitudes coordinates to pinpoint the sample collection sites.

Sediment type typical of this region (silts, clays) have high scattering characteristics in channel 1 (red) which, when images are viewed successively, allows better understanding of circulation and sediment transport processes in these turbid coastal waters. Two variations of dark pixel atmospheric correction were tested, based on methods developed by Stumpf (1999) and modified by Walker and Hammack (2000):

1) by subtracting the dark (clear water) pixel value of the visible band 1 (red) from the entire band 1 (red) image, or
2) by subtracting the dark (clear water) pixel value of the infrared band 2 from the entire band 1 (red) image.

This was accomplished by finding the dark pixel in channel 1 and choosing that same pixel in channel 2 to evaluate whether it was also the dark pixel in band 2. The consistency between dark pixels in each band was good. The dark pixel subtraction values in band 1 were less than 1% reflectance higher than in band 2 across multiple days' images (Table 3.2). The ERDAS Imagine Modeler function was employed to produce two new aerosol corrected image files for each day. The new pixel data values from these images were used as input for creation of the suspended sediment model.

Table 3.2 SSC Model Development: Dark Pixel Values

Image ID	Date	Latitude (N)	Longitude (W)	dark pixel value ch. 1	dark pixel value ch. 2
2001080	March 21, 2001	28.392483	-92.364289	.0095	.0060
2001142	May 22, 2001	29.433394	-92.710181	.0421	.0380
2002327	Nov 23, 2002	28.361259	-91.451795	.0100	.0063
2003303	Oct 30, 2003	29.121462	-91.365082	.0177	.0080

3.1.2 Field Sample Processing for SSC Model Development

Research cruises for the project *Application of Remote Sensing to Assessing Impacts of Short Term Climate Variability on Coastal Sedimentation* were made into the Atchafalaya Bay, Four League Bay, the Atchafalaya Navigation Channel and the Chenier Plain just west of Atchafalaya Bay on the following dates: March 21, 2001; May 20 through 22, 2001; November 23, 2002; and October 30, 2003. The project was funded by NASA Goddard grant # NA65-9688 in collaboration with the University of Wisconsin-Madison, Space Science and Engineering Center. The data from these cruises represents the autumn and winter seasons (March, October, and November) as well as spring/summer conditions (May). Water samples were collected from within 0.5 meter of the surface in 500 ml quantities. The locations were determined using GPS, and samples were taken within one to two hours of satellite overpass. Figures 3.1 through 3.4

demonstrate the locations of sample collection stations overlaid on their respective days' images. The water samples were processed in the Marsh Hydrology Laboratory at Louisiana State University for suspended sediment concentration (SSC) using the glass microfiber (GF/F diameter 47 mm, pore size 0.7µm) filter method: dried at 60°C, combusted at 500°C and weighed to distinguish inorganic and organic sediment proportions (USGS, 1987). These data were readily available for use in this project.

3.1.3 Statistical Analysis for SSC Model Development

The four days of field collection yielded 92 surface water samples (Appendix A). Of these, 22 were eliminated due to land contamination, 4 due to frontal boundary uncertainty, 7 were in cloud shadow, and 8 due to absorption from chlorophyll *a* concentration distorting the reflectance signal from sediments. The inorganic suspended sediment concentration data from the remaining 51 samples were plotted against the aerosol corrected reflectance of channel 1, determined by using two methods: channel 1 dark pixel value subtraction (Figure 3.5 (a)) and channel 2 dark pixel value subtraction (Figure 3.5 (b)). While the two scatterplots are nearly identical in shape and distribution, the channel 2 dark pixel subtraction demonstrates slightly higher reflectance values overall. This suggests that the channel 1 dark pixel subtraction removes more aerosol scattering.

Regression analysis of channel 1 corrected reflectance data to sea-truth samples produced two suspended sediment concentration models, one for each dark pixel correction method (data in Appendix B and Appendix C). Reflectance was input as the independent variable and suspended sediment was the dependent variable. The exponential curves for both variations of the dark pixel correction methods are shown below in Figure 3.6 (a) and (b). For both, x is the atmospherically corrected reflectance and y is the SSC in mg/l.

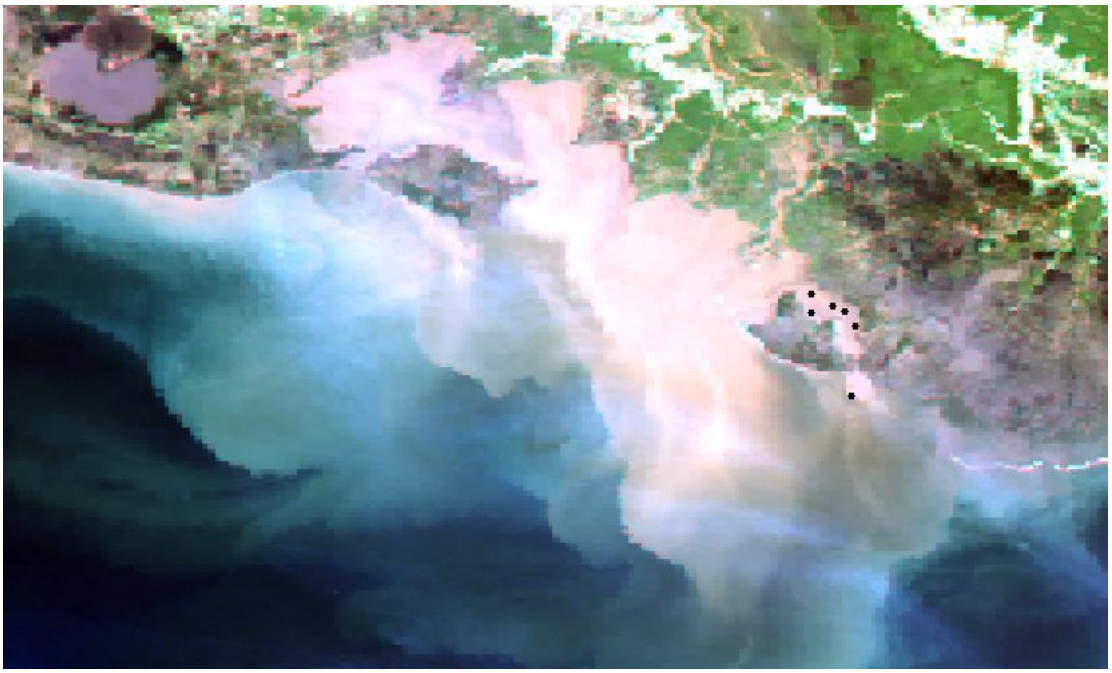

Figure 3.1 March 21, 2001 stations. MODIS “true color” image with black dots indicating locations of water samples.

Figure 3.2 May 22, 2001 stations. MODIS “true color” image with black dots indicating locations of water samples.

Figure 3.3 November 23, 2002 stations. MODIS “true color” image with black dots indicating locations of water samples.

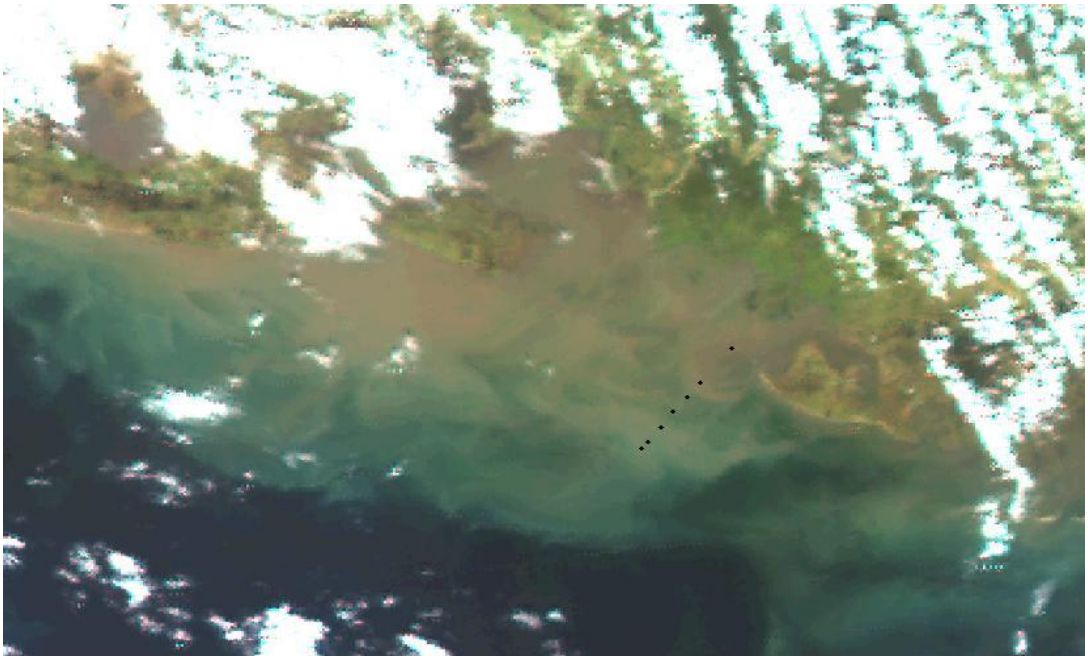

Figure 3.4 October 30, 2003 stations. MODIS “true color” image with black dots indicating locations of water samples.

(a)

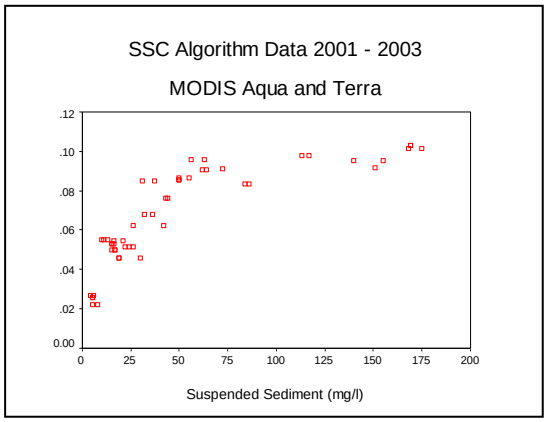

(b)

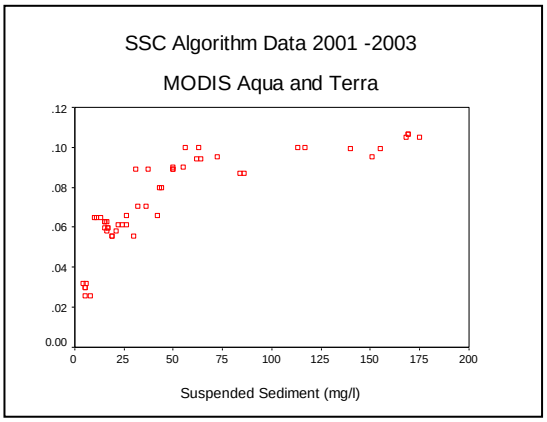

Figure 3.5 Scatterplots of dark pixel corrected reflectance and suspended sediment. (a) channel 1 – channel 1 and (b) channel 1 – channel 2.

(a)

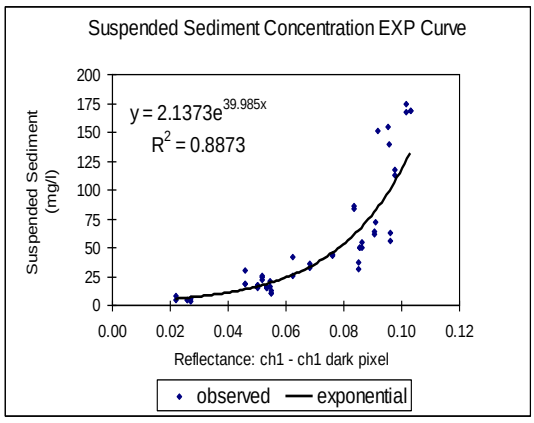

(b)

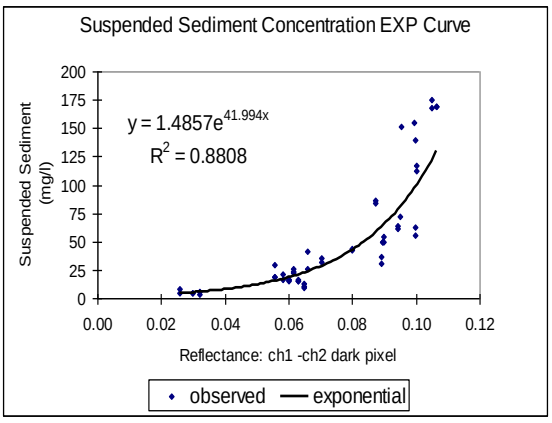

Figure 3.6 Exponential regressions of dark pixel corrected reflectance and suspended sediment. (a) channel 1 – channel 1 and (b) channel 1 – channel 2. Blue dots are the observed data; the black line is the exponential model.

Comparison of the two regressions confirms that the channel 1 (red) dark pixel subtraction was as effective as the channel 2 (infrared) dark pixel subtraction in removing atmospheric scattering in these turbid waters; all subsequent image processing for this project utilized this procedure. These findings also indicate that atmospherically corrected channel 1 reflectance values reliably predict suspended sediment concentrations in the Atchafalaya plume, both within the bay and on the inner continental shelf. This model was applied to the entire Atchafalaya Bay Complex and the inner shelf environments to map the extent of various surface concentration boundaries and track movement of surface sediments in response to meteorological and oceanographic forcing.

3.1.4 Suspended Sediment Concentration Model Testing

Two research cruises were undertaken by LSU faculty and students aboard Louisiana Universities Marine Consortium's RV Pelican, from January 6 – 11, 2006 and from March 31 – April 6, 2006. During both cruises, cold fronts crossed the Atchafalaya Bay region. For the January cruise, two days (January 6 and 7) provided good quality imagery. Unfortunately, the January 6 image (Figure 3.7) contained fires on land with smoke plumes extending out over the bay region near sampling locations. The January 7 image was cloud free and four stations matched the satellite overpass time window. Four surface water samples were collected, although all were taken outside the sediment plume.

For the March-April cruise, 5 days of images were processed with one discarded for cloudiness. Although there were a number of satellite overpass time-matched stations for these days, the stations were located too far from shore and well outside the sediment plume. Processing for suspended sediment concentration was discontinued on these samples. In addition

Figure 3.7 MODIS “true color” image showing smoke plumes on January 6, 2006.

to the above samples, sea-truth data was available from north-south transect lines on the inner shelf from February, April and June 2002 and January 2003 (N. Rabalais, LUMCON, unpublished data). An additional 6 samples coincided with time-matched imagery, although isolated clouds were in the proximity of several collection sites.

All imagery was processed in the same manner as the SSC model imagery. The SSC equation (see Figure 3.6 (a))

$$y = 2.1373\ e^{39.985x} \qquad (3.1)$$

was applied to the reflectance values to obtain predicted SSC. Poor test results ($R^2 = .15$) were due to several factors:

- atmospheric contamination on collection days,
- low availability of samples overall ($n = 10$),
- smaller range of SSC values (0 – 56 mg/l),
- possibility of sediment advection from the Chenier Plain to the west.

Attempts to find other suspended sediment samples from this region to further validate the model proved unsuccessful.

3.2 Case Studies of Cold Front Passages

3.2.1 Field Data from the Wave-Current-Surge Information System (WAVCIS)

The Wave-Current-Surge Information System (http://www.wavcis.lsu.edu) provides both meteorological and oceanographic hourly data for analysis of the intensity of wind-wave interaction and the influences on currents in shallow waters that drive sediment resuspension and transport. This study accessed data from CSI-3, which is located south of Vermillion Bay, seaward of Marsh Island (coordinates: 92°03.68', 29°26.47') (Figure 1.1).

The station is equipped with meteorological sensors including an anemometer, a barometer and an electronic thermometer to provide measurements of wind speed (adjusted to a standardized 10 meters height), wind direction, air temperature and barometric pressure. For purposes of this study, wind direction is expressed using the meteorological convention, that is, the direction from which the wind blows. The hydrodynamic sensors include a digiquartz pressure transducer and an electronic thermometer to provide measurements of waves, water level, and near-surface water temperature.

CSI-3 was equipped with an Acoustic Doppler Current Profiler (ADCP) for ocean current profiling. For this study, current direction is designated using standard oceanographic convention, as the direction toward which it flows. Current direction and speed are measured at thirteen depths ('bins') from the sea bottom to the sea surface. For this study, hourly current measurements from particular bins were selected (Table 3.3) to correspond most closely with:

1) the depths of turbidity measurements taken at the same site (bins 2, 5, and 7) and

2) an allowance for water level set down during cold front passage (bin 11).

Table 3.3 ADCP Bin Depth Selections

Bin #	Depth from sea floor (meters)	
11	4.12	(near surface)
7	2.72	(mid-depth)
5	2.03	(mid-depth)
2	0.98	(bottom)

From 2003 to 2005, CSI-3 housed a rack of three McVan Analite NEP 195-4-30-g turbidity probes which operate by sending a beam of infrared light (780-900 nm) into the water. The beam is scattered by suspended particles and the detector then measures the quantity of light

that is reflected back to a detector set at a 90° angle, in Nephelometric Turbidity Units (NTU), scaled from 0 to 1000.

Salinity measurements were also taken every 20 minutes from bins 2, 5 and 7 (Table 3.3), and are labeled SAL1, SAL2 and SAL3 respectively, denoting their distance from the sea bed. Meteorological and oceanographic measurements were plotted on the same temporal scale as the sediment data (sections 3.2.3, 3.2.4 and 3.2.5 below) to reveal the forces which drive the sediment dynamics.

3.2.2 Identifying Cold Front Passages

National Weather Service Daily Weather Charts (http://www.spc.noaa.gov/obswx/maps/) were examined for the presence of cold air masses which passed over the Atchafalaya Bay region during the winters of 2004 and 2005. These were confirmed with the hourly meteorological data from CSI-3 to include: a 10◦ C drop in air temperature, a drop in barometric pressure and a clockwise rotation of the winds from southerly or south-easterly to northwesterly, northerly, or (less commonly) northeasterly. Time periods investigated include both frontal passages and the subsequent cold air outbreaks, with winds having a northerly component ranging from 271◦ to 89◦. The term "post-frontal" refers to the period from onset of frontal passage until winds resume with a southerly component and vary in length from hours to days. The terms "inter-frontal" or "non-frontal" refer to periods when winds ranged between 90◦ and 270◦ with a southerly orientation. Selection of fronts to be further analyzed was based on the availability of clear sky imagery and turbidity data which coincided with the fronts. For each front selected, several days prior to and afterwards were also examined for a more complete picture of the effects of winter storms in this shallow water, fluid mud environment. The weeks selected are shown in Table 3.4, each of which includes at least one cold front event. "Duration"

represents the length of time of winds with a northerly component (post-frontal) impacted the station (Table 3.4).

Table 3.4 Case Study Weeks Selected

Case Study Selections	duration	begin date/time	end date/time
January 6 – 12, 2004	53 hrs	1/9/04 10:00	1/11/04 14:00
January 16 -22, 2004	53 hrs	1/18/04 12:00	1/20/04 16:00
January 24 -30, 2004	41 hrs	1/27/04 3:00	1/28/04 20:00
March 30 – April 5, 2005	51 hrs	4/1/05 12:00	4/3/05 13:00
April 20 – 26, 2005	41 hrs	4/23/05 4:00	4/24/05 20:00

3.2.3 Turbidity Probe Data – Conversion of NTU to TSS

From April 10, 2003 to May 6, 2005 at the CSI-3 station, turbidity measurements were obtained every 20 minutes from probes mounted at 1 meter (NTU1), 2 meters (NTU2) and 3 meters (NTU3) above the sea floor. For April 2005, the CSI-14 station also provided hourly turbidity readings at 1 meter from the bottom. The Field Support Group of the Coastal Studies Institute, Department of Oceanography and Coastal Science, Louisiana State University regularly maintains all instrumentation and calibrated the turbidity probes (Analite 195) with Formazin to NTU's at the time of installation.

In order to match CSI-3's NTU sensor recording cycle (every 20 minutes) to the meteorological and ADCP hourly readings, hourly means were calculated on each of the three NTU readings (hh:mm) from 00:19 minutes, 00:39 minutes and 00:59 minutes for each hour, at each of the three depths.

These means (NTU1hrly, NTU2hrly and NTU3hrly) were converted to TSS hourly values (TSS1, TSS2, and TSS3) with the linear relationship:

$$y = 0.75x + 21.32 \qquad (3.2)$$

where *y* is TSS in mg/l and *x* is the hourly NTU value (Walker, 2001). The model was developed within the East Cote Blanche Bay-Atchafalaya Bay area, with a time series of data, sampling every 6 hours over 4 days. Water samples were collected with an automatic water sampler at a depth of 1.5 meters, concurrent with YSI 6600 turbidity readings. The regression analysis R^2 = .97 indicates that the turbidity measurements accurately reflected the variability in temporal TSS fluctuation. For the CSI-14 data, the measurements were already provided at 1 hour intervals and Formula 3.2 was applied here as well. For this study, the term "fluid mud" refers to high TSS concentrations resuspended near-bottom.

3.2.4 Calculation of Sediment Flux at CSI-3

Each TSS hourly value was converted to g/l then matched with the hourly data taken the following minute (i.e. 01:00) from the ADCP current data. By multiplying the total suspended sediment at each depth (1, 2 and 3 meters from the sea bed) and time by the corresponding current speed at that same depth and time, the sediment flux (g/l * cm/s) was derived. By combining this output with the current direction for its corresponding depth and time, the sediment hourly flux was plotted in stick vector format for each depth, where values from bins 2, 5, and 7 were given the names SEDFLX1, SEDFLX2, and SEDFLX3 respectively. When the plots were "stacked" by depth, a more complete analysis of the sediment transport throughout the water column during cold front passage was made. There was no continuous turbidity measurement which corresponded to bin 11 current data; therefore, the uppermost meter of water did not have sufficient data to create a time series sediment flux plot.

3.2.5 Calculation of TSS for Surface Waters at CSI-3

Suspended sediment concentration for the surface waters could be calculated only for those particular points in time when the satellite was making an overpass providing a reflectance

value for the calculation of TSS. For each case study image, the atmospherically corrected pixel value from channel 1 was selected at the CSI-3 station position. To derive the SSC at the site, equation 3.1 was applied (Table 3.5).

Table 3.5 Case Study Images Suspended Sediment at CSI-3 Location.

Date	pixel ID	reflectance ch1-ch1 dk	TSSRefl susp sed mg/l
20040110	CSI3 2004010.1855	0.1036	135
20040111	CSI3 2004011.1940	0.0525	17
20040119	CSI3 2004019.1850	0.0963	100
20040127	CSI3 2004027.1940	0.1002	117
20040128	CSI3 2004028.1845	0.0923	86
20050401	CSI3 2005091.1950	0.0851	64
20050402	CSI3 2005092.1855	0.0837	61
20050403	CSI3 2005093.1940	0.0449	13
20050424	CSI3 2005114.1955	0.0365	9

The remotely sensed reflectance signals which were converted to surface TSS estimates at CSI-3 (TSSRefl) were plotted with the oceanographic measurements of NTU (also converted to TSS estimates) for the mid- and bottom depths. The purpose was to determine whether the surface plume sediment concentration is indicative of sediment patterns below the surface, that is, in the lower 3 meters of the 5 meter water column.

3.3 Plume Contours, Area Measurements and Bathymetry

In order to map the changes in extent and shape of the surface sediment plume in response to cold front passage, raster contours were created using Imagine Interpreter's Topographic function. It was first necessary to determine the reflectance values desired to select points which will simulate the 10 mg/l, 25 mg/l, 50 mg/l and 100 mg/l boundaries. This was accomplished by inputting reflectance values into equation 3.1 to compute the result closest to the desired concentration level. The Raster Contour function of Imagine was used to create Arc Coverage layers. Table 3.6 gives the reflectance values contoured to plot the four selected levels of sediment concentration.

Table 3.6 Equivalents for SSC and Reflectance Contours

SSC (mg/l)	contour reflectance
10	0.0386
25	0.0616
50	0.0789
100	0.0962

Occasionally, the presence of clouds or a smoke plume distorted the placement of a small segment of a contour line. To remedy this and to allow for area measurements using a scale tool, each images' four contour lines in the Arc Coverage layer were then hand digitized into individual Annotation (.ovr) layers. The results of plume area measurements are found in Appendix D and discussed in the next chapter. The satellite imagery was annotated with the location of the CSI-3 station, the satellite derived TSS estimate (which corresponds to TSSRefl on the TSS plot for each cold front event) and suspended sediment concentration plume contours. In the plume contour analysis, the term "mud-plume" refers to the area(s) of satellite observed surface suspended sediment concentration of 100 mg/l or more.

Bathymetry files from the DBDB2 (Digital Bathymetric Data Base) from a project of the Naval Research Laboratory were converted to Annotation (.ovr) files as well, to display 5m, 10m, and 20m contours to reveal general inner shelf characteristics and the locations of shoals.

3.4 CSI 3 Water Level Comparison to Eugene Island Tidal Prediction

In order to distinguish the water level set-down attributed to a cold front, the astronomical tidal fluctuation should be excluded. The nearest National Oceanographic and Atmospheric Administration station for which such predictions are made is Eugene Island (station ID 8764311), located at 29° 22.3'N, 91° 23.1'W (Figure 1.1).

The hourly prediction from Mean Low Water Level (MLW) in meters was downloaded from http://tidesandcurrents.noaa.gov/tide_pred.html. The mean from January 2004 through May 2005 was calculated at 0.33 m, and subtracted from each hourly prediction to derive the expected hourly tidal variance.

In similar fashion, the mean water level at CSI-3 was calculated at 4.92 m, based on the same period January 2004 through May 2005. This mean was also subtracted from the actual hourly water level measurements to derive he water level variance.

Both variances were graphed together to show the amount of water level decrease which is attributed to cold front passages, the "set-down" (Figure 3.8).

3.5 Limitations

A number of factors involved in sediment dynamics are not specifically examined: high or low frequency wave energy damping, fetch length, wind stress on the sea surface, shoaling depth, particle size of the sediment, bottom friction and the process of flocculation. It should be noted that while the imagery was atmospherically corrected, adjustments for absorption by CDOM or phytoplankton were not specifically addressed since this region is dominated by sediment backscatter.

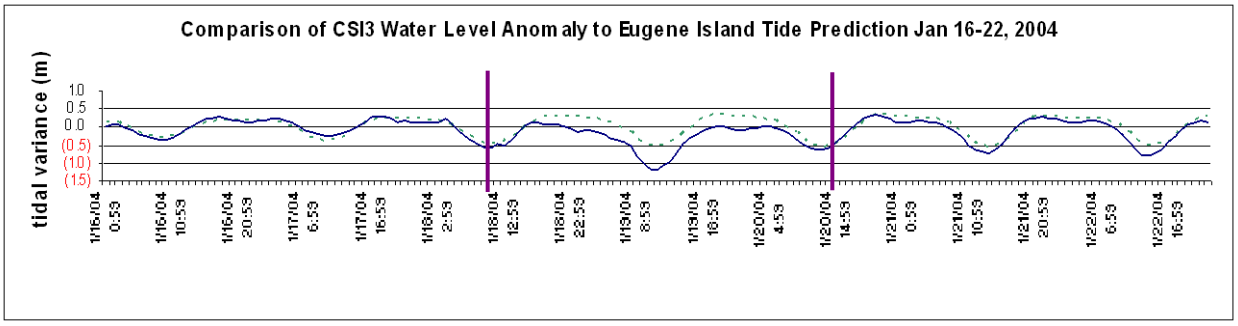

Figure 3.8 Comparison of CSI-3 Water Level Anomaly to Eugene Island Tidal Prediction January 16 – 22, 2004. Sample showing variance in water level ("set-down") attributed to cold front passage.

CHAPTER 4 RESULTS

4.1 Introduction to Case Studies

Five case study events were studied 1) to investigate whether spatial and temporal changes in surface sediment concentrations reflect the characteristics of sediment resuspension and transport throughout the water column, 2) to gain a comprehensive view of the common characteristics of cold front passages which impact sediment dynamics and 3) to reveal the unique features of each event. These particular cold front passages in 2004 and 2005 were selected based on the availability of in-situ measurements of TSS at WAVCIS CSI-3, other important oceanographic and meteorological in-situ measurements and clear sky MODIS satellite imagery. These events provide a view of sediment delivery, resuspension and transport characteristics under various meteorological and river discharge conditions during January 2004 and March/April 2005.

The following table (Table 4.1) summarizes the satellite observations of TSS from MODIS and is discussed in detail in the next section (Section 4.2).

Table 4.1 Summary of Satellite Observations from MODIS TSS Analysis

Date/Time (GMT)	TSS at CSI-3 (mg/l)	Maximum TSS in mud-plume (mg/l)	contour area (km^2)			
			100 mg/l	50 mg/l	25 mg/l	10 mg/l
1/10/2004 18:55	135	285	1,210	3,315	5,414	7,569
1/11/2004 19:40	17	301	733	1,780	2,957	5,149
1/19/2004 18:50	100	399	2,268	4,709	7,611	11,116
1/27/2004 19:40	117	427	2,542	5,064	8,724	10,763
1/28/2004 18:45	86	722	1,698	3,331	4,509	8,841
4/1/2005 19:50	64	142	176	3,204	4,440	6,133
4/2/2005 18:55	61	482	1,416	3,686	5,207	8,172
4/3/2005 19:40	13	324	351	1,467	2,867	4,267
4/24/2005 19:55	9	271	366	1,004	1,728	2,992

4.2 Case Studies of Cold Front Passages over WAVCIS CSI-3 on the Inner Shelf

4.2.1 January 6 - 12, 2004 Case Study Event

During the first week under observation, this cold front passage followed a prior cold front which had concluded within the previous 48 hours. River discharge during this period was steadily increasing from the previous autumn season low of 90,000 cfs (2,549 $m^3 s^{-1}$) and had sustained 200,000 cfs (5,663 $m^3 s^{-1}$) for several weeks before this front's arrival.

In the pre-frontal period from January 6 - 8, SE winds from 9 - 12 m s^{-1} (Figure 4.1 (a),(b)) caused a relatively small but sustained water level set-up, as shown in the comparison of CSI-3 water levels to the Eugene Island tidal prediction (Figure 4.2 (c)). The water column was well-mixed and salinity fluctuated with the tidal signal between 10 – 20 psu (Figure 4.1 (c)). Significant wave heights (H_s) (Figure 4.2 (a)) in the pre-frontal phase were 0.8 m and decreased steadily to ~ 0.3 m as the wind speed decreased and the wind direction shifted from SE to SW prior to frontal passage. This response may have been partially attributable to wave energy damping from a concurrent peak in TSS on January 8 (Figure 4.4) (Sheremet and Stone, 2003). Currents were generally northwestward/westward at 20 – 40 cm s^{-1} in the upper water column and 10 – 35 cm s^{-1} at the bottom from the dominant alongshore current which was evident throughout the water column (Figure 4.3). Currents flowed intermittently offshore but maintained westward flow throughout January 6 - 8. TSS concentrations at CSI-3 (Figure 4.4) were fairly uniform throughout the water column during the pre-frontal period, peaking at 567 mg/l on January 6; 502 mg/l on January 7; and 311 mg/l on January 8; in response to tidal low water. This strong tidal component in the TSS signal was not as evident in the other four pre-frontal periods studied. Sediment flux at CSI-3 (Figure 4.5) in the pre-frontal period was 5 - 15

g/l * cm/s to the northwest throughout the water column, then weakened and "paused" during the wind shift into the frontal passage.

The cold front approached the coast obliquely from the northwest. On January 9, 2004 at 10:00 GMT, the winds rotated rather abruptly, skipped over the typical period of rotation through westerly winds, and established northerly/northeasterly winds at reduced wind speeds of 5 - 11 m s^{-1}, which were maintained for the next 53 hours. Total water depth at CSI-3 (Figure 4.2 (b)) decreased from 5.3 m to 4.2 m; with 0.4 m of the water level set-down attributed to the frontal passage, the remainder is due to the astronomical diurnal tidal cycle. Water levels remained suppressed on January 9 and 10. Dips in salinity of 5 psu occurred simultaneously with tidal lows, showing that lower salinity river/bay water was discharged onto the inner shelf with the outgoing tides. During periods of higher water (~ 5 m), even though northeasterly winds were sustained at 6 - 9 m s^{-1}, currents weakened to ~ 5 - 25 cm $s^{-1}$and flowed onshore. On January 9, maximum values of near-bottom TSS1 were ~ 250 - 375 mg/l, and ~150 mg/l in the mid-depths (Figure 4.4). Near-bottom SEDFLX1 was weak and slightly onshore to the northeast with a short-lived "peak" of 9 g/l * cm/s, while sediment flux was minimal in the mid-depths. On January 10, TSS at all levels peaked at ~ 350 mg/l during a transition to weak offshore southeasterly sediment flux (11 - 13 g/l * cm/s) simultaneous with the tidal water level decrease. The first MODIS image for this event was January 10, 2004 at 18:55 GMT, with a satellite derived TSS of 135 mg/l in the surface plume at CSI-3 (Figure 4.6) and a maximum TSS in the main mud-plume (which extended over the CSI-3 location) of 285 mg/l (Table 4.1). The plume contours for January 10 (Figure 4.6) show the 100+ mg/l (area: 1,210 km^2) extending from the river mouth and forced by winds and currents seaward and downcoast, bypassing the western bays (at 50+ mg/l). The 25 mg/l contour conforms to a bi-lobate shape which mimics the 5 m

bathymetry of the seabed. The 10 mg/l contour (area: 7,569 km^2) encroaches across the 10 m bathymetry, encompassing two offshore shoals to the south and southwest. Eastern lobes of the 10 mg/l and 25 mg/l contours extended past Point au Fer Island, but not as far as Ship Shoal. CSI-3 was located within the mud-plume, yet the 135 mg/l satellite derived surface TSS was considerably less than the 200+ mg/l in the water column below. By January 11, TSS had decreased to 60 – 100 mg/l throughout the water column, and only weak onshore flux was evident at mid- and bottom depths with maximums of 4 g/l * cm/s. During this post-front period, the tidal influence was observed in both TSS and salinity signals more distinctly than in the post-front periods; water level highs and lows dominated currents and sediment flux throughout the water column in the absence of powerful winds.

The inter-frontal period commenced on January 11 with the return of SE winds and a corresponding drop in wind speeds and significant wave heights. Currents returned to downcoast (westward) flow at 50 - 70 cm s^{-1} at the surface, 20 – 55 cm s^{-1} in the mid-depths and 5 – 23 cm s^{-1} at the bottom. TSS was less than 100 mg/l at all depths and sediment flux was minimal (Figure 4.5). The second MODIS image acquired was in the inter-frontal period on January 11, 2004 at 19:40 GMT. The satellite derived TSS at CSI-3 was 17 mg/l in the surface water in comparison to 50 - 75 mg/l in the water column below (Figure 4.7). The maximum TSS in the mud-plume to the east of CSI-3 was 301 mg/l (Table 4.1). Sediments had quickly settled out of suspension within 5 - 6 hours of cessation of northeasterly winds. The mud-plume lost its extension south of Marsh Island and was pushed shoreward by onshore currents (area: 733 km^2). A small, isolated area of 100+ mg/l concentration was located within West Cote Blanche Bay. Comparing post-front and inter-frontal periods, all concentration levels showed between 30 - 45% decreases in area.

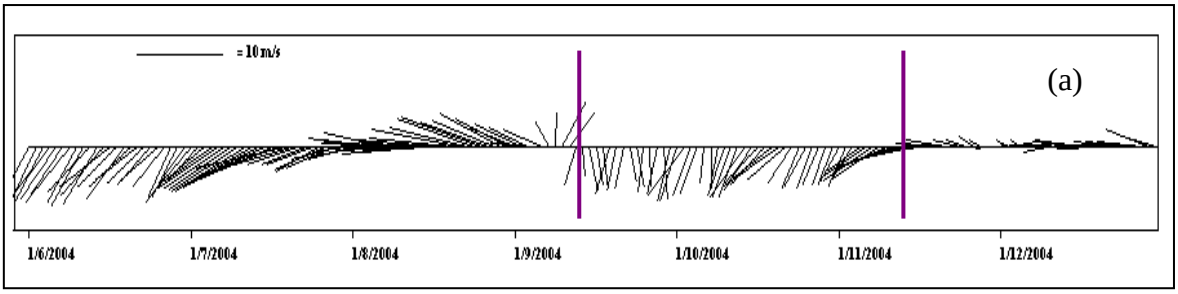

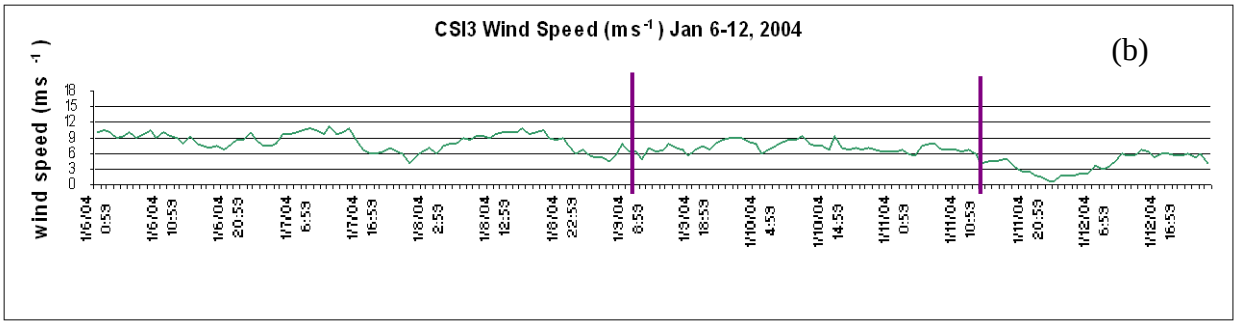

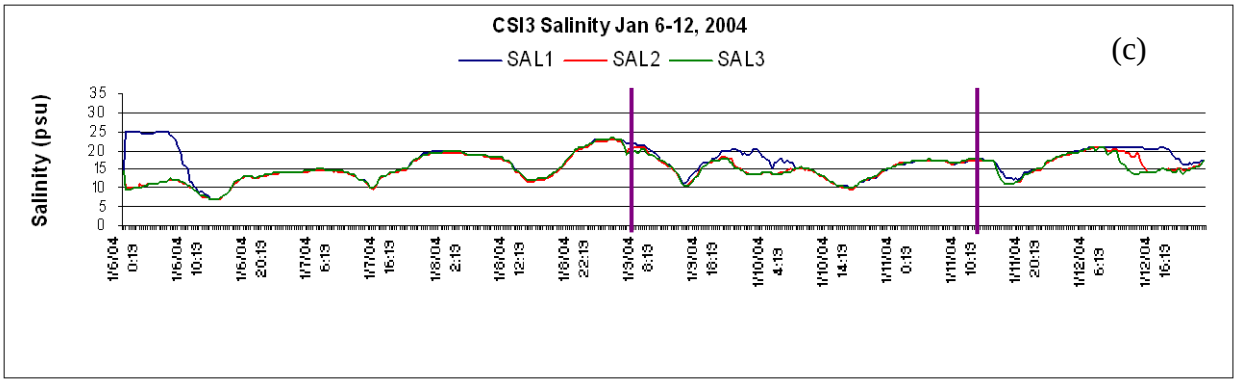

Figure 4.1 CSI-3 observations of winds and salinity during the week of January 6 – 12, 2004: (a) vector plot of wind direction and speed; (b) wind speed; (c) salinity at 1 meter from bottom (SAL1), 2 meters from bottom (SAL2), and 3 meters from bottom (SAL3). Purple lines mark boundary of winds with a northerly component, including the cold front passage and the subsequent cold air outbreak.

Figure 4.2 CSI-3 observations of waves and water level during the week of January 6 – 12, 2004: (a) significant wave height; (b) water depth; (c) water level variation (solid blue line) from nearby Eugene Island tidal prediction (dashed green line). Purple lines mark boundary of winds with a northerly component, including the cold front passage and the subsequent cold air outbreak.

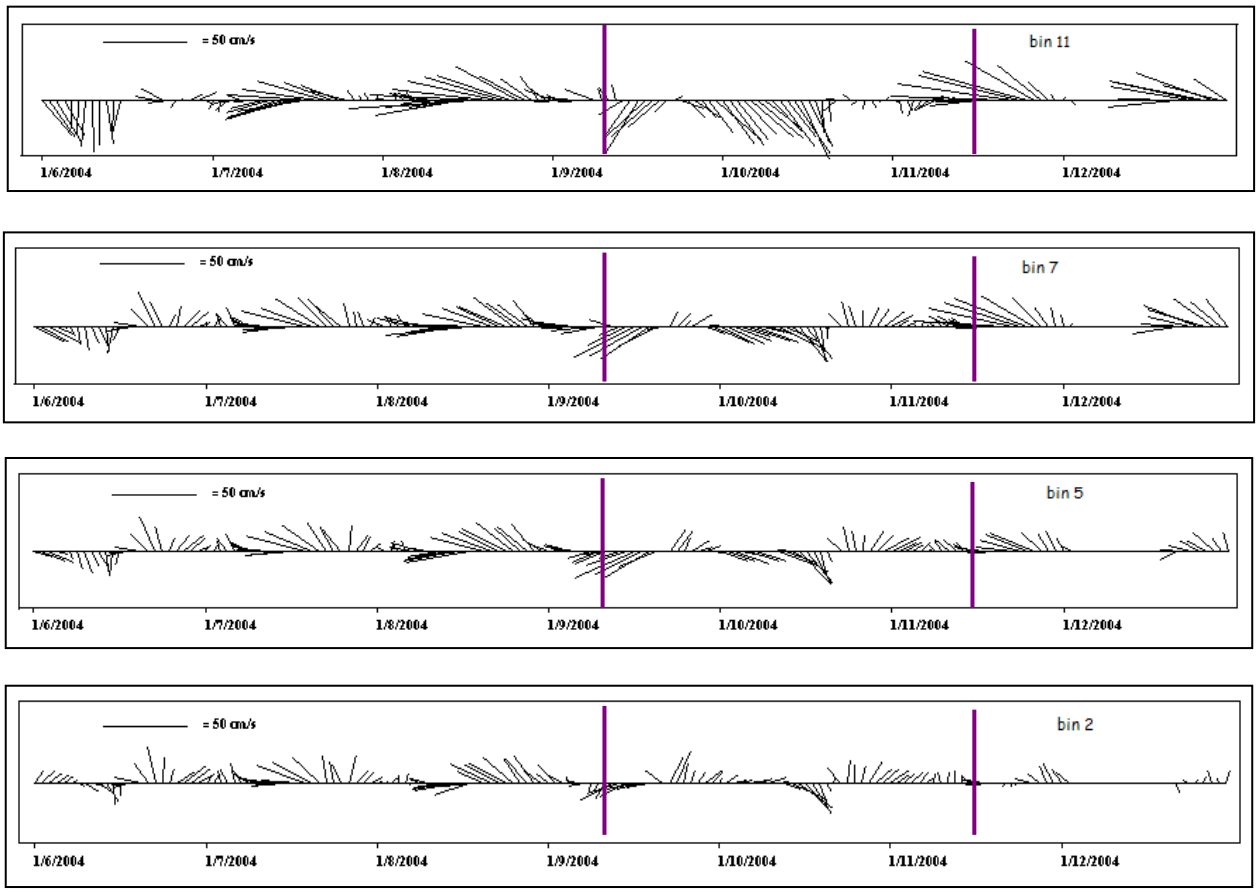

Figure 4.3 CSI-3 observations of currents during the week of January 6 – 12, 2004: vector plots of current direction and speed at various depths: bin 11 is ~ 4 m from the bottom (near surface); bin 7 is ~ 3 m from the bottom (mid-depth); bin 5 is ~ 2 m from the bottom (mid-depth); and bin 2 is ~ 1 m from the bottom. Purple lines mark boundary of winds with a northerly component, including the cold front passage and the subsequent cold air outbreak.

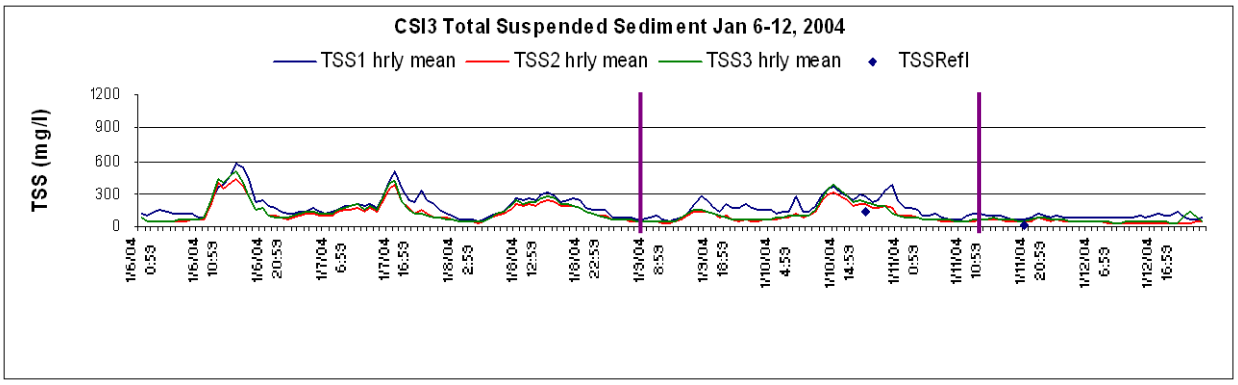

Figure 4.4 CSI-3 observations of total suspended sediment during the week of January 6 – 12, 2004: TSS at 1, 2 and 3 meters from the bottom (blue, red and green lines respectively), and at the surface plume (two dots).

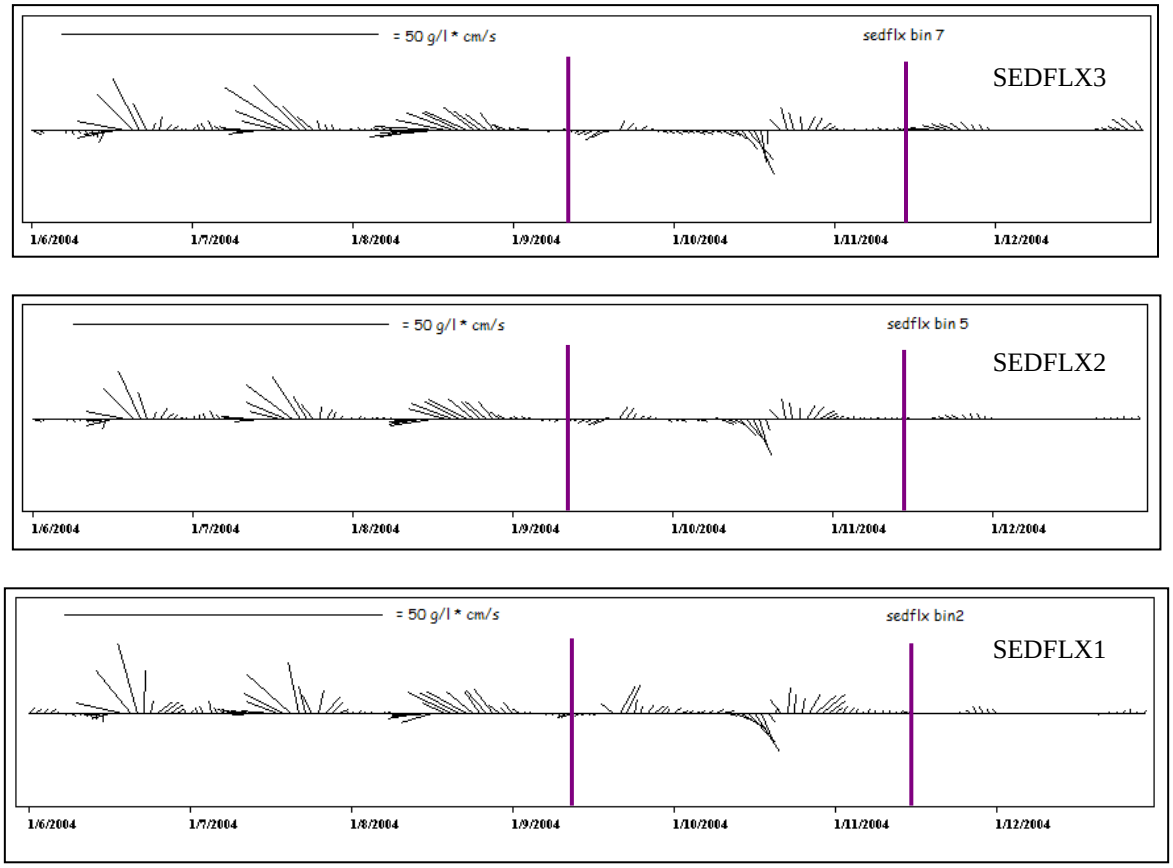

Figure 4.5 CSI-3 observations of sediment flux during the week of January 6 – 12, 2004: vector plots of sediment flux at various depths: SEDFLX3 is ~ 3 m from the bottom (mid-depth); SEDFLX2 is ~ 2 m from the bottom (mid-depth); and SEDFLX1 is ~ 1 m from the bottom. Purple lines mark boundary of winds with a northerly component, including the cold front passage and the subsequent cold air outbreak. Note: no sediment flux is calculated for bin 11 (near surface) since NTU was not available at that depth.

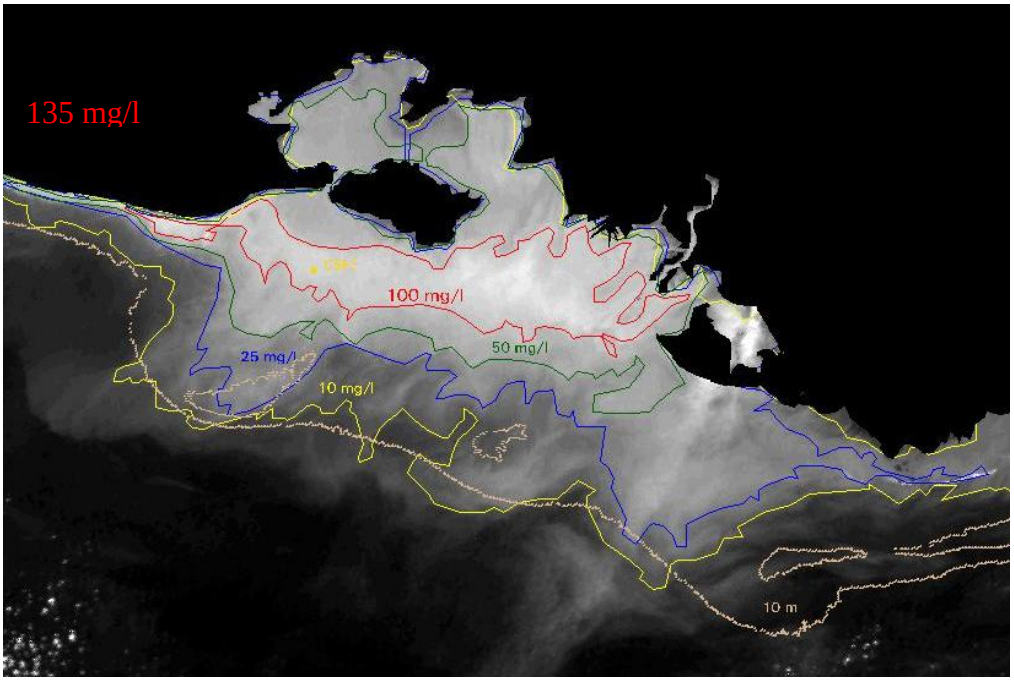

Figure 4.6 January 10, 2004 MODIS image showing location of CSI-3 on the inner shelf, having a satellite derived TSS of 135 mg/l in the surface plume during the post-front phase. Contour lines for surface TSS are 100 mg/l (red); 50 mg/l (green); 25 mg/l (blue); and 10 mg/l (yellow). The 10 m isobath contour is tan, as are the three 5 m shoals (tan polygons).

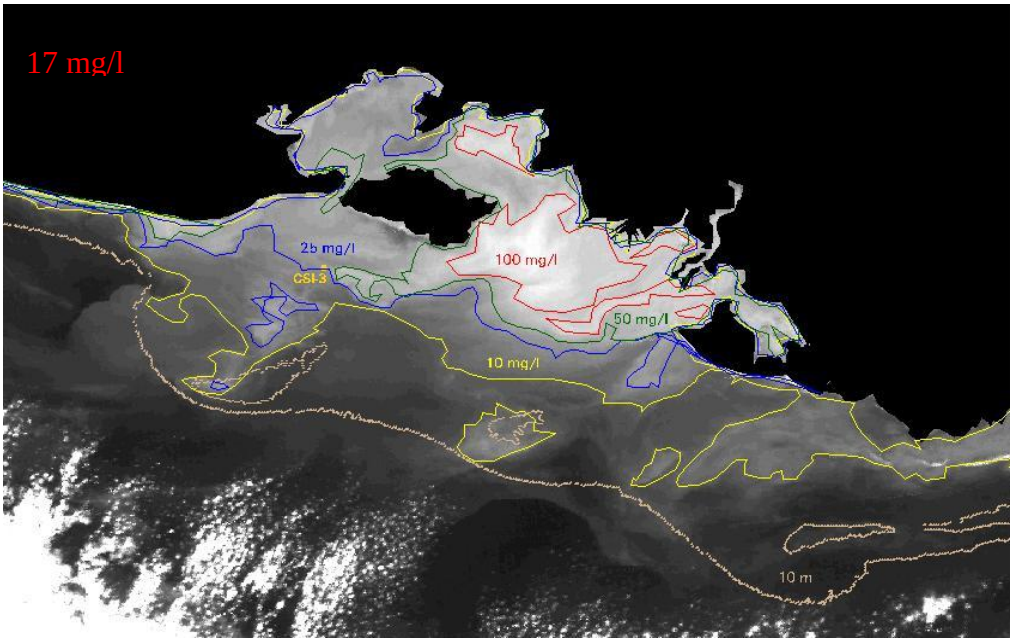

Figure 4.7 January 11, 2004 MODIS image showing location of CSI-3 on the inner shelf, having a satellite derived TSS of 17 mg/l in the surface plume during the inter-frontal phase. Contour lines for surface TSS are 100 mg/l (red); 50 mg/l (green); 25 mg/l (blue); and 10 mg/l (yellow). The 10 m isobath contour is tan, as are the three 5 m shoals (tan polygons).

4 2.2 January 16 – 22, 2004 Case Study Event

The second cold front under observation arrived as an Arctic air mass which pushed south from the Great Lakes region and encompassed the entire mid-section of the continental United States. The Atchafalaya River discharge had been steadily increasing since the first week of January, and had reached flow rates of 250,000 cfs (7,079 $m^3 s^{-1}$) to 290,000 cfs (8,212 $m^3 s^{-1}$) during the week of observation. Sediment concentrations upstream at two USGS stations had increased from seasonal autumn lows of less than 100 mg/l each to 214 mg/l (Simmesport, LA station ID: 07381490, on January 13, 2004) and 502 mg/l (Melville, LA station ID: 07381495, on January 14, 2004).

Pre-frontal conditions on January 16 and 17 consisted of S and SE winds at 7 – 10 ms^{-1}, rotating through SW and W winds at 4 – 10 ms^{-1} on January 17 and 18 (Figure 4.8 (a),(b)). During this period, water levels fluctuated in sync with the astronomical tidal prediction (Figure 4.9 (c)). On January 16, 2004, the water column was stratified with a surface lens of river water over CSI-3 (Figure 4.8 (c)). On January 17, the water column became fresher and well-mixed with river water at 5 - 7 psu due to strong southwesterly winds. On January 18, the water column once again developed a temporary stratification (Figure 4.8 (c)). SAL1 rose to 24 psu, SAL2 to 22 psu and SAL3 rose to 16 psu due to a higher salinity water mass advected in with the tide. During the pre-frontal period, the bottom meter current flowed onshore at ~ 17 cm s^{-1}, and at two meters from the bottom, onshore at ~ 20 - 40 cm s^{-1} (Figure 4.10), bringing higher salinity water toward shore. This state persisted until the northeasterly winds were well established on January 18 and the water level rose with the diurnal tide some 18 hours later. TSS1 in the pre-frontal period was ~ 150 mg/l and ~ 60 mg/l at TSS2 and TSS3 (Figure 4.11). Sediment flux was minimal in the pre-frontal and the early hours of the frontal passage phases (Figure 4.12).

The passage of the cold front on January 18, 2004 at 12:00 GMT, with increasing northwesterly and northerly winds to 11 m s^{-1}, forced water level set-down, overpowering and offsetting the rising astronomical tide by 0.4 m and then enhancing the next predicted low tide drop by 0.7 m (Figure 4.9 (c)). With the onset of post-front northwesterly winds, TSS1 spiked briefly to 366 mg/l. TSS also began to increase at the mid-depths while wind speeds were erratic, significant wave heights were moderate, and currents were weak. With the increasing northwesterly winds on January 19, sediment flux ranged from 8 to 22 g/l * cm/s offshore to the southeast. The rotation to northerly winds induced a water level set down to 3.8 m (Figure 4.9 (b)), rendered the uppermost ADCP measurements null (Figure 4.10 (bin 11)) and continued to suppress the water level below tidal prediction for another 24 hours. Significant wave height peaked at 0.6 m (Figure 4.9 (a)) then slowly decreased throughout the northerly component gradually decreasing winds, which lasted 53 hours. The water column became well-mixed at 15 - 20 psu and then dropped uniformly to 10 psu in response to the wind-forced water level set-down and discharge from the bays onto the shelf. Currents throughout the water column became offshore and southeastward at 50 – 60 cm s^{-1} sustained for about 12 hours. As the winds persisted from the north, TSS at all depths on January 19 climbed to 450 - 560 mg/l, concurrent with the water level set-down.

The second day post-front (January 19) was characterized by weakening northerly winds, strong enough to inhibit the water level increase from attaining the tidal inflow prediction by 0.3 m. Offshore currents (Figure 4.10) were also weakening, SE at ~ 15 cm s^{-1} in the bottom two meters and SE 20 – 50 cm s^{-1} in the upper levels. Salinity was 26 - 27 psu due to a higher salinity water mass, having no influence from river discharge, being advected in from the west. While the mid-depth's TSS tapered off gradually to pre-frontal levels, TSS1 peaked to 946 mg/l, then

stabilized in the following few hours. Since this peak occurred with the incoming tide and was short-lived, it was probably the advection of fluid mud from the west, concurrent with the higher salinity water influx noted. As the tidal flow shifted onshore, SEDFLX1 peaked to 25 g/l * cm/s to the northeast, corresponding with the brief TSS peak. Sediment flux dropped quickly throughout the water column when the winds changed to northeasterly and decreased in strength; although the direction of sediment flux alternated between SE and SW then SE, flux was only 1 – 3 g/l * cm/s until the storm abated.

The MODIS image for this event was acquired January 19, 2004 at 18:50 GMT, about 8 hours after the TSS peaks, during northerly (but decreasing) winds (Figure 4.13). TSS1 was 281 mg/l, but the surface TSS estimate was 100 mg/l, similar to the mid-depth values of 108 mg/l and 135 mg/l (TSS2 and TSS3 respectively). The maximum TSS in the mud-plume which extended over the CSI-3 location was 399 mg/l. The mud-plume (area: 2,268 km^2) filled Atchafalaya Bay, extended well downcoast seaward of the eastern Chenier Plain, and had a branch extending close to Trinity Shoal and another into West/East Cote Blanche Bays. The 50 mg/l contour (area: 4,709 km^2) filled Vermillion Bay and a western arm reached the Chenier Plain; an eastern lobe of the 50 mg/l contour extended to the Isles Dernieres, with a detached area over Ship Shoal. Both the 25 mg/l and the 10 mg/l eastern contours approached the boundary of Terrebonne Bay and over Ship Shoal. The 10 mg/l contour extended well beyond the 10 m isobath, with an area of 11,116 km^2.

Inter-frontal winds were ENE at 1 - 6 m s^{-1} from January 21 to 22 and currents flowed westward during this period, with tidal influences moderating onshore/offshore flow and water column stratification, which highlighted the flow from the bays most prominently in the upper water column. During this period, TSS and sediment flux were minimal at all depths.

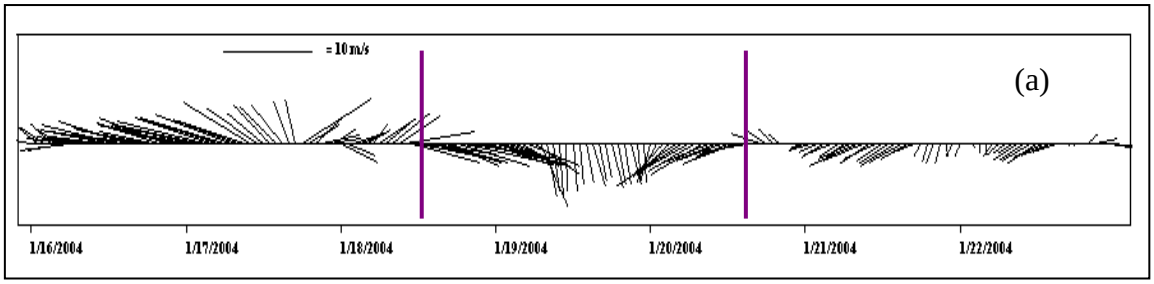

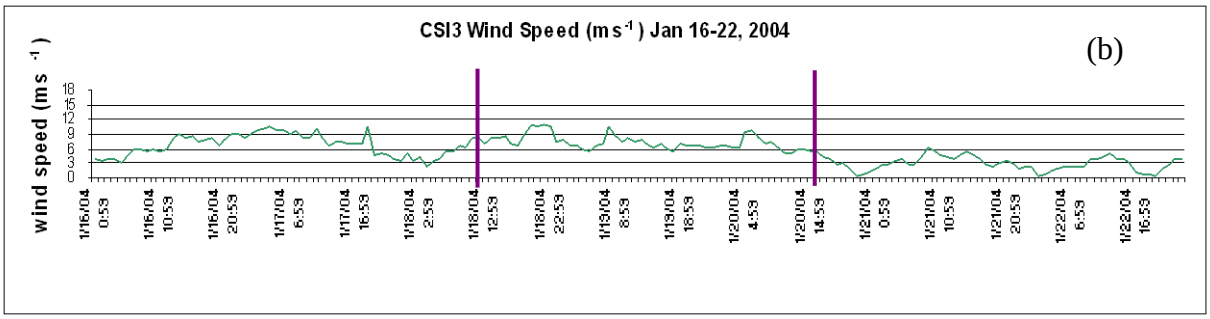

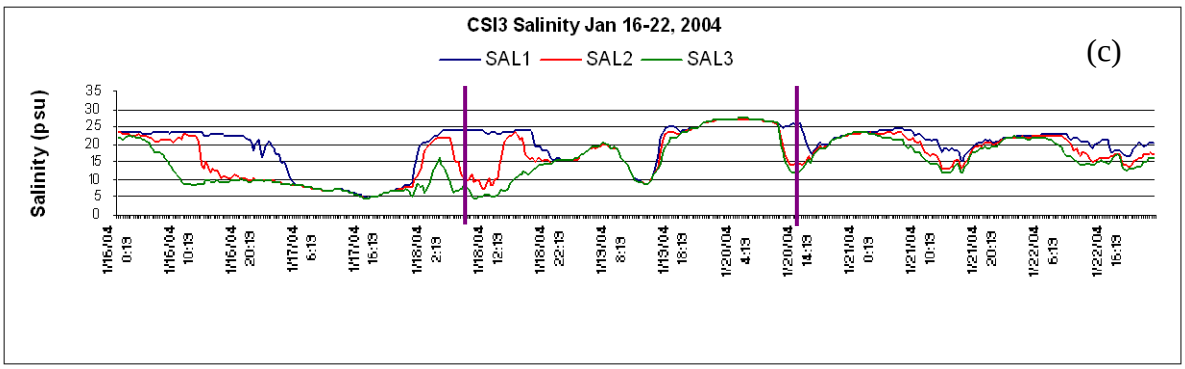

Figure 4.8 CSI-3 observations of winds and salinity during the week of January 16 – 22, 2004: (a) vector plot of wind direction and speed; (b) wind speed; (c) salinity at 1 meter from bottom (SAL1), 2 meters from bottom (SAL2), and 3 meters from bottom (SAL3). Purple lines mark boundary of winds with a northerly component, including the cold front passage and the subsequent cold air outbreak.

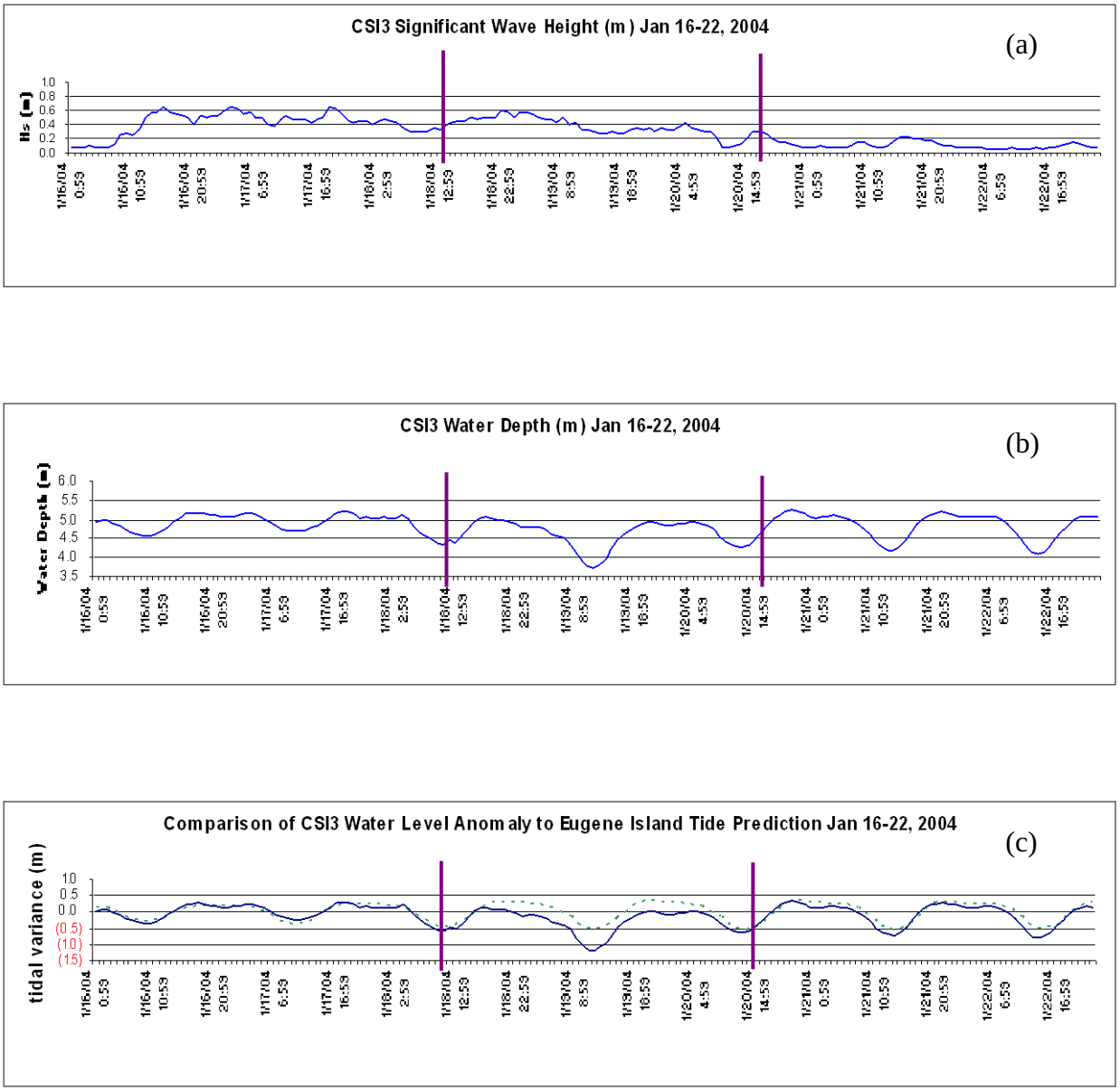

Figure 4.9 CSI-3 observations of waves and water level during the week of January 16 – 22, 2004: (a) significant wave height; (b) water depth; (c) water level variation (solid blue line) from nearby Eugene Island tidal prediction (dashed green line). Purple lines mark boundary of winds with a northerly component, including the cold front passage and the subsequent cold air outbreak.

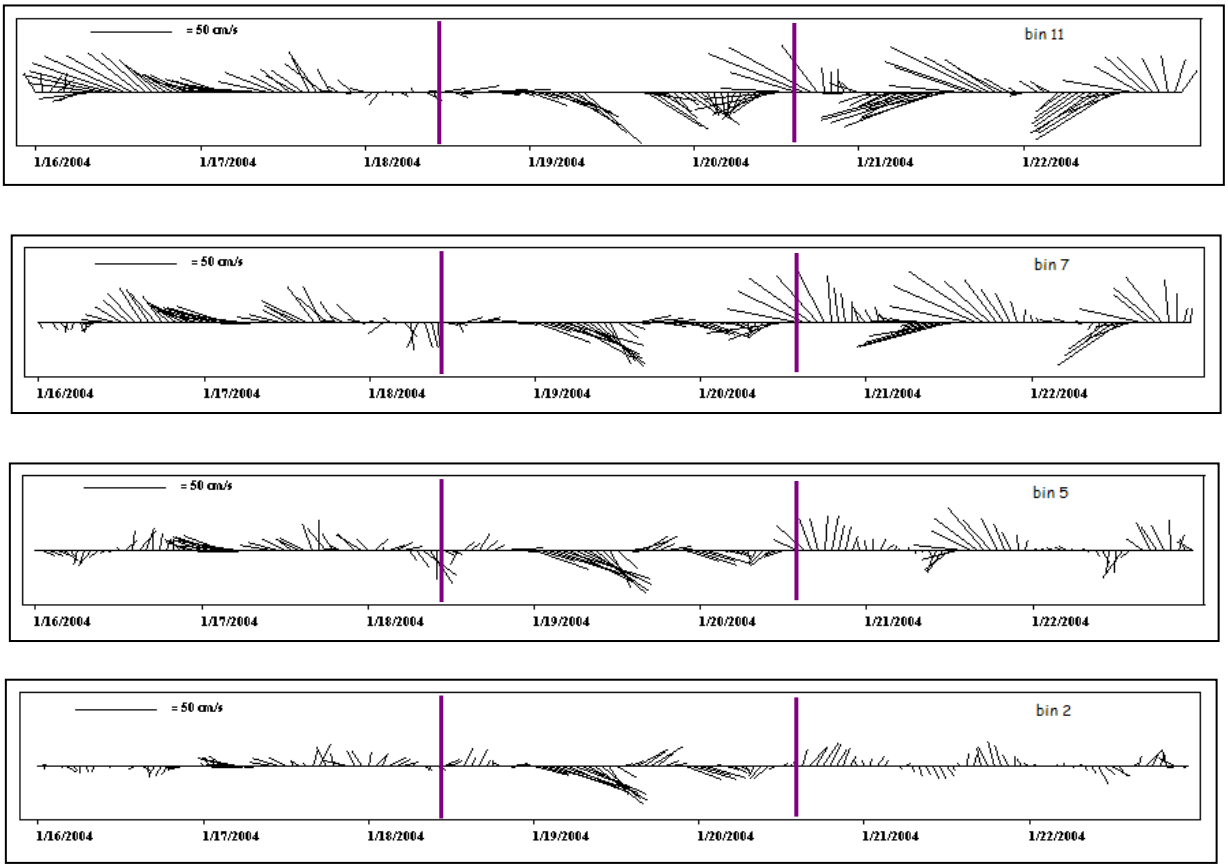

Figure 4.10 CSI-3 observations of currents during the week of January 16 – 22, 2004: vector plots of current direction and speed at various depths: bin 11 is ~ 4 m from the bottom (near surface); bin 7 is ~ 3 m from the bottom (mid-depth); bin 5 is ~ 2 m from the bottom (mid-depth); and bin 2 is ~ 1 m from the bottom. Purple lines mark boundary of winds with a northerly component, including the cold front passage and the subsequent cold air outbreak.

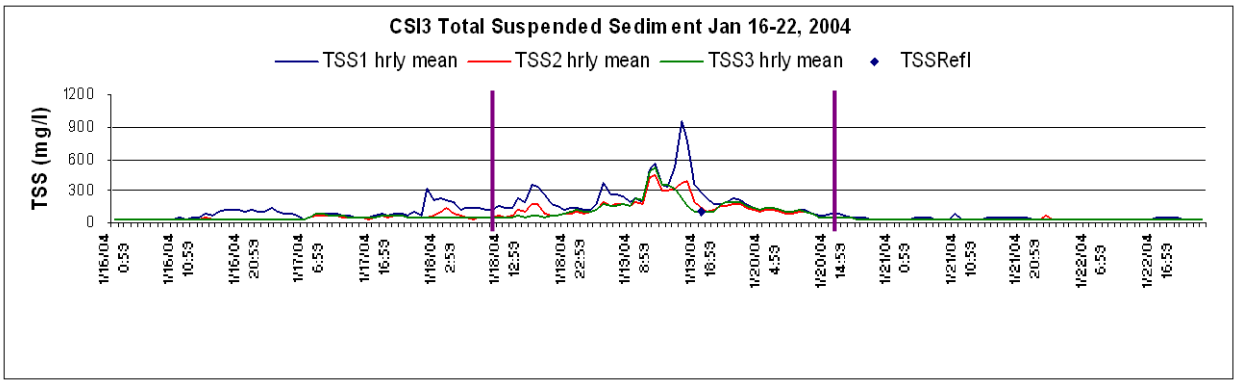

Figure 4.11 CSI-3 observations of total suspended sediment during the week of January 16 – 22, 2004: TSS at 1, 2 and 3 meters from the bottom (blue, red and green lines respectively), and at the surface plume (one dot).

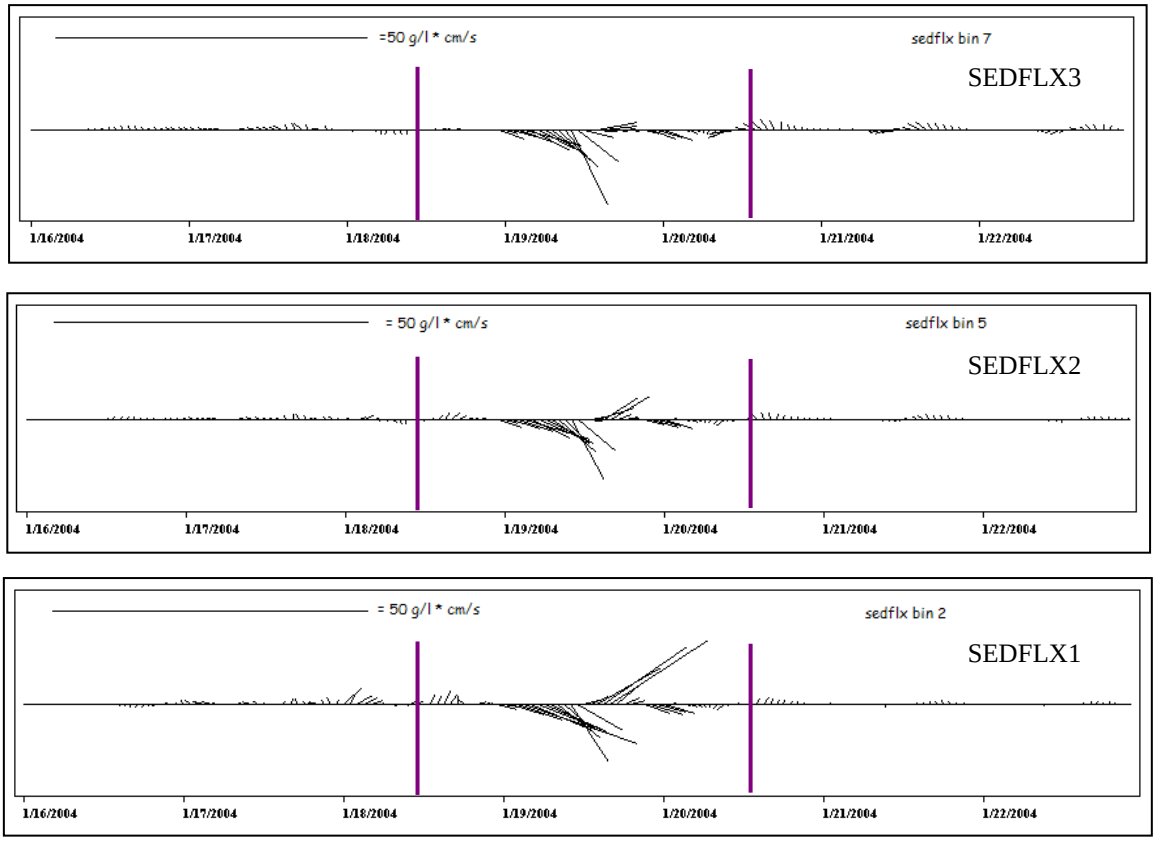

Figure 4.12 CSI-3 observations of sediment flux during the week of January 16 – 22, 2004: vector plots of sediment flux at various depths: SEDFLX3 is ~ 3 m from the bottom (mid-depth); SEDFLX2 is ~ 2 m from the bottom (mid-depth); and SEDFLX1 is ~ 1 m from the bottom. Purple lines mark boundary of winds with a northerly component, including the cold front passage and the subsequent cold air outbreak. Note: no sediment flux is calculated for bin 11 (near surface) since NTU was not available at that depth.

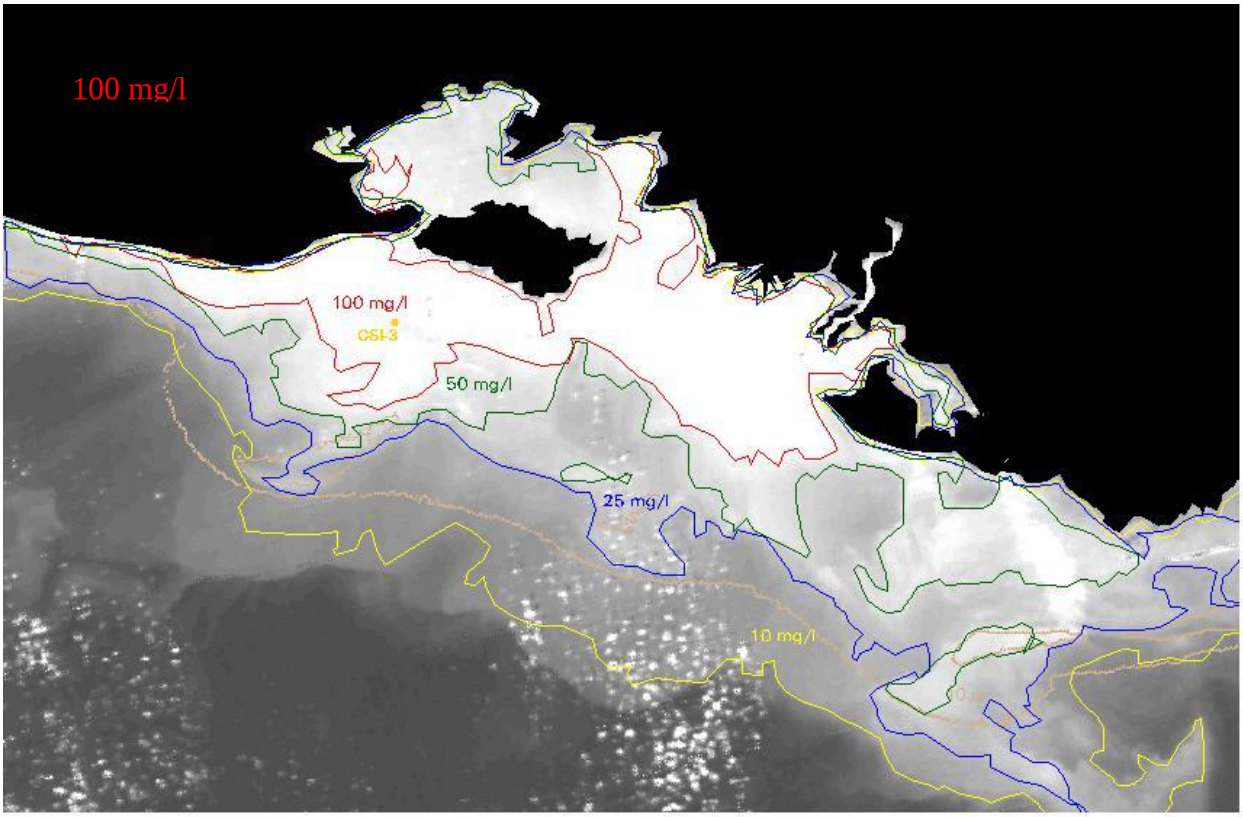

Figure 4.13 January 19, 2004 MODIS image showing location of CSI-3 on the inner shelf, having a satellite derived TSS of 100 mg/l in the surface plume during the post-front phase. Contour lines for surface TSS are 100 mg/l (red); 50 mg/l (green); 25 mg/l (blue); and 10 mg/l (yellow). The 10 m isobath contour is tan, as are the three 5 m shoals (tan polygons).

4.2.3 January 24 – 30, 2004 Case Study Event

During the third week of January, the Atchafalaya River discharge rate increased from 290,000 cfs (8,212 $m^3 s^{-1}$) to 320,000 cfs (9,061 $m^3 s^{-1}$) on January 26, 2004. The upstream Melville, LA USGS station (ID 07381495) showed increases in sediment concentration from 502 mg/l on January 14, 2004 to 968 mg/l on January 28, 2004, having the highest river TSS of the events studied. Thus, the steady increases in river discharge and in sediment concentration increased the volume of sediments available for delivery and resuspension in the bays and on the inner shelf. This was not the highest discharge rate for the flood season (390,000 cfs (11,044 $m^3 s^{-1}$) in March 2004), and this season had the lowest peak of the five year period 2001 – 2005 (Figure 2.6). The frontal passage approached from the west, out of Texas.

Pre-frontal winds on January 24 were moderate southerly and southwesterly winds 11 m s^{-1} decreasing to 1 m s^{-1} by January 26 (Figure 4.14 (a),(b)). Water levels (Figure 4.15(b)) were in agreement with tidal prediction level (Figure 4.15 (c)) from January 24 - 26. The water column showed weak stratification between 15 - 20 psu (Figure 4.14 (c)) and significant wave heights decreased from 0.6 m to 0.2 m between January 24 – 26 Figure 4.15 (a)). Currents were variable at all depths (Figure 4.16). TSS fluctuated generally between 40 to 80 mg/l in the mid-depths for several days (Figure 4.17). TSS at the bottom was much higher and demonstrated several peaks, the first of which reached 646 mg/l, probably in response to a tidal water level low and brief ebb-tide flow at ~ 35 cm s^{-1}. A second peak of 573 mg/l occurred as the reversal to an onshore current was returning higher salinity water toward shore. Several smaller bottom peaks of 250 to 360 mg/l occurred as variable winds shifted SW and W. Since significant wave heights were decreasing, the peaks do not appear to be wave-induced resuspension, but rather advection from nearshore fluid mud accumulations in response to bottom currents up to 34 cm s^{-1}. In spite

of the frequent TSS peaks at the bottom, sediment flux in the water column (Figure 4.18) was minimal during the pre-frontal period.

The rotation of the wind direction from southeasterly to northwesterly on January 27, 2004 at 3:00 GMT was coupled with wind speed increases to 15 m s^{-1} with frontal passage. Post-front water level set-down (to 4.14 m) dropped beyond the tidal prediction by 0.7 – 0.8 m, once again thwarting ADCP measurements at the surface. Significant wave heights more than doubled to 0.55 m and currents flowed offshore and southeastward at 40 to 60 cm s^{-1} throughout the water column. The water column became well-mixed by mid-day on January 27 and remained well-mixed even while salinity rose steadily from 10 psu to 25 psu, probably due to advection of higher salinity waters from the west. As the wind speeds relaxed (6 – 9 m s^{-1}) in the second 12 hrs post-front, significant wave heights decreased to 0.3 to 0.4 m, and water levels rose slightly to 4.5 to 4.8 m, still below the mean MSL (4.92 m) and the tidal prediction level. The northerly winds maintained offshore southeastward currents: 35 to 40 cm s^{-1} at the bottom and 37 to 50 cm s^{-1} in the mid-depths. The total duration of northerly component winds for this storm was 41 hours. TSS responded with steady increases at all depths in the first 12 hours post-front: the bottom reached a maximum of 560 mg/l, and then soon after decreased to values close to the mid-depths maxima of 396 to 421 mg/l. Sediment flux responses to the moderate but steady TSS increase were rapid, from 2 to 20 g/l * cm/s over the first 12 hours post-front at all depths. Once the northerly wind speeds began decreasing, the TSS levels decreased uniformly at mid- and bottom depths. The sediment flux response to decreasing wind speed and TSS was rapid, decreasing to 2 – 4 g/l * cm/s in the subsequent 4 hours and remained at this rate well into the inter-frontal phase.

The first MODIS image was acquired on January 27, 2004 at 19:40 GMT; about 16 hours post-front (Figure 4.19). The satellite derived surface TSS at CSI-3 was 117 mg/l, considerably less than the near-bottom concentrations values of ~ 300 mg/l in the water column. The maximum TSS in the mud-plume which extended over the CSI-3 location was 427 mg/l. The mud-plume (100+ mg/l) (area: 2,542) was the largest of all the days examined; it filled Atchafalaya Bay, Fourleague Bay, East Cote Blanche Bay and about half of West Cote Blanche Bay. An extension of the mud-plume passed Marsh Island downcoast and extended westward, to the entire Chenier Plain coastline. The mud-plume also had an easterly lobe which included most of the length of Point au Fer Island. The 50 mg/l contour (area: 5,064 km^2) extended westward to the Chenier Plain coast and eastward beyond Point au Fer Island. There were also a number of detached 50 mg/l areas close to the 10 m isobath, often found in close proximity to the offshore shoals. The 25 mg/l (area: 8,724 km^2) and 10 mg/l (area: 10,763 km^2) contours extended beyond the 10 m isobath for most of their contour lengths; both extended southeastward to include the Isles Dernieres and Ship Shoal.

The second MODIS image (Figure 4.20) was acquired on January 28, 2004 at 18:45 GMT; near the end of the cold air outbreak event as NE winds were in decline. The satellite derived TSS of the surface plume was 86 mg/l, comparable to the 60 - 75 mg/l levels in the waters below. The maximum TSS in the mud-plume (to the east of CSI-3) was 722 mg/l. The mud-plume had lost its westward extension seaward of Marsh Island to the Chenier Plain coast and the eastern lobe had regressed from to the tip of Point au Fer; it now covered 67% of the area it had the previous day (1,698 km^2). The 50 mg/l and 25 mg/l showed similar losses, but the 10mg/l contour retained its position beyond the 10 m isobath along its eastern length and still held 82% of the previous day's coverage area (8,841 km^2) including over the shoals.

The inter-frontal period January 29 and 30 was dominated by moderate to strong easterly winds from 3 - 12 m s^{-1} which raised significant wave heights to 0.5 - 0.7 m. Water level fluctuation during this period was minimal, within 0.2 m of the mean, matching the tidal prediction. Strong westward /northwestward current flow dominated (20 – 60 cm s^{-1}), but sediment flux was negligible since sediments had already dropped out of suspension.

4.2.4 March 30 to April 5, 2005 Case Study Event

The fourth cold front passage analyzed approached from the Rocky Mountain region. Atchafalaya River discharge rates had already peaked at a 5 year high on February 2, 2005 at 527,000 cfs (14,923 m^3 s^{-1}) and had decreased to between 190,000 cfs (5,380 m^3 s^{-1}) and 220,000 cfs (6,230 m^3 s^{-1}). Upstream, sediment concentrations slowly increased between March 21 and April 13: at the USGS Simmesport, LA station (ID 07381490) from 151 – 223 mg/l and at the USGS Melville, LA station (ID 07381495) from 69 - 164 mg/l.

Pre-frontal winds ranged from 2 – 7 m s^{-1} from the south/southeast (Figure 4.21 (a),(b)), but the wind speeds were variable so that significant wave heights were decreasing overall from 0.6 m to 0.2 m from March 30 to April 1 (Figure 4.22 (a)). Currents flowed northwest at 12 – 51 cm s^{-1} in the upper water column and 1 – 27 cm s^{-1} at the bottom, with only slight decreases to the onshore flow due to tidal fluctuation (Figure 4.23). Water levels matched the tidal prediction very well (Figure 4.22 (c)), and water level remained above 4.5 m (Figure 4.22 (b)). The water column was generally well-mixed by the southerly winds, with salinity at 25 – 29 psu, but surface water salinity temporarily dipped 5 psu further below the overall pattern with ebb-tides (Figure 4.21 (c)). In two days, the entire water column showed a progressive drop to 12 psu as currents turned more westward, drawing fresher river water toward CSI-3.

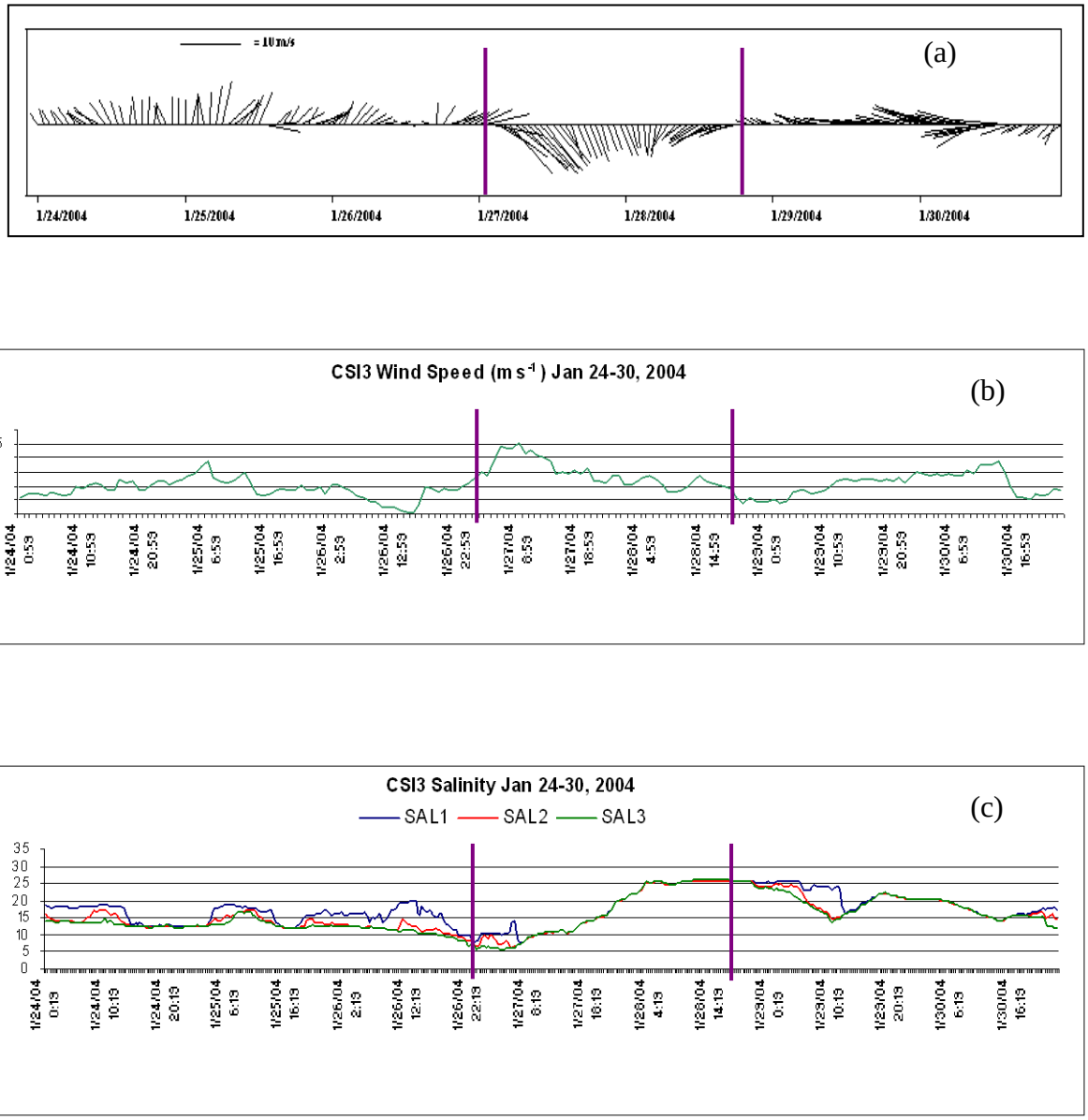

Figure 4.14 CSI-3 observations of winds and salinity during the week of January 24 – 30, 2004: (a) vector plot of wind direction and speed; (b) wind speed; (c) salinity at 1 meter from bottom (SAL1), 2 meters from bottom (SAL2), and 3 meters from bottom (SAL3). Purple lines mark boundary of winds with a northerly component, including the cold front passage and the subsequent cold air outbreak.

Figure 4.15 CSI-3 observations of waves and water level during the week of January 24 – 30, 2004: (a) significant wave height; (b) water depth; (c) water level variation (solid blue line) from nearby Eugene Island tidal prediction (dashed green line). Purple lines mark boundary of winds with a northerly component, including the cold front passage and the subsequent cold air outbreak.

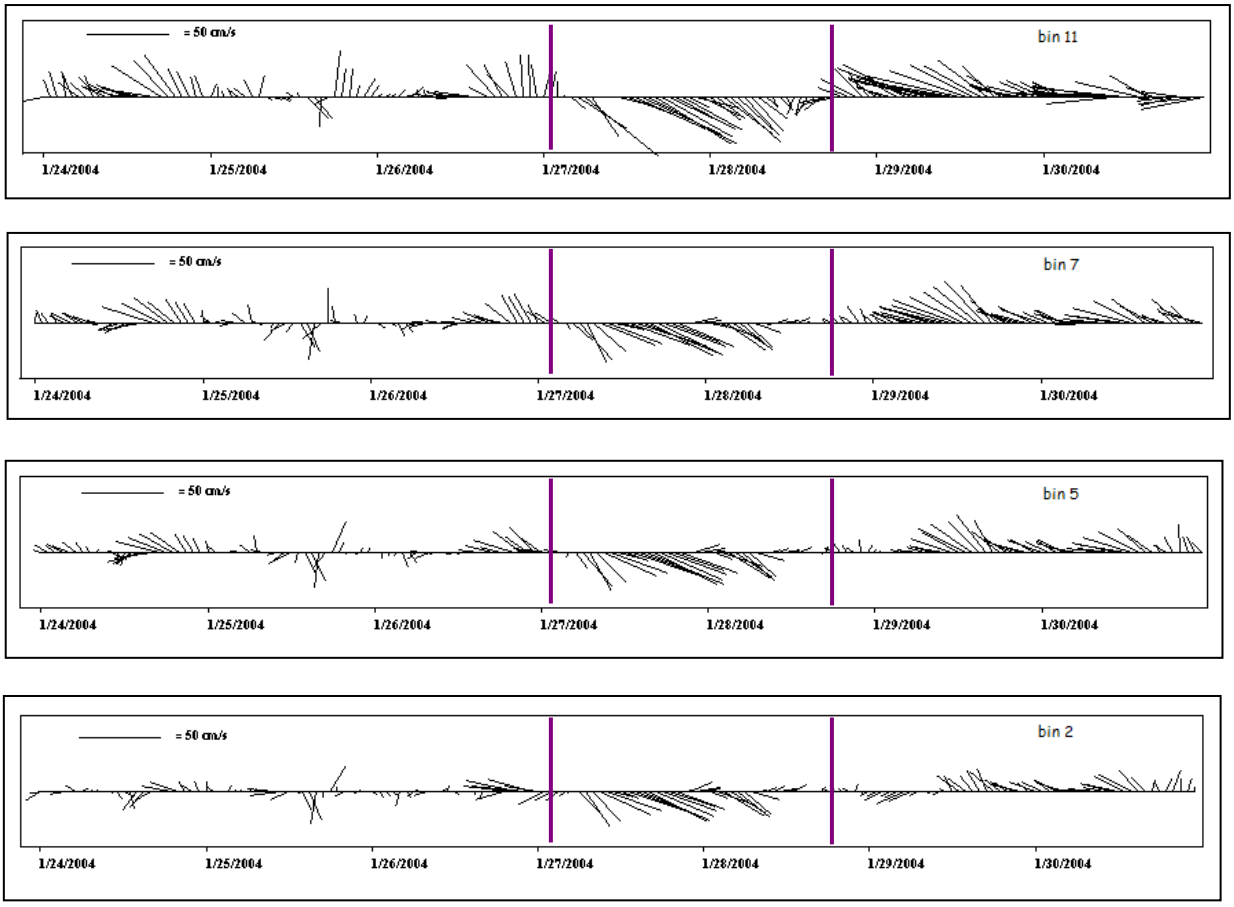

Figure 4.16 CSI-3 observations of currents during the week of January 24 – 30, 2004: vector plots of current direction and speed at various depths: bin 11 is ~ 4 m from the bottom (near surface); bin 7 is ~ 3 m from the bottom (mid-depth); bin 5 is ~ 2 m from the bottom (mid-depth); and bin 2 is ~ 1 m from the bottom. Purple lines mark boundary of winds with a northerly component, including the cold front passage and the subsequent cold air outbreak.

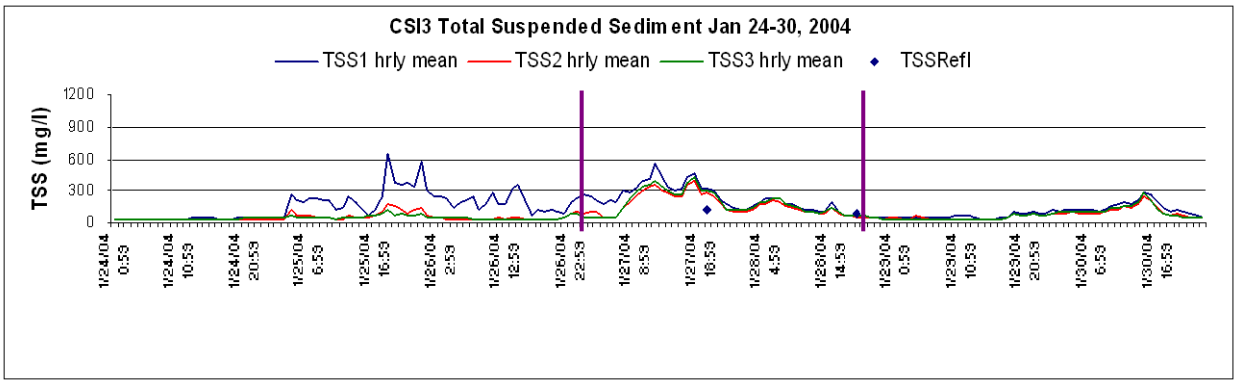

Figure 4.17 CSI-3 observations of total suspended sediment during the week of January 24 – 30, 2004: TSS at 1, 2 and 3 meters from the bottom (blue, red and green lines respectively), and at the surface plume (two dots).

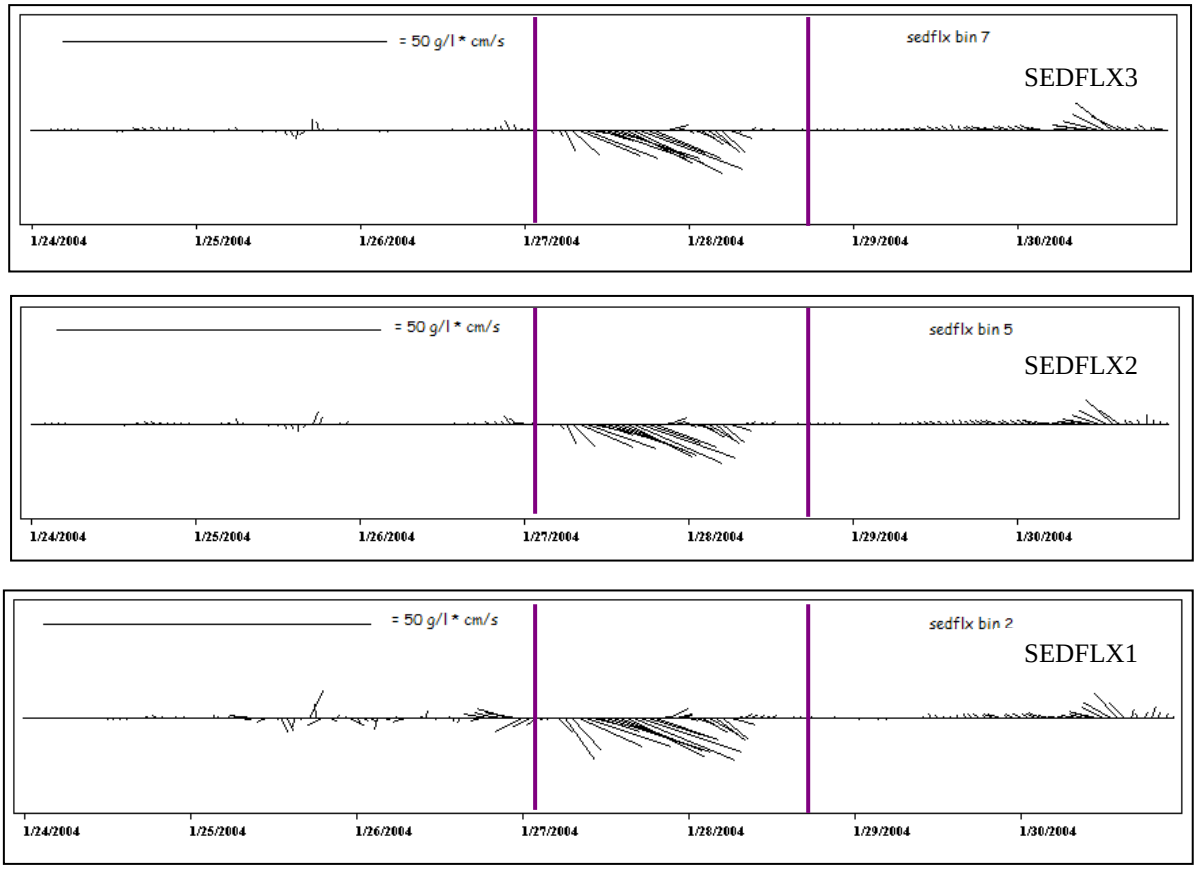

Figure 4.18 CSI-3 observations of sediment flux during the week of January 24 – 30, 2004: vector plots of sediment flux at various depths: SEDFLX3 is ~ 3 m from the bottom (mid-depth); SEDFLX2 is ~ 2 m from the bottom (mid-depth); and SEDFLX1 is ~ 1 m from the bottom. Purple lines mark boundary of winds with a northerly component, including the cold front passage and the subsequent cold air outbreak. Note: no sediment flux is calculated for bin 11 (near surface) since NTU was not available at that depth.

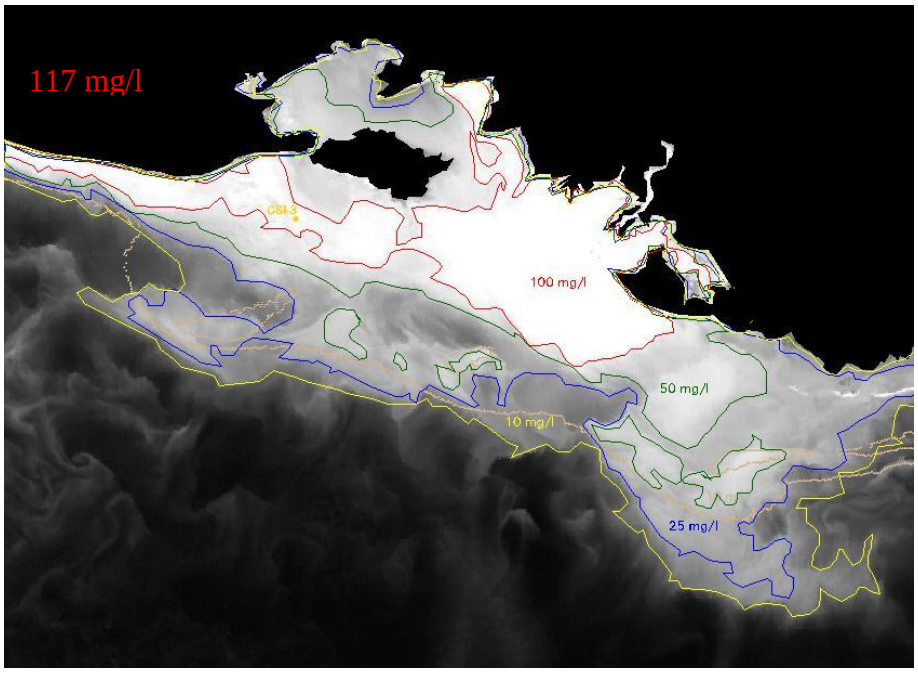

Figure 4.19 January 27, 2004 MODIS image showing location of CSI-3 on the inner shelf, having a satellite derived TSS of 117 mg/l in the surface plume during the post-front phase. Contour lines for surface TSS are 100 mg/l (red); 50 mg/l (green); 25 mg/l (blue); and 10 mg/l (yellow). The 10 m isobath contour is tan, as are the three 5 m shoals (tan polygons).

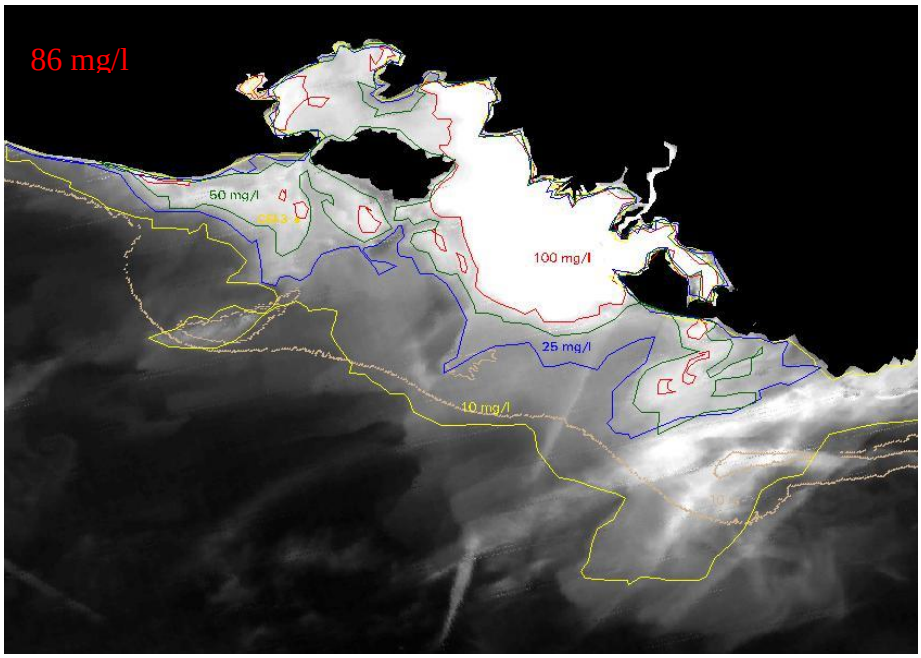

Figure 4.20 January 28, 2004 MODIS image showing location of CSI-3 on the inner shelf, having a satellite derived TSS of 86 mg/l in the surface plume during the post-front phase. Contour lines for surface TSS are 100 mg/l (red); 50 mg/l (green); 25 mg/l (blue); and 10 mg/l (yellow). The 10 m isobath contour is tan, as are the three 5 m shoals (tan polygons).

The NTU3 sensor was not functioning due to bio-fouling during this period; therefore, TSS3 could not be calculated at this depth (Figure 4.24). Sediment concentrations showed sustained elevated levels in the pre-frontal phase: TSS2 at ~ 100 to 200 mg/l and TSS1 at ~ 200 to 300 mg/l (Figure 4.26). It appears that these elevations were not responses to a particular meteorological event, excessive current speed, or tidal fluctuation, but may have been the cumulative result of overall river discharge and sediment availability over the entire flood season.

There was a radical but short-lived peak at TSS1 to 1,141 mg/l and at TSS2 to 428 mg/l, which occurred during the pre-frontal period on March 30 which lasted only 3 hours. There are no meteorological or oceanographic indicators for this spike; it is assumed that the cause was an anthropogenic or biological disturbance, perhaps by a boat or a school of fish. A second, lesser peak at TSS1 of 524 mg/l occurred on March 31 to which the TSS2 sensor showed no similar peak . The current at the bottom meter had been onshore at 15 – 33 cm s^{-1} with the incoming tide, which may have temporarily caused a resuspension event. A comparison of the TSS1 at CSI-3 (inner shelf) with CSI-14 (East Cote Blanche Bay) during the pre-frontal period shows bay values consistently low (~ 50 mg/l) in contrast to the erratic peaks which occur on the shelf (Figure 4.25).

SEDFLX3 could not be calculated due to missing TSS3 data. SEDFLX1 and SEDFLX2 transport was generally westward and northwestward at 2 – 8 g/l * cm/s. Sediment flux demonstrated little variation in response to the TSS peaks at either depth; relatively low current speeds and the short-duration of high resuspension concentrations prevented marked increases in transport.

The frontal passage on April 1 at 12:00 GMT caused dramatic changes on the inner shelf at CSI-3. The winds rotated from westerly at 5 m s^{-1} to northwesterly and doubled in speed to 10 m s^{-1} in 3 hours time. Winds strengthened to 16.5 m s^{-1}, driving significant wave heights to 0.7 m and forcing the water level set-down to 3.7 m depth, which was 0.7 m lower than the tidal prediction. Total duration of northerly component winds was 51 hours. The water column became well-mixed from 13 - 17 psu as a very strong offshore southeastward flow ensued (from both the winds and the outgoing tide) at 60 – 98 cm s^{-1}. As water depths rebounded with the incoming tide on April 2 - 3, the water column remained well-mixed but became very saline at 31 psu.

TSS1 spiked again to 1,143 mg/l for a few hours, this time apparently due to wind/wave forcing. Although TSS1 values decreased, they were maintained at 270 – 550 mg/l for the next 21 hours. TSS2 was 300 – 600 mg/l and sustained for 18 hours. The TSS peaks which occurred in the lower half of the water column coincided with 1) the initial swift increase in wind speed and wind direction rotation, and 2) the water level set-down concurrent with low tide. Sediment flux in the lower half of the water column this first day post-front was 20 - 30 g/l * cm/s offshore and southeastward for 9 hours, representing the highest rate for the longest period of time for all of the cold front events examined. The first MODIS image was acquired on April 1, 2005 at 19:50 GMT, about 7 hours into the frontal phase (Figure 4.27). Although the lower water column at CSI-3 demonstrated strong resuspension, the satellite derived surface TSS was only 64 mg/l, showing that the surface was unaffected by the resuspension from the depths below. The maximum TSS in the surface waters was 142 mg/l, but the three isolated areas of 100+ mg/l at the surface (area: 176 km^2) could not be designated as a mud-plume from the river mouth; these patches were probably due to resuspension from strong winds in the early post-front hours. The

remainder of the bays and the bordering eastern/western regions (area: 3,204 km ^{2}) had surface SSC of 50 mg/l, with the 25mg/l contour tightly beside it. The 10 mg/l contour was generally confined along the 5 m isobath, except that it had extensions over the shoals.

The second 24 hours post-front (April 2 - 3, 2005) was calmer, with winds northerly , then turning westerly at 3 – 8 m s^{-1}, significant wave heights were moderate at 0.2 – 0.4 m and the incoming tide brought seawater to the inner shelf (32 - 33 psu). The northerly winds were still able to slightly suppress the water level from reaching the tidal prediction level by a small margin, about 0.2 m. As the saline waters intruded, the winds were strong enough to keep the water column well-mixed throughout the post-front period. Currents continued offshore and southeastward but weakened to 10 -50 cm $s^{-1.}$ Total suspended sediment at TSS1 and TSS2 leveled off, remaining between 125 – 300 mg/l, and sediment flux diminished rapidly to 1 - 14 g/l * cm/s offshore and southeastward. The second MODIS image was obtained on April 2, 2005 at 18:55 GMT (Figure 4.28). The satellite derived surface TSS was 61 mg/l, not reflecting the resuspension in the water column beneath and far from the mud-plume (area: 1,416 km^2) which now dominated the surface waters in the bays. The maximum TSS in the mud-plume was 482 mg/l. The 50 mg/l contour (area: 3,686 km^2) extended seaward of the bays and the eastern Chenier Plain coast. The 10 mg/l contour approached the 10 m isobath for most of its length, maintaining position over the shoals as it had the previous day.

The inter-frontal period began on April 3 with southerly winds at 2 –5 m s^{-1}, significant wave heights < 0.2 m, and water levels in sync with tidal prediction. The high salinity water mass (30 psu) remained well-mixed and current direction varied from weakly onshore to offshore: 6 – 21 cm s^{-1}. During this time, TSS2 was ~ 100 mg/l, but TSS1 appeared very sensitive to minor changes in current direction from the tides (especially at low water),

exhibiting a range of values from 70 – 580 mg/l over 24 hours. In spite of these variations, sediment flux remained low at 1 – 6 g/l * cm/s. On April 5, downcoast westward flow was re-established by increasing SE winds at 6 - 9 m s^{-1} and a corresponding rise in significant wave heights to 0.7 m. Fresher river water flowed from the east, and salinity decreased to 20 psu. As wind speeds and wave heights varied, TSS2 and SEDFLX2 changed accordingly, ranging from 2 – 30 g/l * cm/s. TSS1 was still elevated at 200 – 750 mg/l, but SEDFLX1 remained moderate at 12 g/l * cm/s. The third MODIS image was obtained on April 3, 2005 at 19:40 GMT, about 7 hours after the shift to southerly winds (Figure 4.29). Over the study region, surface sediments had fallen out of suspension on most of the inner shelf and at CSI-3, the satellite derived surface TSS was 13 mg/l. With clearer water moving into the bays, all plume contours decreased in area by 44 - 75% and the mud-plume was restricted to a "tongue" along a NW to SE axis from within the bays to Point au Fer Island (Moeller et al, 1993; Walker and Hammack, 2000). The maximum TSS in the mud-plume was 324 mg/l.

4.2.5 April 20 - 26, 2005 Case Study Event

The final winter storm observed was caused by an Artic air mass which encompassed the mid-continental U.S. The Atchafalaya River discharge had been increasing in the intervening weeks, up from ~ 220,000 (6,230 m^3 s^{-1}) to reach 340,000 cfs (9,628 m^3 s^{-1}) as this cold front approached. Upstream sediment discharge rates were 223 mg/l (USGS Simmesport, LA station ID 07381490) and 164 mg/l (USGS Melville, LA station ID 0381495) in the week prior to the cold front, and were declining slowly.

One of the most prominent features of the pre-frontal period from April 20 – 22 was the evidence of the neap tide in the water level signal; the fluctuation around the mean water level was very small (Figure 4.31 (b)). This left the currents even more responsive to southeasterly and

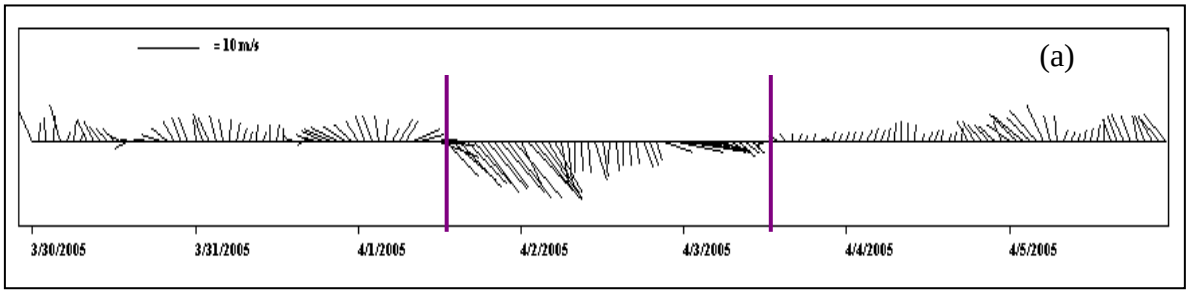

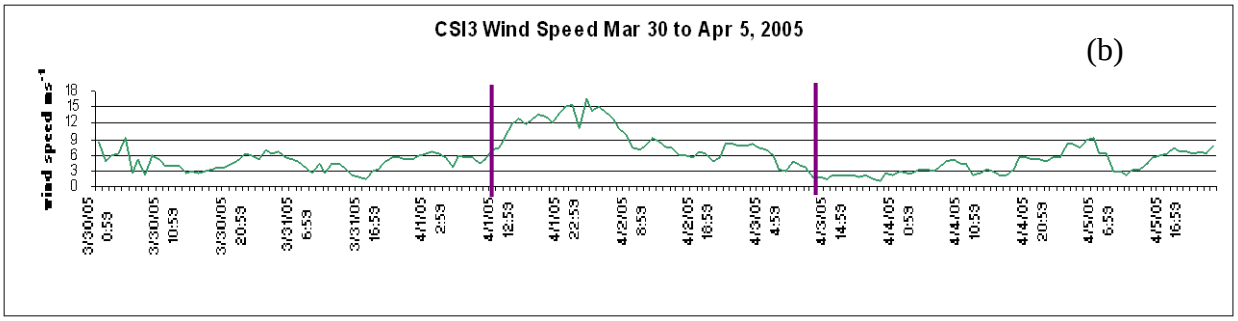

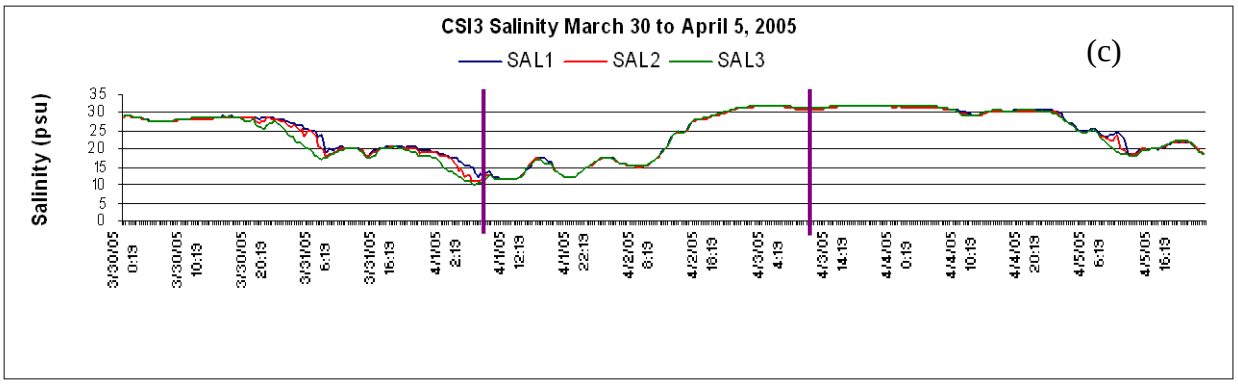

Figure 4.21 CSI-3 observations of winds and salinity during the week of March 30 – April 5, 2005: (a) vector plot of wind direction and speed; (b) wind speed; (c) salinity at 1 meter from bottom (SAL1), 2 meters from bottom (SAL2), and 3 meters from bottom (SAL3). Purple lines mark boundary of winds with a northerly component, including the cold front passage and the subsequent cold air outbreak.

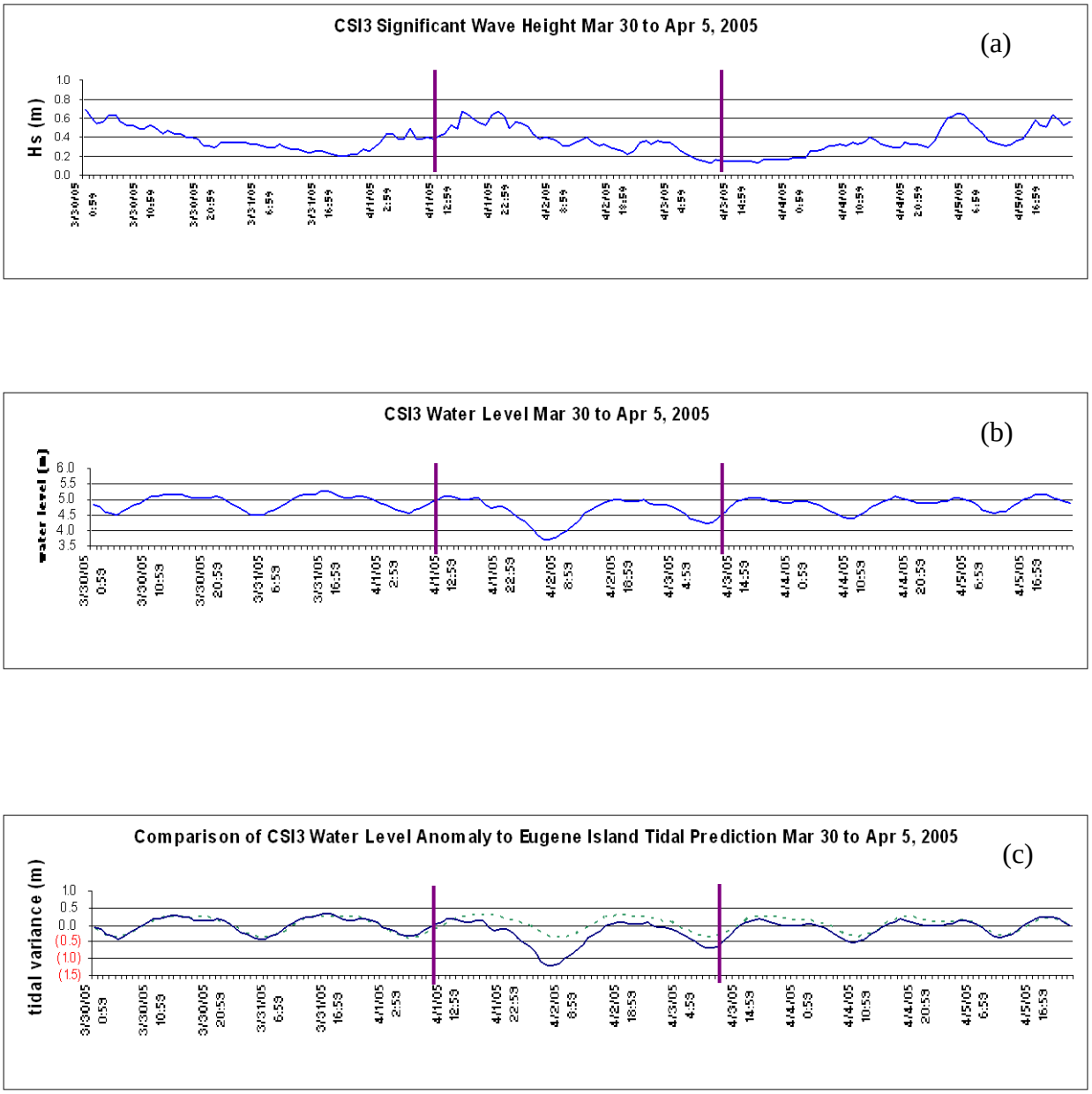

Figure 4.22 CSI-3 observations of waves and water level during the week of March 30 – April 5, 2005: (a) significant wave height; (b) water depth; (c) water level variation (solid blue line) from nearby Eugene Island tidal prediction (dashed green line). Purple lines mark boundary of winds with a northerly component, including the cold front passage and the subsequent cold air outbreak.

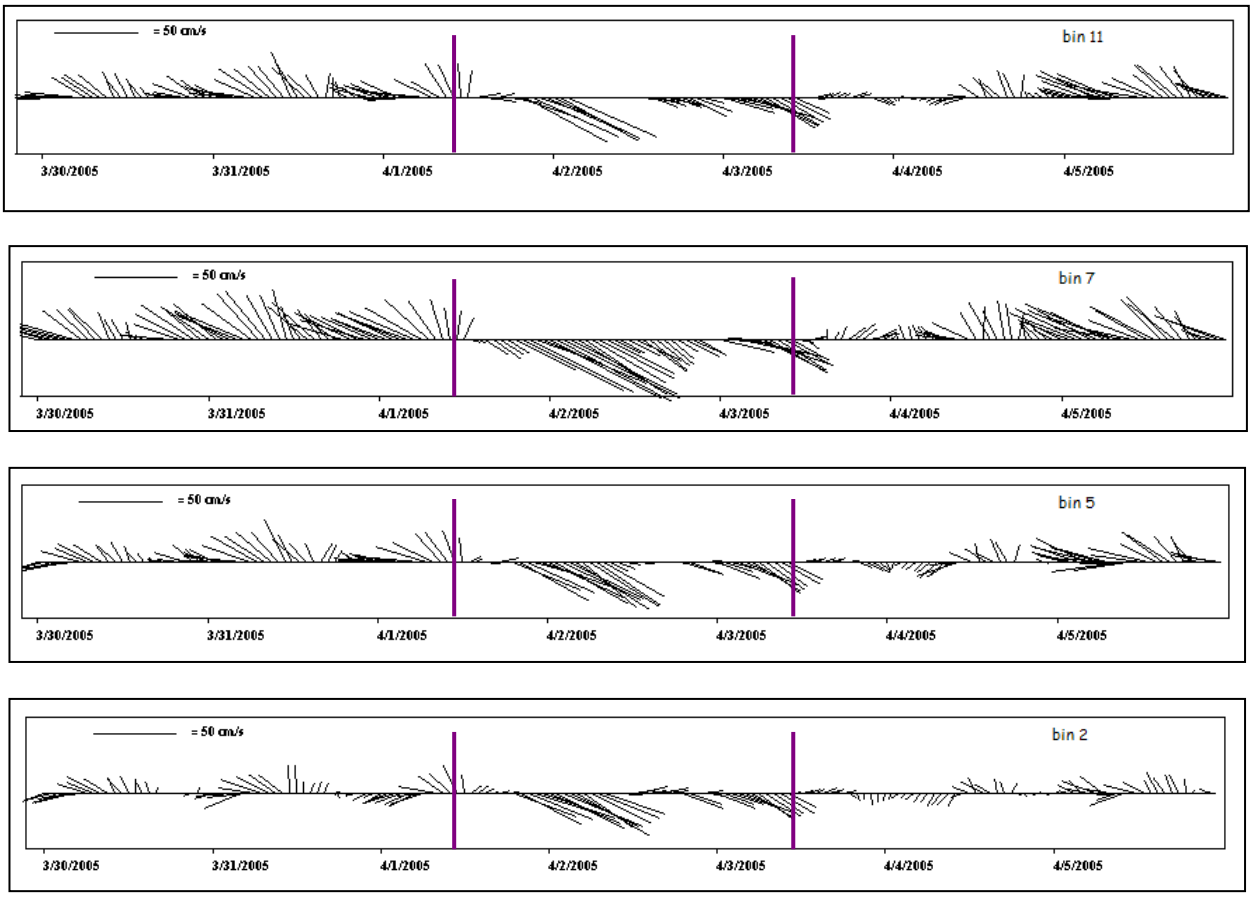

Figure 4.23 CSI-3 observations of currents during the week of March 30 – April 5, 2005: vector plots of current direction and speed at various depths: bin 11 is ~ 4 m from the bottom (near surface); bin 7 is ~ 3 m from the bottom (mid-depth); bin 5 is ~ 2 m from the bottom (mid-depth); and bin 2 is ~ 1 m from the bottom. Purple lines mark boundary of winds with a northerly component, including the cold front passage and the subsequent cold air outbreak.

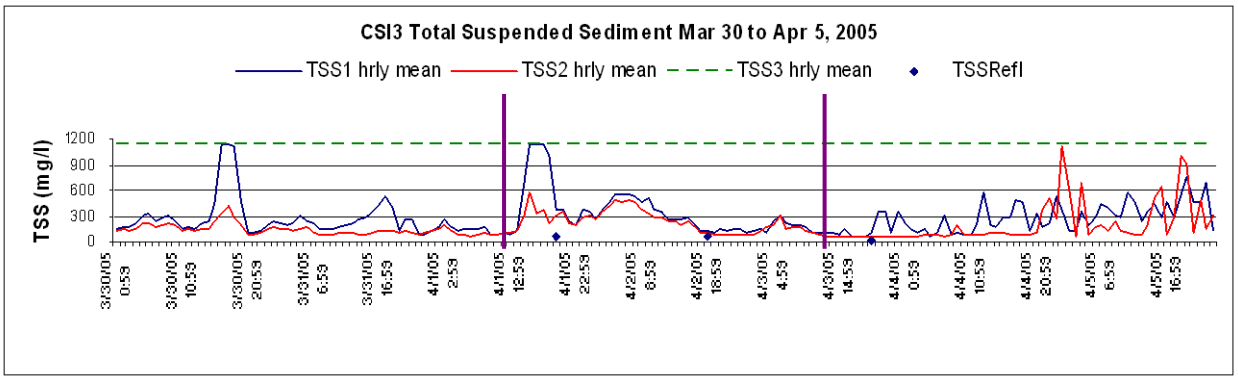

Figure 4.24 CSI-3 observations of total suspended sediment during the week of March 30 – April 5, 2005: TSS at 1, 2 and 3 meters from the bottom (blue, red and green lines respectively), and at the surface plume (three dots).

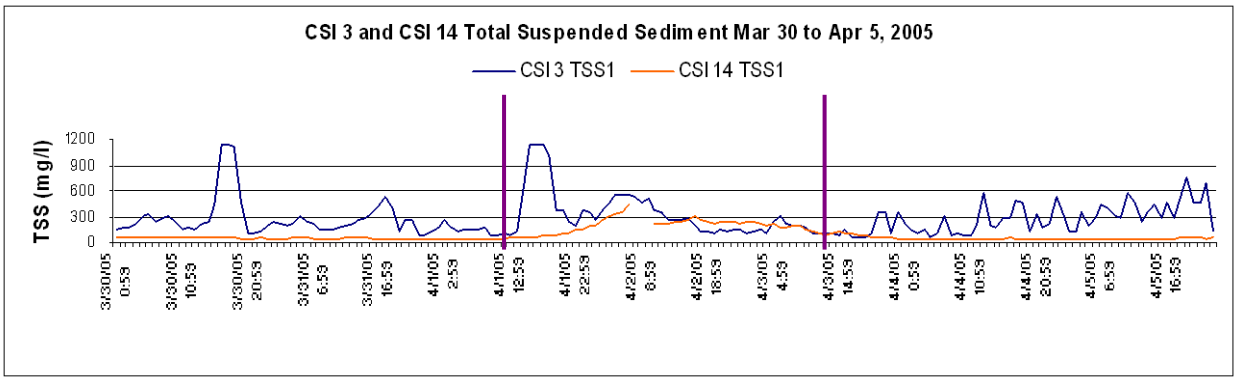

Figure 4.25 Comparison of CSI-3 (inner shelf) and CSI-14 (bay) TSS observations at 1 meter from bottom during the week of March 30 – April 5, 2005.

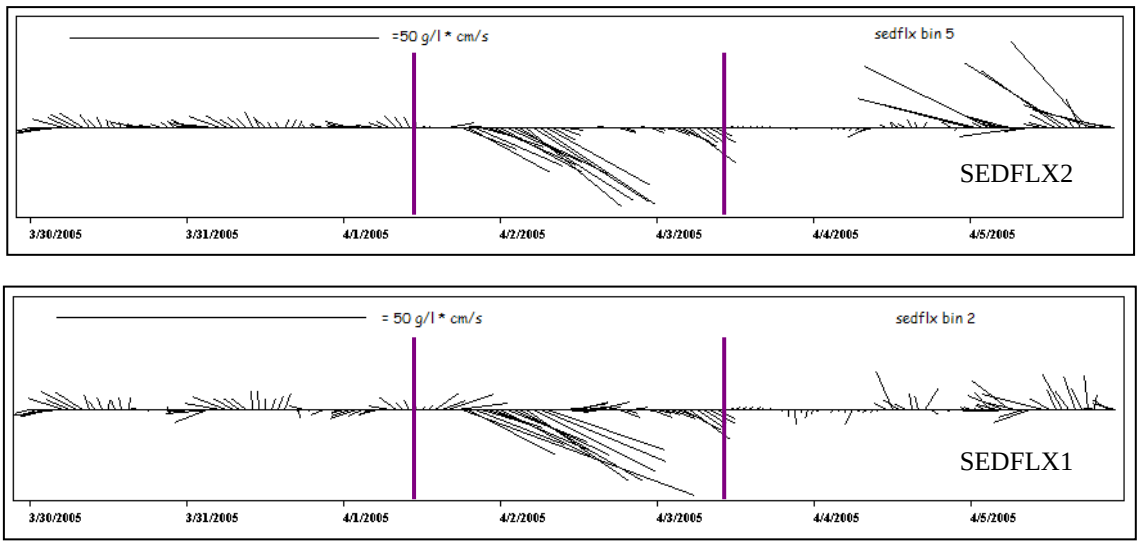

Figure 4.26 CSI-3 observations of sediment flux during the week of March 30 – April 5, 2005: vector plots of sediment flux at various depths: SEDFLX2 is ~ 2 m from the bottom (mid-depth); and SEDFLX1 is ~ 1 m from the bottom.

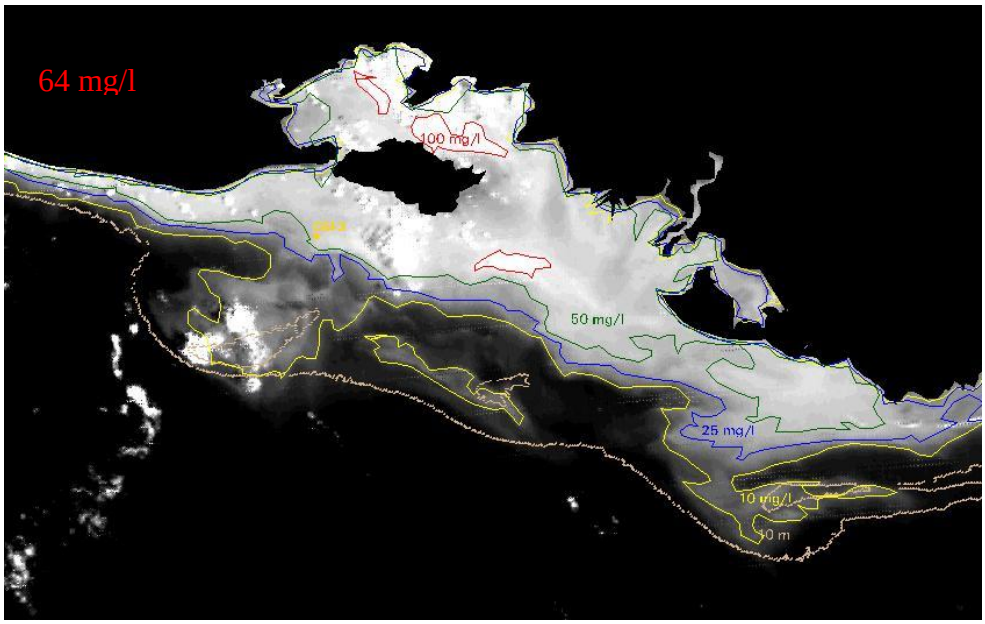

Figure 4.27 April 1, 2005 MODIS image showing location of CSI-3 on the inner shelf, having a satellite derived TSS of 64 mg/l in the surface plume during the early post-front phase. Contour lines for surface TSS are 100 mg/l (red); 50 mg/l (green); 25 mg/l (blue); and 10 mg/l (yellow). The 10 m isobath contour is tan, as are the three 5 m shoals (tan polygons).

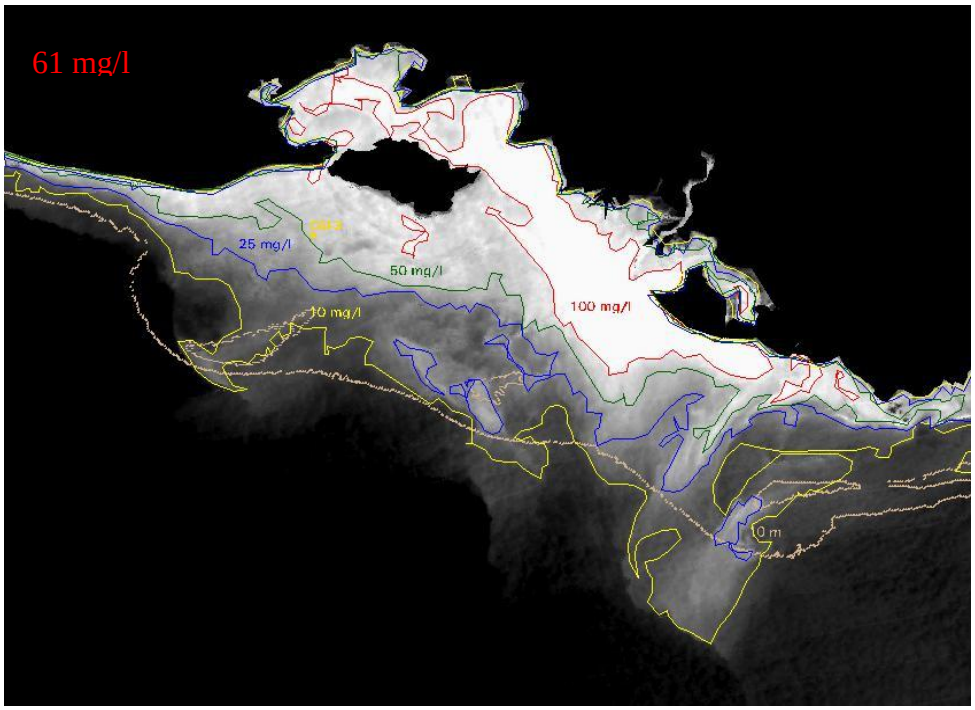

Figure 4.28 April 2, 2005 MODIS image showing location of CSI-3 on the inner shelf, having a satellite derived TSS of 61 mg/l in the surface plume during the second day of the post-front phase. Contour lines for surface TSS are 100 mg/l (red); 50 mg/l (green); 25 mg/l (blue); and 10 mg/l (yellow). The 10 m isobath contour is tan, as are the three 5 m shoals (tan polygons).

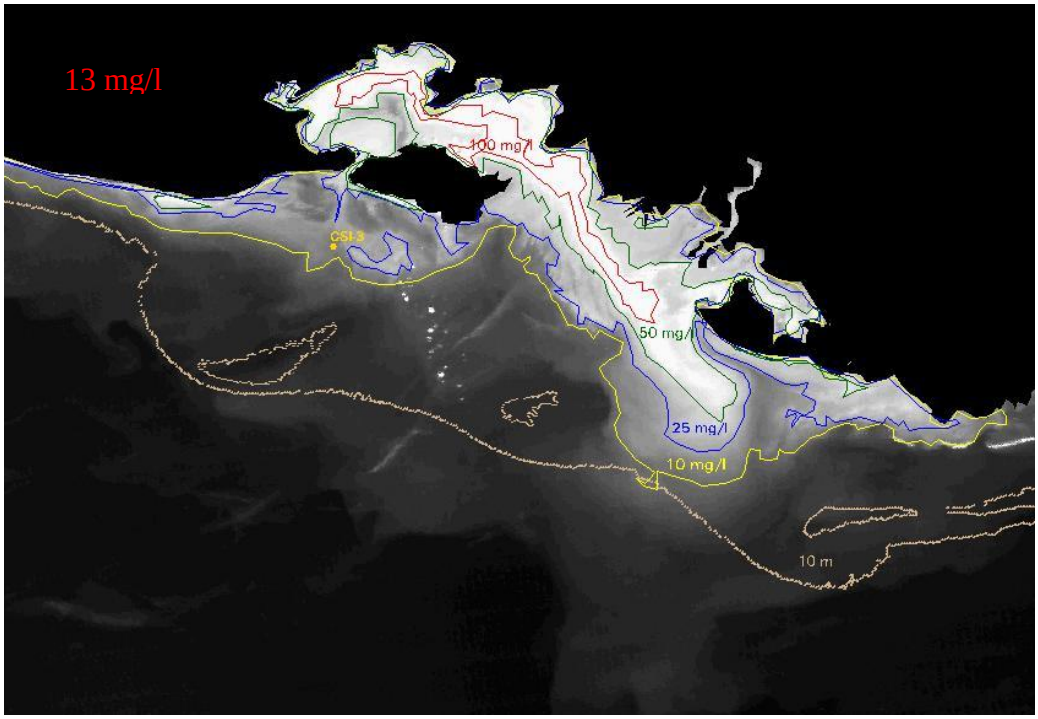

Figure 4.29 April 3, 2005 MODIS image showing location of CSI-3 on the inner shelf, having a satellite derived TSS of 13 mg/l in the surface plume during the inter-frontal phase. Contour lines for surface TSS are 100 mg/l (red); 50 mg/l (green); 25 mg/l (blue); and 10 mg/l (yellow). The 10 m isobath contour is tan, as are the three 5 m shoals (tan polygons).

southerly winds in the pre-frontal phase (Figure 4.32). Although the maximum wind speed was no more than 7 m s^{-1} (Figure 4.30 (b)), currents were steadily northwestward, especially in the upper water column (20 - 57 cm s^{-1}); the typical oscillations (onshore/offshore) with tides were noticeably absent. The bottom meter exhibited weaker current speeds (4 - 33 m s^{-1}) as is often the case, but displayed a bit more variation in current direction than the other depths. Water level slightly exceeded predicted tide throughout the period (Figure 4.31 (c)). Salinity showed the pre-frontal water mass to be fresh (5 – 20 psu), but the SAL1 sensor malfunctioned (Figure 4.30 (c)).

Total suspended sediment levels were elevated in the water column in the pre-frontal phase, never below 300 mg/l at any depth (Figure 4.33). TSS3 was fairly consistent throughout the pre-frontal period at very high levels from 740 – 900 mg/l indicating the presence of a westward flowing river plume or "mudstream". TSS2 exhibited a slow but relatively steady increase from 305 – 875 mg/l, but remained at lower values than the waters both above and below it. This was an unusual break from the typical pattern of TSS2 having similar values as TSS3. It is probably due to the presence of the mud-plume which elevated TSS3 while the strong and steady currents kept the sediments suspended at that depth. TSS1 responded erratically between 396 – 1146 mg/l, with peaks and valleys likely due to the oscillations of a mobile fluid mud layer as the bottom current varied in direction and speed. Overall, the water column shows the cumulative results of the generous supply of sediments from the seasonal succession of river flooding events and flocculation.

SEDFLX3 in the pre-frontal phase was uncharacteristically high due to the presence of the concentrated surface mud-plume (Figures 4.35, 4.36, 4.37). Transport ranged from 20 – 50 g/l * cm/s downcoast with the persistent southeasterly winds (Figure 4.30 (a)) driving the water column. SEDFLX2 was 8 – 20 g/l * cm/s, also steadily westward. SEDFLX1 was predominantly

onshore, but inconsistent in magnitude and direction when compared with the layers above; the fluid mud layer exhibited spatial patchiness.

The frontal passage on April 23, 2005 at 4:00 GMT was ushered in with a definite rotation from southwesterly through westerly winds at 6 – 9 m s^{-1}, and to northerly winds at ~ 11 m s^{-1}. The duration of northerly component winds was 41 hours. Significant wave heights rose to 0.5 – 0.6 m for about 8 hours, then leveled off to 0.2 – 0.4 m (Figure 4.31 (a)). Evidence of spring tides began to appear in that water level prediction exhibited a greater range between high and low tide (about 0.5 m) on April 24, 2005 with the return of the full moon. The moderate northerly winds forced a set-down on April 23, 2005 by 0.3 m, even before spring tides were re-established. The water level decrease, however, was not extreme, as the depth was 4.5 m. The water column was well-mixed in the mid-depths at 15 – 23 psu. Currents reversed from northwestward before the frontal passage to southeastward, strengthening in response to westerly and northerly winds, the cold front induced set-down on April 23 and the outgoing tide on April 24. Current speeds in the upper water column were 50 – 75 cm s^{-1} during peak flows and 25 – 47 cm s^{-1} at the bottom.

Post-front sediment concentrations remained elevated overall on April 23 and 24, but TSS3 demonstrated a slow decline from 750 to 325 mg/l as the offshore current persisted and significant wave heights waned. TSS2 levels responded to the set-down and outgoing tide with decreases to ~ 600 mg/l, still carrying a significant amount of sediment load. TSS1 remained erratic, dropped suddenly from 1,110 mg/l to 200 mg/l, then increased with a slow (but still erratic) climb back to 800 mg/l as the post-front currents advected fresher water offshore. It is interesting to note that while TSS1 and TSS3 did not maintain their respective pre-frontal values consistently, TSS2 did. Sediment flux reversed direction from northwestward in the pre-frontal

phase to southeastward with northerly wind conditions; the maximum ~ 30 g/l cm s^{-1}, coincided with water level decreases. There were also marked differences in TSS1 values between the inner-shelf (CSI-3) and the bay (CSI-14) (Figure 4.34). By the time the MODIS image on April 24, 2005 at 19:55 GMT was acquired near the end of the post-front phase, CSI-3 was no longer under the influence of the surface mud-plume (Figure 4.38) and the satellite derived surface TSS was 9 mg/l. The maximum TSS in the mud-plume to the east of CSI-3 was 271 mg/l. The surface plume's 10 mg/l contour was within the 5 m isobath and bordered CSI-3; the surface waters at CSI-3 showed no indication of the 600 – 900 mg/l concentrations measured near-bottom.

The inter-frontal winds on April 25 were variable at < 3 m s^{-1}, significant wave heights were < 0.1 m, and the water column remained well-mixed at ~ 23 psu. In the mid-depths, TSS2 decreased from 650 mg/l to 300 mg/l, matching TSS3 levels, and sediment flux was onshore at 2 - 10 g/l * cm/s. Near-bottom, TSS1 varied between 600 mg/l to 1,100 mg/l with SEDFLX1 exhibiting sporadic flux variation (5 – 22 g/l cm s^{-1}) and transport direction (SW, NE, N, NE, SE). This is probably due to the bottom meter of the water column's sensitivity to tidal fluctuations and the mobility of the fluid mud layer. On April 26, the winds developed the typical SE pattern, and later turned SW, then NW, increasing to 6 – 10 m s^{-1} so that significant wave heights rose to 0.5 – 0.7 m. Salinity dropped to 14 psu when the tidal outflow caused replacement with fresher water from the bays/river. Currents were westward, then northwestward (maxima 40 - 65 cm s^{-1}) throughout the water column, somewhat slower at the bottom. TSS1 had decreased so that TSS throughout the water column became relatively uniform between 300 – 500 mg/l. The sediment flux throughout the water column was predominantly northwestward at 7 – 22 g/l * cm/s, then finally shifted southeastward at 1 - 19 g/l * cm/s in response to the NW winds, signaling the approach of the next cold front event.

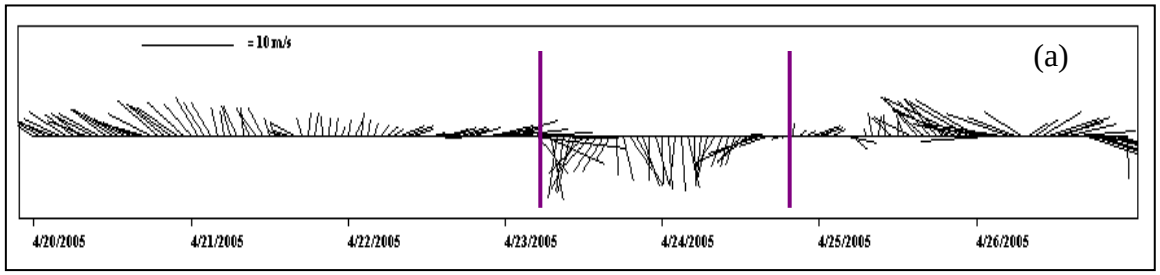

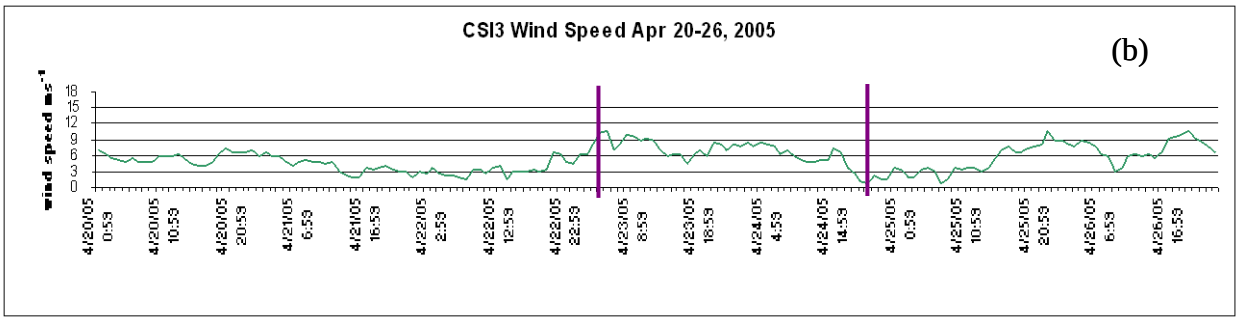

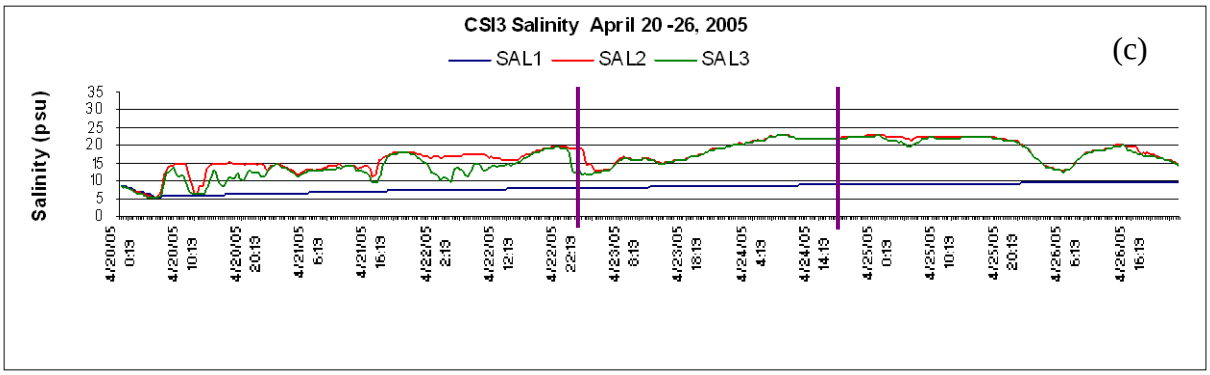

Figure 4.30 CSI-3 observations of winds and salinity during the week of April 20 -26, 2005: (a) vector plot of wind direction and speed; (b) wind speed; (c) salinity at 1 meter from bottom (SAL1), 2 meters from bottom (SAL2), and 3 meters from bottom (SAL3). Purple lines mark boundary of winds with a northerly component, including the cold front passage and the subsequent cold air outbreak.

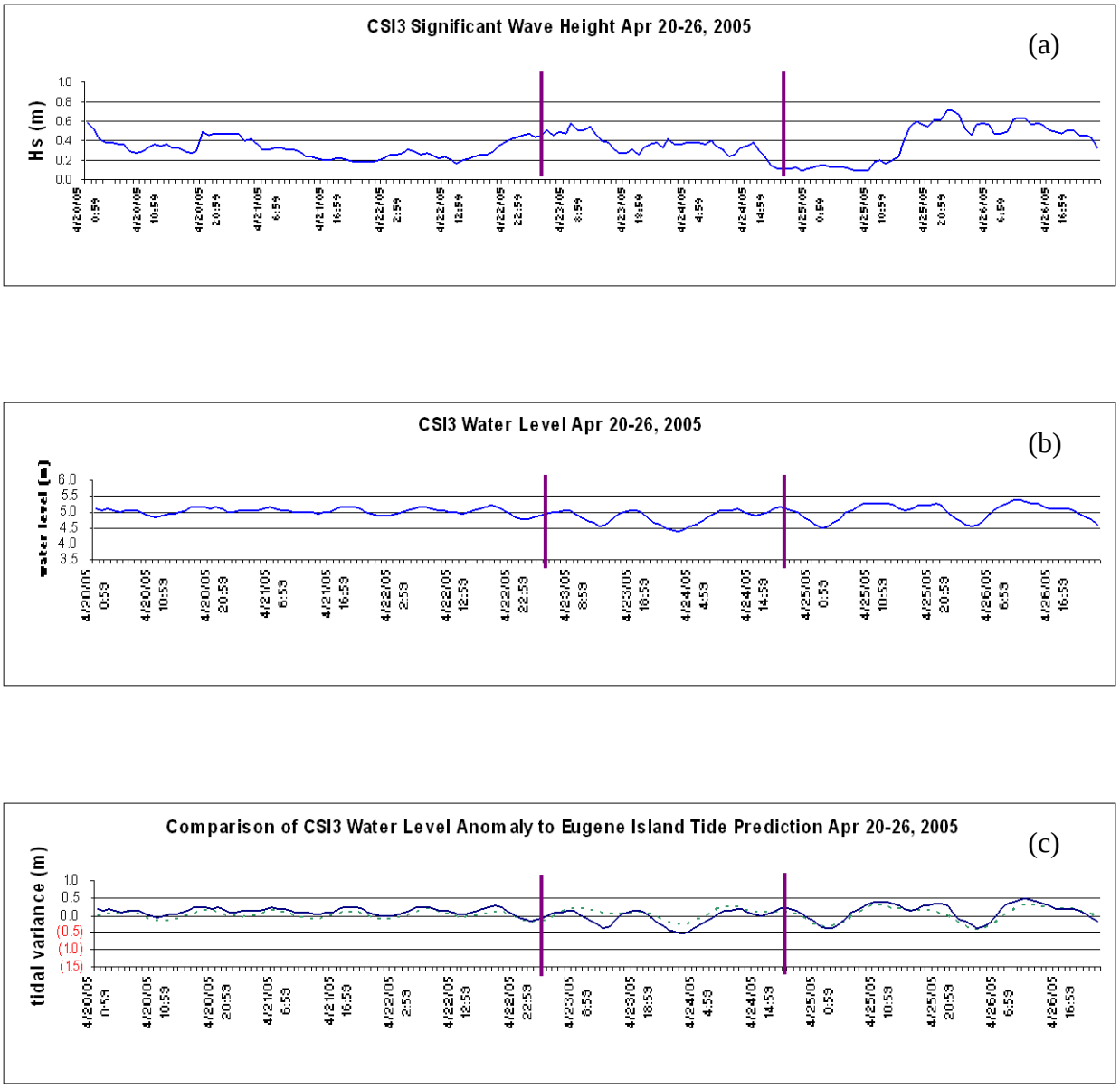

Figure 4.31 CSI-3 observations of waves and water level during the week of April 20 - 26, 2005: (a) significant wave height; (b) water depth; (c) water level variation (solid blue line) from nearby Eugene Island tidal prediction (dashed green line). Purple lines mark boundary of winds with a northerly component, including the cold front passage and the subsequent cold air outbreak.

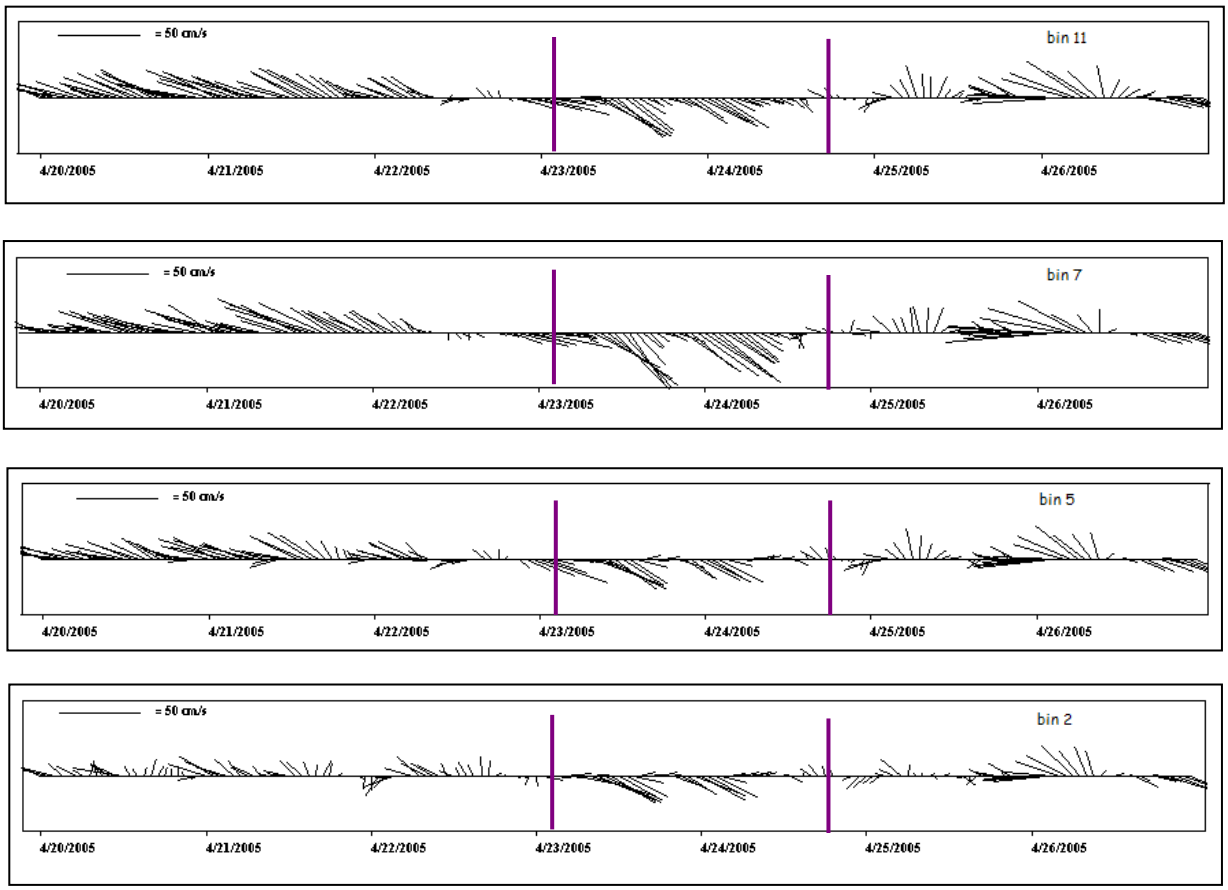

Figure 4.32 CSI-3 observations of currents during the week of April 20 – 26, 2005: vector plots of current direction and speed at various depths: bin 11 is ~ 4 m from the bottom (near surface); bin 7 is ~ 3 m from the bottom (mid-depth); bin 5 is ~ 2 m from the bottom (mid-depth); and bin 2 is ~ 1 m from the bottom. Purple lines mark boundary of winds with a northerly component, including the cold front passage and the subsequent cold air outbreak.

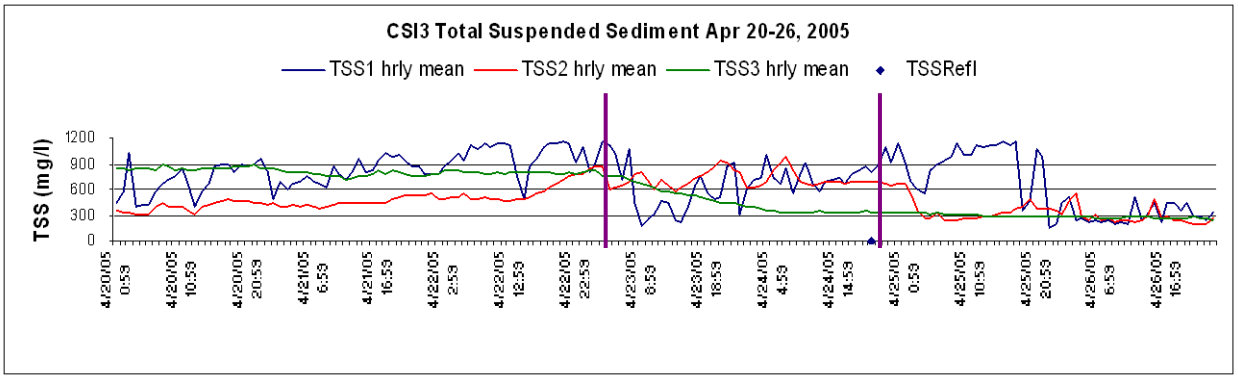

Figure 4.33 CSI-3 observations of total suspended sediment during the week of April 20 - 26, 2005: TSS at 1, 2 and 3 meters from the bottom (blue, red and green lines respectively), and at the surface plume (one dot).

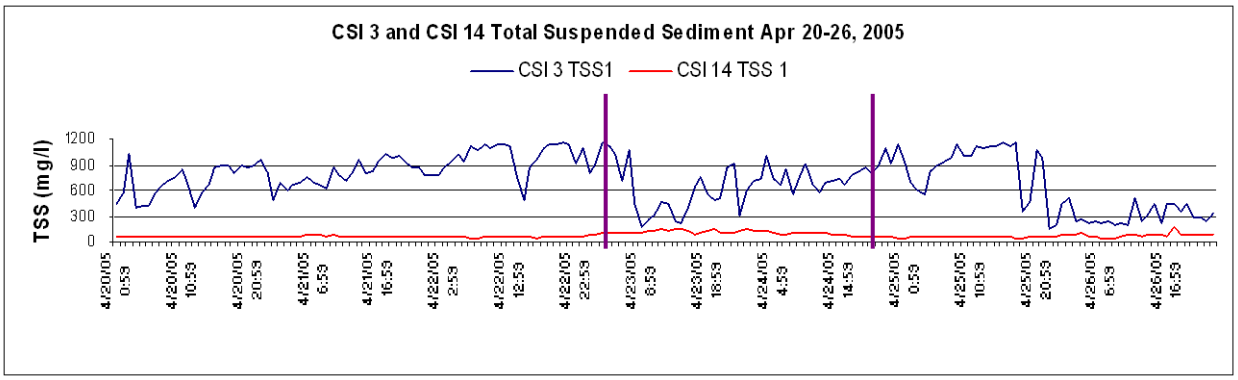

Figure 4.34 Comparison of CSI-3 (inner shelf) and CSI-14 (bay) TSS observations at 1 meter from bottom during the week of April 20 - 26, 2005.

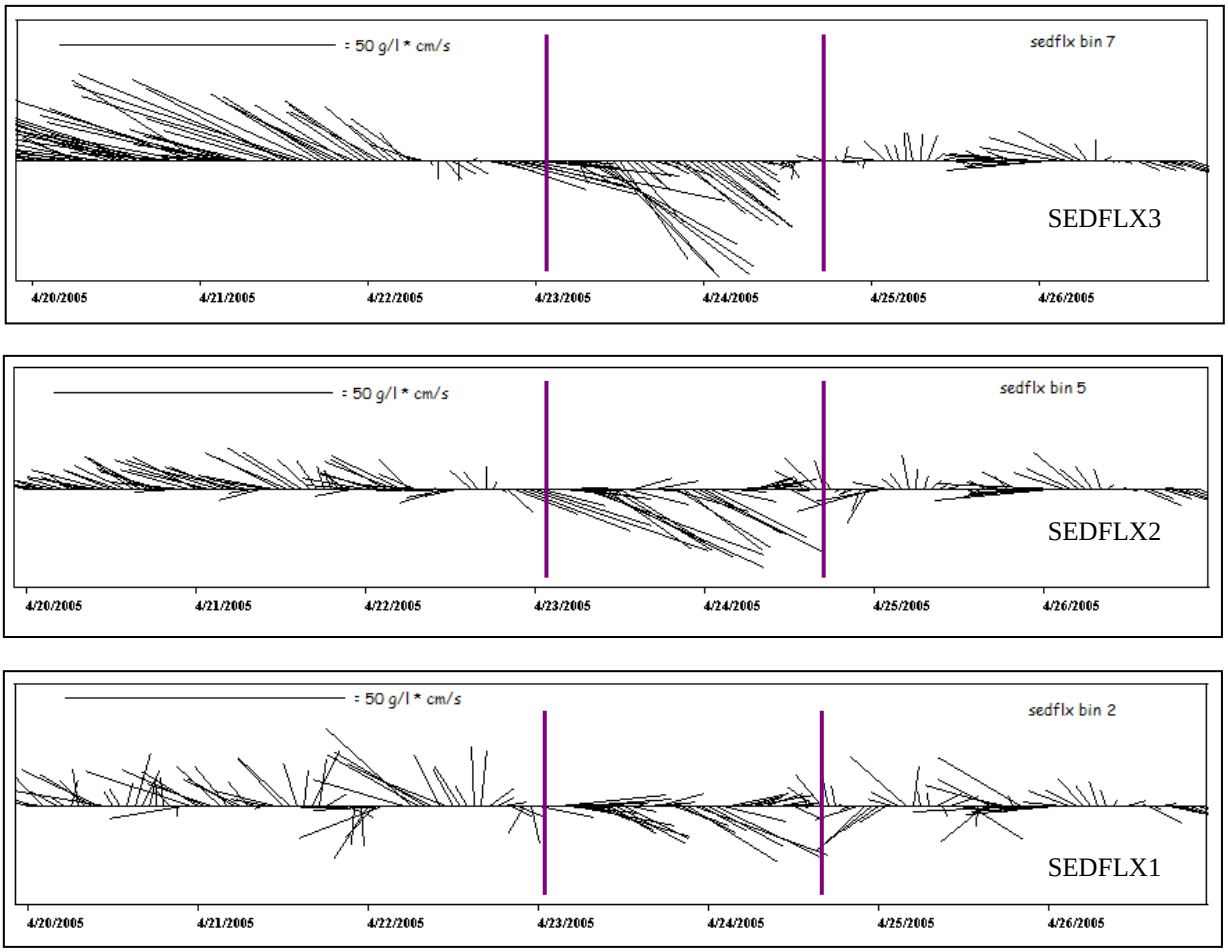

Figure 4.35 CSI-3 observations of sediment flux during the week of April 20 - 26, 2005: vector plots of sediment flux at various depths: SEDFLX3 is ~ 3 m from the bottom (mid-depth); SEDFLX2 is ~ 2 m from the bottom (mid-depth); and SEDFLX1 is ~ 1 m from the bottom. Purple lines mark boundary of winds with a northerly component, including the cold front passage and the subsequent cold air outbreak. Note: no sediment flux is calculated for bin 11 (near surface) since NTU was not available at that depth.

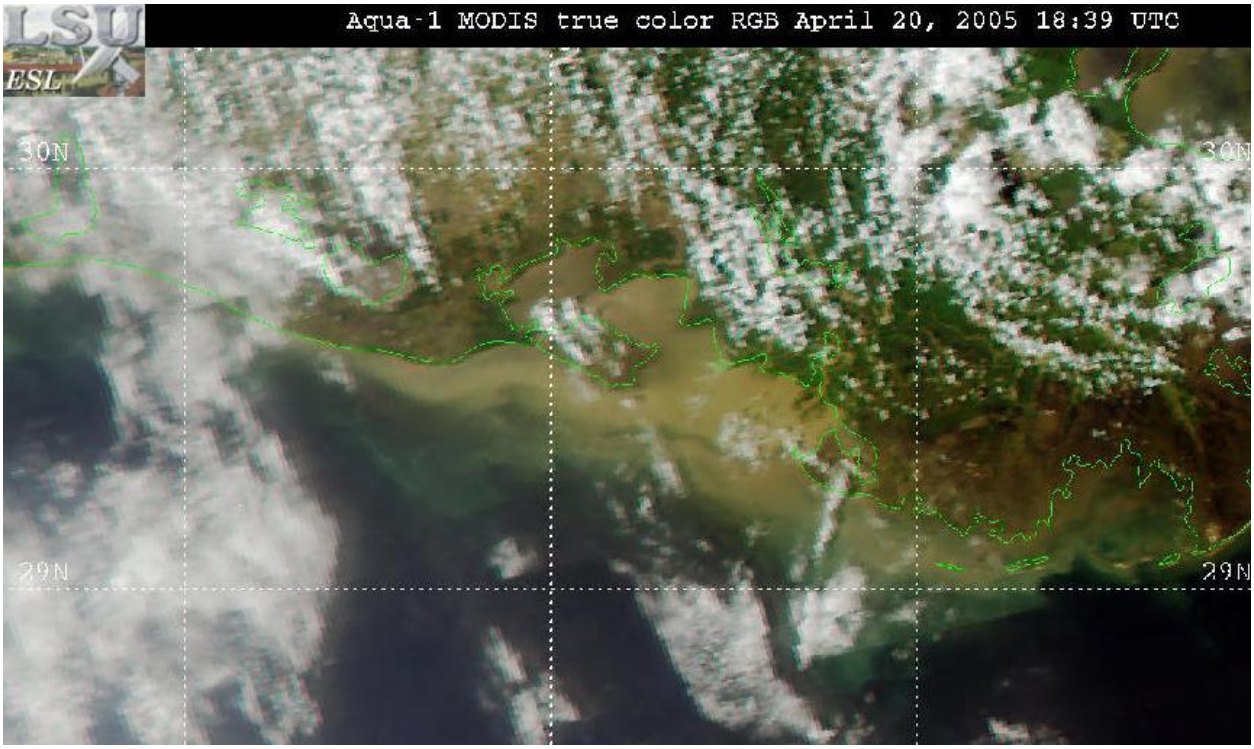

Figure 4.36 April 20, 2005 MODIS image showing surface mud-plume position in the pre-frontal phase. TSS from satellite reflectance was not calculated using this image due to cloud contamination.

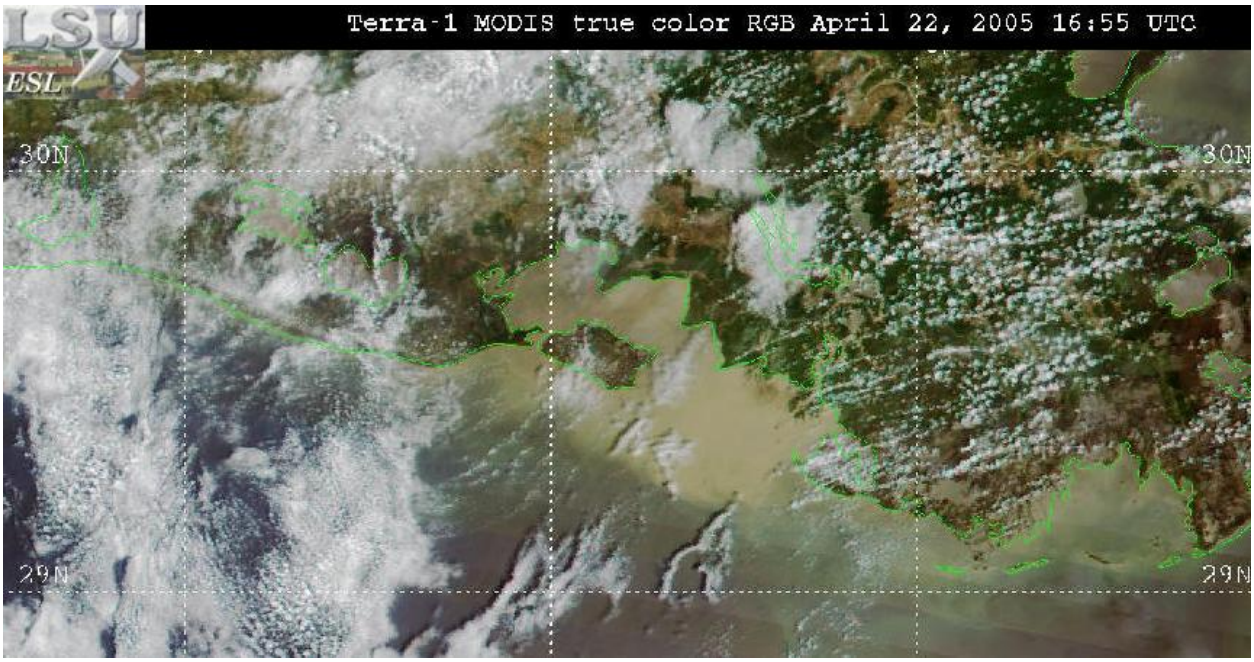

Figure 4.37 April 22, 2005 MODIS image showing surface mud-plume position in the pre-frontal phase. TSS from satellite reflectance was not calculated using this image due to cloud contamination .

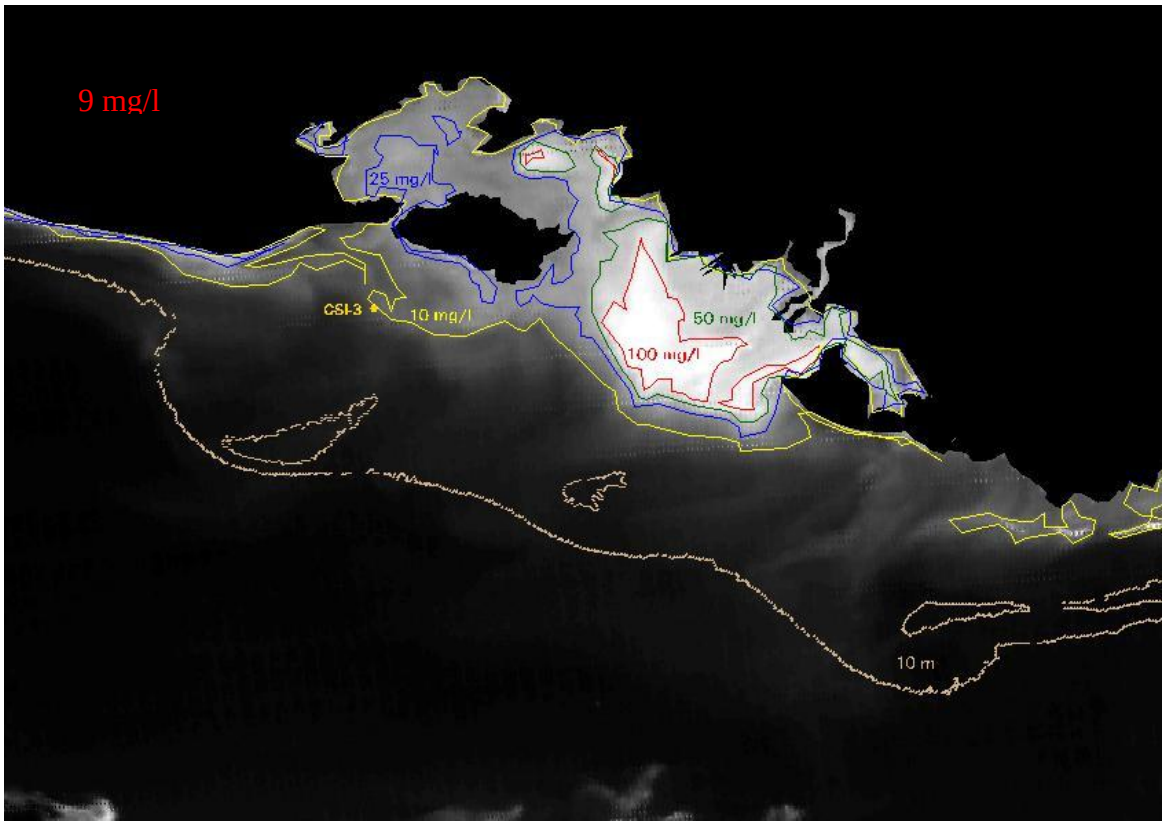

Figure 4.38 April 24, 2005 MODIS image showing location of CSI-3 on the inner shelf, having a satellite derived TSS of 9 mg/l in the surface plume at the close of the post-front phase. Contour lines for surface TSS are 100 mg/l (red); 50 mg/l (green); 25 mg/l (blue); and 10 mg/l (yellow). The 10 m isobath contour is tan, as are the three 5 m shoals (tan polygons).

CHAPTER 5 DISCUSSION

This study was based on time series of measurements at WAVCIS CSI-3 and satellite imagery in a shallow water area during five cold front events. Satellite imagery provided the "big picture" of surface sediment transport while the WAVCIS station provided measurements of the vertical structure of sediment resuspension and transport at one location in the water column, albeit some distance away from the main sediment plume during frontal passage.

Table 5.1 summarizes pre-frontal conditions of the five case study events at CSI-3. Prefrontal conditions at CSI-3 exhibited southeasterly wind speed maxima (7 – 12 m s^{-1}) which were strong enough to generate significant wave heights up to 0.8 m. Evidence of a pre-frontal influence from resuspended sediment causing a reduction of significant wave height, like that of the relationship of resuspended fine-grained sediments on wave energy dissipation discussed by Sheremet and Stone (2003), was not obvious. Northwestward currents (integrated over the water column) in the pre-frontal phase averaged 15 - 28 cm s^{-1}, with maxima from 42 – 66 cm s^{-1}. Water level set-up was < 0.3 m for all pre-frontal periods examined. Salinity was generally < 20 psu, showing the flow of fresh water from the mouth of the Atchafalaya River and from the bays. A tidal influence was evident on salinity, with outgoing tides causing temporary decreases of 5 - 8 psu. In one event, total suspended sediment peaks were noticeable in the water column as the onset of onshore currents followed ebb-tide low water. Total suspended sediment and sediment flux was higher in the near-bottom than in the mid-depths due to the presence of the fluid mud layer. Some peaks in total suspended sediment and sediment flux can be attributed to the mobility of this high concentration layer. Sediment flux maxima in the bottom meter was from 2 - 21 g/l * cm/s. Since pre-frontal conditions are often cloudy, no satellite imagery was available

to be processed to examine and quantify surface sediment plumes. It should be noted that these conditions may not be representative of the entire region.

Table 5.1 Case Study Summary Table: Pre-frontal Phase at CSI-3 on the Inner Shelf

	January 6-8, 2004	January 16-17, 2004	January 24-26, 2004	March 30 - April 1, 2005	April 20-22, 2005
Atchafalaya River Discharge ($m^3 s^{-1}$)	5,663	8,212	9,061	6,230	9,628
Upstream Sediment Concentration (mg/l)	n/a	502	968	151	223
Max Wind Speed ($m s^{-1}$)	12	10	11	7	7
Max Significant Wave Height (m)	0.8	0.7	0.8	0.7	0.6
Minimum Water Depth (m)	4.2	4.4	4.3	4.5	4.9
Mean TSS3 (mg/l)	165	45	50	n/a	808
Mean TSS2 (mg/l)	151	45	55	148	470
Mean TSS1 (mg/l)	209	76	160	269	830
Max TSS3 (mg/l)	510	81	134	n/a	885
Max TSS2 (mg/l)	441	76	441	428	780
Max TSS1 (mg/l)	567	138	567	524[a]	1,146
Mean Current[b] NW ($cm s^{-1}$)	22	20	15	28	24
Maximum Current[b] NW ($cm s^{-1}$)	51	47	42	61	66
Mean SEDFLX3 ($g/l * cm s^{-1}$)	4	1	1	n/a	24
Mean SEDFLX2 ($g/l * cm s^{-1}$)	4	1	1	4	12
Mean SEDFLX1 ($g/l * cm s^{-1}$)	4	1	2	4	13
Max SEDFLX3 ($g/l * cm s^{-1}$)	17	3	4	n/a	50
Max SEDFLX2 ($g/l * cm s^{-1}$)	15	2	4	7	39
Max SEDFLX1 ($g/l * cm s^{-1}$)	21	2	8	8	31

[a] Maximum TSS which can be attributed to meteorological/oceanographic forcing.

[b] Currents integrated over water column.

Table 5.2 summarizes post-front conditions of the five case study events at CSI-3. Post-front winds were NW, N or NE with maxima between 9 - 16.5 m s^{-1}. In spite of higher wind speeds, maximum significant wave heights were reduced by 0.1- 0.3 m less than in the pre-frontal phase, due to fetch length reduction from the mainland coast and from Marsh Island. However, these post-front winds were strong enough to suppress tidal inflow from reaching predicted tidal high water and to produce water level set-down up to 0.7 m below predicted tidal

low. Sustained frontal winds were able to keep the water column well-mixed, even during transitions between low and high salinity water masses during current variations. Southeastward currents (integrated over the water column) averaged 20 - 29 cm s^{-1} with maxima from 55 – 98 cm s^{-1}, approximately a 30% increase over pre-frontal current speeds. The water column was generally well-mixed in the post-front phase. Three events showed steady increases in salinity from the first to second day post-front. One event showed a "resistant" stratification of the water column under NW wind conditions until the winds rotated to northerly. In four events, a well-mixed water column was a proxy for similarity in total suspended sediments in the mid-depths, but not in the near-bottom as the fluid mud layer has higher viscosity. Sediment flux maxima at 3 meters from the bottom were higher than at 2 meters from the bottom due to more powerful currents in the upper water column in response to frontal winds. Near-bottom sediment flux maxima were also higher than at 2 meters from the bottom due to higher total suspended sediment values. Both offshore wind-forcing of currents in the upper water column and sediment availability in the bottom meter are important contributors to sediment flux rates. Based on this limited number of case studies, the weather type of cold front passage, Frontal Over-running (FOR) or Continental High (CH) did not appear to affect total suspended sediment values, sediment flux rates or total sediment transport.

Post-front satellite imagery shows that the dominant post-front surface sediment transport direction is to the southeast, extending from the river mouth in Atchafalaya Bay. The multi-lobate contours often conform to bottom 5 and 10 meter bathymetry, indicating that such cold front events may have historically been the source of sediment supply for the underwater shoals. Satellite-derived total suspended sediment values for the surface waters at CSI-3 show substantially lower values than in the water column beneath, with maxima in the water column as

much as 5 to 10 times higher, especially in the bottom meter. This shows that the surface mud-plume sediment transport process is distinctly different from the mid-depths and bottom, as revealed by CSI-3. In the lower water column, it is reasonable to expect high rates of sediment transport into at CSI-3 during the post-front period; as the currents flow southeastward from the Chenier Plain coast region, the area of the highest fluid mud concentrations on the coast.

Table 5.2 Case Study Summary Table: Post-front Phase at CSI-3 on the Inner Shelf

	January 9-11, 2004	January 18-20, 2004	January 27-28, 2004	April 1-3, 2005	April 23-24, 2005
River Discharge ($m^3 s^{-1}$)	5,663	8,212	9,061	6,230	9,628
Upstream Sediment Concentration (mg/l)	n/a	502	968	151	223
Cold Front Weather Type	FOR	CH	FOR	FOR	CH
Max Wind Speed ($m s^{-1}$)	9	11	15	16.5	11
Duration of N Component Winds (hrs)	53	53	41	51	41
Max Significant Wave Height	0.5	0.6	0.6	0.7	0.6
Minimum Water Depth (m)	4.2	3.7	4.1	3.7	4.5
TSSRefl surface (mg/l)	137	100	117	64	n/a
Mean TSS3 (mg/l)	109	122	171	n/a	477
Mean TSS2 (mg/l)	101	129	161	205	724
Mean TSS1 (mg/l)	158	207	218	306	703
Max TSS3 (mg/l)	379	515	421	n/a	829
Max TSS2 (mg/l)	315	451	396	572	967
Max TSS1 (mg/l)	379	946	560	1,143	1,146
Mean Current[a] SE ($cm s^{-1}$)	20	24	22	29	22
Maximum Current[a] SE ($cm s^{-1}$)	55	65	61	98	75
Mean SEDFLX3 ($g/l * cm s^{-1}$)	3	3	5	n/a	15
Mean SEDFLX2 ($g/l * cm s^{-1}$)	2	3	5	7	14
Mean SEDFLX1 ($g/l * cm s^{-1}$)	3	4	6	8	11
Max SEDFLX3 ($g/l * cm s^{-1}$)	14	24	20	n/a	48
Max SEDFLX2 ($g/l * cm s^{-1}$)	12	19	18	30	41
Max SEDFLX1 ($g/l * cm s^{-1}$)	12	25	20	46	29
Post-Front Sediment Transport[b]	**1,526**	**1,908**	**2,362**	**2,754**	**5,904**
Post-Front Max 100 mg/l area (km^2)	1,210	2,268	2,542	1,416	366

[a] Current integrated over water column.

[b] Transport in the lower three meters of the water column, in metric tons, over the duration of each post-front event.

Post-front sediment transport in the lower three meters of the water column was derived using mean sediment flux (which includes sediment concentration and flow rates of transport), obtaining the equivalent of g/l s^{-1} transported into metric tons/hour, and converting to a total volume of sediment transported for each post-front period by multiplying each by its respective time (Duration of N Component Winds). The units are expressed in metric tons and show marked differences across the five case study events. Comparison of post-front sediment transport with river discharge and upstream sediment concentration revealed no obvious correlation. Again, it should be noted that these conditions may not be representative of the entire region.

Sediment concentrations throughout the water column during post-front conditions from Table 5.2 compare favorably with other studies. Allison (2000) found concentrations during high post-front winds and high river discharge conditions ranging from 50 – 1000 mg/l at the Chenier Plain coast, with higher concentrations closer to shore and settling to the bottom as winds decreased. Kineke et al found similar concentrations and process from surface to bottom at the Chenier Plain coast, with maxima bottom sediment concentrations near 2000 mg/l, being measured at 0.15 m from the bottom.

Table 5.3 shows a comparison of total suspended sediment: 1) satellite-derived at the surface at CSI-3, 2) WAVCIS measurements of total suspended sediment from each depth at CSI-3; and 3) the satellite-derived maximum in the mud-plume, *all at the time of satellite overpass*. The maximum total suspended sediment in the mud-plume was some distance from CSI-3 in every case, either to the east of CSI-3, or in one case within West Cote Blanche Bay (April 1, 2005). In two post-front periods (highlighted in green) there were similarities in sediment concentration at the CSI-3 site from the surface into the water depths. Since these

images were all post- or inter-frontal, the maximum total suspended sediment in the mud-plume did not correlate to the surface TSSRefl at CSI-3, since the dominant direction of transport after frontal passage was southeastward, away from the station. The near-bottom fluid mud concentration values were 2 – 10 times that of the surface total suspended sediment at CSI-3.

Table 5.3 Case Study Comparison of Total Suspended Sediment

Date/Time (GMT)	Post- or Inter-frontal Image	Mud-plume encompass CSI-3 location?	Surface TSSRefl at CSI-3 (mg/l)	TSS3 at CSI-3 (mg/l)	TSS2 at CSI-3 (mg/l)	TSS1 at CSI-3 (mg/l)	Maximum TSS in mud-plume (mg/l)
1/10/2004 18:55	Post-front	yes	135	225	209	286	285
1/11/2004 19:40	Inter-frontal	no	17	59	52	73	301
1/19/2004 18:50	Post-front	yes	100	108	135	281	399
1/27/2004 19:40	Post-front	yes	117	308	278	329	427
1/28/2004 18:45	Post-front	no	86	66	61	72	722
4/1/2005 19:50	Post-front	no	64	n/a	319	385	142
4/2/2005 18:55	Post-front	no	61	n/a	121	143	482
4/3/2005 19:40	Inter-frontal	no	13	n/a	67	110	324
4/24/2005 19:55	Post-front[1]	no	9	341	697	789	271

[1] Image was obtained very late in the post-front period; within a few hours inter-frontal.

CHAPTER 6 CONCLUSIONS

The observations of pre-frontal and post-front conditions disclose the variability and uniqueness of cold front event effects on sediment transport. Based on the analysis of both meteorological/oceanographic observations and MODIS satellite imagery, the following conclusions were made:

- My hypothesis, that the spatial and temporal changes in surface sediment concentrations at CSI-3 reflect the characteristics of sediment resuspension and transport throughout the water column, was not supported by the data analyzed.
- Near-bottom fluid mud layers at CSI-3 appeared to be decoupled from the upper water column. In pre- or post-front periods, near-bottom sediment concentrations were often twice that of the waters above.
- River sediment concentrations, total suspended sediments, sediment flux and total sediment transport were not easily predicted by Atchafalaya River water discharge rates.
- High rates of sediment flux in the surface and upper water column were primarily in response to strong currents from wind-forcing; high rates of sediment flux in the near-bottom were due to high sediment concentrations.
- Maximum sediment flux in the bottom occurred during the post-front period; maximum currents forced fluid mud from the Chenier Plain region southeastward to the inner shelf at CSI-3.
- Maximum sediment transport in the surface mud-plume was also during the post-front period; sediment supplied from the river, bays and resuspension flowed southeastward, away from the CSI-3 site on the inner shelf.

Future study to examine sediment concentration and fluxes throughout the water column on a greater spatial scale should include multiple stations in array on the inner shelf and in the bays simultaneously, to provide understanding of vertical and horizontal sediment transport patterns. Stations located within the main river plume or within the bays in very shallow water might show greater uniformity in total suspended sediment throughout the water column. Time series data should be collected during all seasons so that non-flood conditions could be compared, as well as those of tropical events to assess the relative impacts on fine-grained sediment transport.

The work should be expanded to examine the processes of wave energy damping, flocculation, energy transfer (such as wind stress) and bottom friction variations due to the presence, height, thickness and mobility of the fluid mud layer. Numerical modeling of this region is currently being studied and should be promoted.

The spatial advantage of remote sensing should be exploited by the development of additional models to predict surface total suspended sediment with imagery from other sensors which acquire data at varying time scales. This would optimize the number of images available which could reveal characteristics which might be otherwise unobserved.

REFERENCES

Allison, M.A., Kineke, G.C., Gordon, E.S., Goñi, M.A., 2000, *Development and Reworking of a Seasonal Flood Deposit on the Inner Continental Shelf off the Atchafalaya River,* Continental Shelf Research, Vol 20, pp. 2267-2294.

Cho, K., Reid, R.O., Nowlin, W.D., 1998, *Objectively Mapped Stream Function Fields on the Texas-Louisiana Shelf Based on 32 Months of Moored Current Meter Data,* Journal of Geophysical Research, Vol.103, No. C5, pp.10,377-10,390.

Chuang, W.S., Wiseman, W. J., 1983, *Coastal Sea Level Response to Frontal Passages on the Louisiana-Texas Shelf,* Journal of Geophysical Research, Vol. 88, No C4, pp. 2615-2620.

Cochrane, J.D., Kelly, F.J., 1986, *Low-Frequency Circulation on the Texas-Louisiana Continental Shelf,* Journal of Geophysical Research, Vol. 91, No. 9, pp. 10,645-10,659.

Draut, A.E., Kineke, G.C., Valasco, D.W., Allison, M.A., Prime, R.J., 2005, *Influence of the Atchafalaya River on Recent Evolution of the Chenier Plain Inner Continental Shelf, Northern Gulf of Mexico, Continental Shelf Research, Vol. 25, pp.91-112.*

D'Sa, E.J., Miller, R.L., 2005, *Bio-Optical Properties of Coastal Waters,* Remote Sensing of Coastal Aquatic Environments, Springer, Netherlands, pp. 129-150.

Fisk, H.N., 1952, *Geologic Investigation of the Atchafalaya Basin and the Problem of Mississippi River Diversion,* U.S. Army Corps of Engineers, Mississippi River Commission, Vicksburg, Mississippi, 138 p.

Georgiou, I.Y., FitzGerald, D.M., Stone, G.W., 2005, *The Impact of Physical Processes Along the Louisiana Coast,* Journal of Coastal Research, SI44, pp. 72-89.

Gordon, E.S., Goñi, M.A., Roberts, Q.N., Kineke, G.A., Allison, M.A., 2001, *Organic Matter Distribution and Accumulation on the Inner Louisiana Shelf West of the Atchafalaya River,* 2001, Continental Shelf Research, Vol.21, No. 16, pp.1691-1721.

Gordon, H.R., Brown, O.B., Jacobs, M.M., 1975, *Computed Relationships Between the Inherent and Apparent Optical Properties of a Flat Homogeneous Ocean,* Applied Optics, Vol.14, pp. 417-427.

Gordon, H.R., 1978, *Removal of Atmospheric Effects from Satellite Imagery of the Oceans,* Applied Optics, Vol.17, pp. 1631-1636.

Gordon, H.R., Clark, D.K., Brown J.W., Brown, O.B., Evans, R.H., Broenkow, W.W., 1983, *Phytoplankton Pigment Concentrations in th Middle Atlantic Bight: Comparison of Ship Determinations and CZCS Estimates,* Applied Optics, Vol.22, pp. 20-36.

Gumley, L., Descloitres, J., Schmaltz, J., 2003, *Creating Reprojected True Color MODIS Images: A Tutorial*, http://rapidfire.sci.gsfc.nasa.gov/faq/MODIS_True_Color.pdf, 19 p.

Huh, O. K., Rouse, L.J., and Walker, N.D., 1984, *Cold Air Outbreaks Over the Northwest Florida Continental Shelf*, Journal of Geophysical Research, Vol. 89, No. C1, pp.717-726.

Huh, O.K., Moeller, C.C., Menzel, W.P., Rouse, L.J., Roberts, H.H., 1996, *Remote Sensing of Turbid Coastal and Estuarine Waters: A Method of Multispectral Water-Type Analysis*, Journal of Coastal Research, Vol. 12, No. 4, pp.984-995.

Huh, O.K., Walker, N.D., Moeller, C.C., 2001, *Sedimentation Along the Eastern Chenier Plain Coast: Down Drift Impact of a Delta Complex Shift*, Journal of Coastal Research, Vol. 17, No. 1, pp.72-81.

Hsu, S.A., 1988, *Coastal Meteorology*, Academic Press, San Diego, California, 260 p.

Hsu, S.A., 1999, *Characteristics of Marine Meteorology and Climatology in the Gulf of Mexico*, in The Gulf of Mexico Large Marine Ecosystem, Kumpf, Steidinger and Sherman (eds.), Blackwell Science, pp. 77-89.

Hsu, S.A., 1999, *Effects of Wave Dynamics on the Wind Setup in Deep Water*, from the Proceedings of the Symposium on the Wind-Driven Air-Sea Interface, Sydney, Australia, January 11-15, 1999, pp. 57-64.

Keen, T.R., 2002, *Waves and Currents During a Winter Cold Front in the Mississippi Bight*, Journal of Coastal Research, vol. 18:4, pp. 622-636.

Kemp, G.P., Wells, J.T., Van Heerden, I.L., 1980, *Frontal Passages Affect Delta Development in Louisiana*, Coastal Oceanography and Climatology News, Vol 3, pp. 4-5.

Kineke, G.C., Higgins, E.E., Hart, K., Velasco, D., 2006, *Fine-Sediment Transport Associated with Cold-Front Passages on the Shallow Shelf, Gulf of Mexico*, Continental Shelf Research, Vol. 26, pp. 2073-2091.

Kirk, J.T.O., 1994, *Light and Photosynthesis in Aquatic Ecosystems, Second Edition*, Cambridge University Press, 509 p.

Li, R.R., Kaufman, Y.J., Gao, B.C., Davis, C.O., 2003, *Remote Sensing of Suspended Sediments and Shallow Coastal Waters*, IEEE Transactions on Geoscience and Remote Sensing, Vol.41, No. 3, pp. 559-566.

Miller, R.L., McKee, B.A., D'Sa, E.J., 2005, *Monitoring Bottom Sediment Resuspension and Suspended Sediments in Shallow Waters*, Remote Sensing of Coastal Aquatic Environments, Springer, Netherlands, pp. 259-276.

Milliman, J.D. and Meade, R.H., 1983, *World-Wide Delivery of Sediment to the Oceans*, The Journal of Geology, Vol. 91, No. 1, pp. 1-21.

Moeller, C.C., Huh, O.K., Roberts, H.H., Gumley, L.E., Menzel, W.P., 1993, *Response of Louisiana Coastal Environments to a Cold Front Passage*, Journal of Coastal Research, Vol 9, No. 2, pp. 434-447.

Moeller, C.C., Huh, O.K., Menzel, W.P., Roberts, H.H., 1996, *The Use of Aircraft-Borne MAS Data for Mapping Sediment Transport Along the Louisiana Coast,* Second International Airborne Remote Sensing Conference and Exhibition, San Francisco, California, ERIM, Vol. II, pp. 673-683.

Morey, S.L., Martin, P.J., O'Brien, J.J., Wallcraft, A.A., Zavala-Hidalgo, J., 2003, *Export Pathways for River Discharged Fresh Water in the Northern Gulf of Mexico,* Journal of Geophysical Research, Vol. 108, No. C10, pp. 3303-3317.

Mossa, J., 1990, *Discharge-Suspended sediment relationships in the Mississippi-Atchafalaya River System, Louisiana*, PhD dissertation, Department of Geography and Anthropology, Louisiana State University, 180 pp.

Mossa, J. and Roberts, H.H., 1990, *Synergism of Riverine and Winter Storm Related Sediment Transport Processes in Louisiana's Coastal Wetlands,* Transactions – Gulf Coast Association of Geological Societies, Volume XL, pp. 635-642.

Murray, S.P., Jarosz, E., Weeks, E.T. III, 1998, *Physical Oceanographic Observations of the Coastal Plume,* from *An Observational Study of the Mississippi-Atchafalaya Coastal Plume Final Report (Murray, S.P., editor),* Minerals Management Service, U.S. Department of the Interior, 513 p.

Myint, S.W., 2002, *Quantification of surface suspended sediments along a river dominated coast with NOAA AVHRR and SeaWiFS measurements: Louisiana, USA,* International Journal of Remote Sensing, Vol.23, No.16, pp. 3229-3249.

Nowlin Jr., W.D., Parker, C.A., 1974, *Effects of a Cold Air Outbreak on Shelf Waters of the Gulf of Mexico,* Journal of Physical Oceanography, Vol 4, pp. 467-486.

Perez, B.C., Day, J.W., Rouse, L.J., Shaw, R.F., Wang, M., 2000, *Influence of Atchafalaya River Discharge and Winter Frontal Passage on Suspended Sediment Concentration and Flux in Fourleague Bay, Louisiana*, Estuarine, Coastal and Shelf Science, Vol. 50, pp 271-290.

Roberts, H.H., 1988, *Delta Switching: Early Responses to the Atchafalaya River Diversion*, Journal of Coastal Research, Vol. 14, No. 3, pp. 882-899.

Roberts, H.H., 1997, *Dynamic Changes of the Holocene Mississippi River Delta Plain: the Delta Cycle*, Journal of Coastal Research, Vol. 13, No.3, pp. 605-627.

Roberts, H.H., Huh, O.K., Hsu, S.A., Rouse, L.R., Rickman, D.A., 1989, *Winter Storm Impacts, on the Chenier Plain Coast of Southwestern Louisiana,* Gulf Coast Association of Geological Societies Transactions, Vol XXXIX, pp. 515-522.

Roberts, H.H., Walker, N.D., Cunningham, R., Kemp, G.P., Majersky, S., 1997, *Evolution of Sedimentary Architecture and Surface Morphology: Atchafalaya and Wax Lake Deltas, Louisiana (1973-1994),* Gulf Coast Association of Geological Societies Transactions, Vol XLVII, pp. 477-484.

Roberts, H.H., Walker, N.D., Sheremet, A., Stone, G.W., 2005, *Effects of Cold Fronts on Bayhead Delta Development: Atchafalaya Bay, Louisiana, USA,* High Resolution Morphodynamics and Sedimentary Evolution of Estuaries, Fitzgerald and Knight (eds.), Kluwer Academic Publishers, Dordrecht, Netherlands, pp. 269-298.

Robinson, I.S., 1985, Satellite Oceanography: An Introduction for Oceanographers and Remote-Sensing Scientists, Prentice Hall, 455 p.

Sheremet, A., Stone, G.W., 2003, *Observations of Nearshore Wave Dissipation Over Muddy Sea Beds,* Journal of Geophysical Research, Vol. 108, No. C11, pp.3357-3367.

Smith, S.R., Jacobs, G.A., 2005, *Seasonal Circulation Fields in the Northern Gulf of Mexico Calculated by Assimilating Current Meter, Shipboard ADCP, and Drifter Data Simultaneously with Shallow Water Equations,* Continental Shelf Research, *Vol 25, pp.157-183.*

Stone, G.W., Kumar, B.P., Sheremet, A., Watzke, D., 2005, *Complex Morpho-Hydrodynamic Response of Estuaries and Bays to Winter Storms: North-Central Gulf of Mexico, USA,* High Resolution Morphodynamics and Sedimentary Evolution of Estuaries, Fitzgerald and Knight (eds.), Kluwer Academic Publishers, Dordrecht, Netherlands, pp. 243-267.

Stumpf, R.P., 1992, *Remote Sensing of Water Clarity and Suspended Sediments in Coastal Waters,* from the proceedings of the First Thematic Conference on Remote Sensing for Marine and Coastal Environments, New Orleans, Louisiana, SPIE, 1930, pp.293-305.

Stumpf, R.P., Pennock, J.R., 1989, *Calibration of a General Optical Equation for Remote Sensing of Suspended Sediments in a Moderately Turbid Estuary,* Journal of Geophysical Research, Vol. 94, No. C10, pp.14,363-14,371.

Tye, R.S. and Coleman, J.M., 1989, *Depositional Processes and Stratigraphy of Fluvially Dominated Lacustrine Deltas: Mississippi Delta Plain,* Journal of Sedimentary Petrology, Vol. 59, No.6, pp. 973-996.

United States Geological Survey, 1987, *Techniques of Water Resources Investigations of the U.S. Geological Survey.* In L.J.Britton and P.E.Greeson (eds.), *Methods for Collection and Analysis of Aquatic Biological and Microbiological Samples.* United States Geological Survey, Washington, D.C.

United States Geological Survey, 2005, TWRI Book 9, Field Manual, *Turbidity,* Chapter A6, Anderson, C.W., version 2.1, Field Measurements. United States Geological Survey, Washington, D.C.

Walker, N.D., 1996, *Satellite Assessment of Mississippi River Plume Variability: Causes and Predictability,* Remote Sensing Environment, Vol. 58, pp. 21-35.

Walker, N.D., 2001, *Tropical Storm and Hurricane Wind Effects on Water Level, Salinity and Sediment Transport in the River Influenced Atchafalaya-Vermillion Bay System, Louisiana, USA,* Estuaries, Vol .24, No. 4, pp.498-508.

Walker, N.D., 2005a, *Effects of River Discharge, Wind Stress and Slope Eddies on Circulation and the Satellite-Observed Structure of the Mississippi River Plume,* Journal of Coastal Research, Vol.21, No. 6, pp.1228-1244.

Walker, N.D., 2005b, *Wind and Eddy-Related Shelf/Slope Circulation Processes and Coastal Upwelling in the Northwestern Gulf of Mexico,* Circulation in the Gulf of Mexico: Observations and Models, Geophysical Monograph Series 161, American Geophysical Union, pp.295-313.

Walker, N.D., Hammack, A.B., 2000, *Impacts of Winter Storms on Circulation and Sediment Transport: Atchafalaya-Vermillion Bay Region, Louisiana,* Journal of Coastal Research, Vol. 16, pp. 996-1010.

Walker, N.D., Roberts, H.H., Stone, G.W., Bentley, S.J., Huh, O.K., Sheremet, A., Rouse, L.J., Inoue, M., Welsh, S. Hsu, S.A., Myint, S.W., 2002, *Satellite-Based Assessment of Sediment Transport, Distribution and Resuspension Associated with the Atchafalaya River Discharge Plume,* Gulf Coast Association of Geological Societies Transactions, Vol. 52, pp.967-973.

Winker, C.D., 1991, *Summary of the Quaternary Framework, Northern Gulf of Mexico,* GCSSEPM Foundation Twelfth Annual Research Conference, Program and Abstracts, pp. 280-284.

Wiseman, W.J. Jr and Sturgis, W., 1999, *Physical Oceanography of the Gulf of Mexico: Processes that Regulate its Biology,* in The Gulf of Mexico Large Marine Ecosystem, Kumpf, Steidinger and Sherman (eds.), Blackwell Science, pp. 77-89.

Woodbury, H.O., Murray, I.B., Pickford, P.J., Akers, W.H., 1973, *Pliocene and Pleistocene Depocenters, Outer Continental Shelf, Louisiana and Texas,* the American Association of Petroleum Geologists Bulletin, Vol. 57, No.12, pp. 2428-2439.

Woodroffe, C.D., 2002, *Coasts: Form, Process and Evolution,* Cambridge University Press, U.K., 638 p.

Zhang, Xiongping, 2004, *Operational Sediment Concentration Conversion for WAVCIS Station CSI3,* unpublished-WAVCIS Laboratory procedures notes

APPENDIX A: SUSPENDED SEDIMENT CONCENTRATION MODEL FIELD DATA

(Strike-through indicates samples eliminated.)

Date	Time (GMT)	Latitude (N)	Longitude (W)	Sample ID	Suspended Sediment (mg/l)	comments
~~21-Mar-01~~	~~1500~~	~~29.48408~~	~~91.27648~~	~~AR-1A~~	~~297~~	land contamination
~~21-Mar-01~~	~~1552~~	~~29.38922~~	~~91.20768~~	~~FLB-1A~~	~~44~~	land contamination
21-Mar-01	1605	29.35873	91.21560	FLB-2A	117	
21-Mar-01	1605	29.35873	91.21560	FLB-2B	113	
21-Mar-01	1616	29.32470	91.21500	FLB-3A	168	
21-Mar-01	1616	29.32470	91.21500	FLB-3B	175	
~~21-Mar-01~~	~~1630~~	~~29.30815~~	~~91.19520~~	~~FLB-4A~~	~~97~~	land contamination
~~21-Mar-01~~	~~1630~~	~~29.30815~~	~~91.19520~~	~~FLB-4B~~	~~99~~	land contamination
21-Mar-01	1641	29.33645	91.17618	FLB-5A	169	
21-Mar-01	1641	29.33645	91.17618	FLB-5B	169	
~~21-Mar-01~~	~~1656~~	~~29.35265~~	~~91.15910~~	~~FLB-6A~~	~~100~~	land contamination
~~21-Mar-01~~	~~1656~~	~~29.35265~~	~~91.15910~~	~~FLB-6B~~	~~111~~	land contamination
~~21-Mar-01~~	~~1707~~	~~29.32633~~	~~91.15307~~	~~FLB-7A~~	~~159~~	
21-Mar-01	1707	29.32633	91.15307	FLB-7B	151	
~~21-Mar-01~~	~~1723~~	~~29.30038~~	~~91.13498~~	~~FLB-8A~~	~~159~~	
~~21-Mar-01~~	~~1723~~	~~29.30038~~	~~91.13498~~	~~FLB-8B~~	~~167~~	
~~21-Mar-01~~	~~1736~~	~~29.26610~~	~~91.13672~~	~~FLB-13A~~	~~203~~	land contamination
~~21-Mar-01~~	~~1736~~	~~29.26610~~	~~91.13672~~	~~FLB-13B~~	~~209~~	land contamination
~~21-Mar-01~~	~~1755~~	~~29.21603~~	~~91.13487~~	~~FLB-14A~~	~~45~~	land contamination
~~21-Mar-01~~	~~1755~~	~~29.21603~~	~~91.13487~~	~~FLB-14B~~	~~45~~	land contamination
~~21-Mar-01~~	~~1814~~	~~29.17478~~	~~91.14177~~	~~FLB-15A~~	~~27~~	frontal area
~~21-Mar-01~~	~~1814~~	~~29.17478~~	~~91.14177~~	~~FLB-15B~~	~~34~~	frontal area
~~22-May-01~~	~~1505~~	~~29.51133~~	~~92.40000~~	~~C10S~~	~~237~~	
22-May-01	1515	29.49483	92.40000	C11S	140	
~~22-May-01~~	~~1526~~	~~29.49800~~	~~92.38667~~	~~C12S~~	~~160~~	

Appendix A: Suspended Sediment Concentration Model Field Data
(Strike-through indicates samples eliminated.)

Date	Time (GMT)	Latitude (N)	Longitude (W)	Sample ID	Suspended Sediment (mg/l)	comments
~~22-May-01~~	~~1540~~	~~29.51383~~	~~92.38633~~	~~C13S~~	~~213~~	cloud shadow
~~22-May-01~~	~~1556~~	~~29.52850~~	~~92.38333~~	~~C14S~~	~~1093~~	near shore
~~22-May-01~~	~~1610~~	~~29.52550~~	~~92.36667~~	~~C15S~~	~~713~~	near shore
~~22-May-01~~	~~1622~~	~~29.51500~~	~~92.36750~~	~~C16S~~	~~385~~	cloud shadow
~~22-May-01~~	~~1633~~	~~29.49895~~	~~92.36717~~	~~C17S~~	~~239~~	
~~22-May-01~~	~~1644~~	~~29.48783~~	~~92.36750~~	~~C18S~~	~~185~~	
22-May-01	1655	29.47117	92.36767	C19S	72	
~~22-May-01~~	~~1705~~	~~29.45500~~	~~92.36700~~	~~C20S~~	~~31~~	cloud shadow
~~22-May-01~~	~~1740~~	~~29.52367~~	~~92.34317~~	~~C21S~~	~~313~~	near shore
~~22-May-01~~	~~1755~~	~~29.50950~~	~~92.34117~~	~~C22S~~	~~203~~	
22-May-01	1805	29.49267	92.34083	C23S	155	
~~22-May-01~~	~~1815~~	~~29.47567~~	~~92.34100~~	~~C24S~~	~~99~~	cloud shadow
~~22-May-01~~	~~1826~~	~~29.45983~~	~~92.34083~~	~~C25S~~	~~50~~	cloud shadow
~~23-Nov-02~~	~~1745~~	~~29.48315~~	~~91.27555~~	~~AR1A~~	~~52~~	land contamination
~~23-Nov-02~~	~~1745~~	~~29.48315~~	~~91.27555~~	~~AR1B~~	~~88~~	land contamination
23-Nov-02	1945	29.17802	91.55490	R2A	5	outside plume
23-Nov-02	1945	29.17802	91.55490	R2B	8	outside plume
23-Nov-02	2000	29.19063	91.54280	R4A	5	outside plume
23-Nov-02	2000	29.19063	91.54280	R4B	5	outside plume
23-Nov-02	2008	29.20373	91.53152	R6A	6	edge of plume
23-Nov-02	2008	29.20373	91.53152	R6B	4	edge of plume
23-Nov-02	2015	29.21700	91.51967	R8A	21	
23-Nov-02	2015	29.21700	91.51967	R8B	16	
23-Nov-02	2022	29.23080	91.50763	R10A	42	
23-Nov-02	2022	29.23080	91.50763	R10B	26	
23-Nov-02	2028	29.24437	91.49920	R12A	36	

Appendix A: Suspended Sediment Concentration Model Field Data
(Strike-through indicates samples eliminated.)

Date	Time (GMT)	Latitude (N)	Longitude (W)	Sample ID	Suspended Sediment (mg/l)	comments
23-Nov-02	2028	29.24437	91.49920	R12B	32	
23-Nov-02	2040	29.25750	91.48433	R14A	31	
23-Nov-02	2040	29.25750	91.48433	R14B	37	
23-Nov-02	2047	29.27048	91.47250	R16A	55	
23-Nov-02	2047	29.27048	91.47250	R16B	50	
23-Nov-02	2052	29.28355	91.46045	R18A	44	frontal area
23-Nov-02	2052	29.28355	91.46045	R18B	43	frontal area
~~23-Nov-02~~	~~2057~~	~~29.29687~~	~~91.44878~~	~~R20A~~	~~22~~	frontal area
~~23-Nov-02~~	~~2057~~	~~29.29687~~	~~91.44878~~	~~R20B~~	~~33~~	frontal area
23-Nov-02	2102	29.30993	91.43712	R22A	63	
23-Nov-02	2102	29.30993	91.43712	R22B	56	
23-Nov-02	2109	29.32310	91.42535	R24A	62	
23-Nov-02	2109	29.32310	91.42535	R24B	64	
23-Nov-02	2113	29.33588	91.41390	R26A	50	
23-Nov-02	2113	29.33588	91.41390	R26B	50	
23-Nov-02	2123	29.34912	91.40223	R28A	84	
23-Nov-02	2123	29.34912	91.40223	R28B	86	
30-Oct-03	1845	29.17802	91.55490	SB1A	10	near edge of plume
30-Oct-03	1845	29.17802	91.55490	SB1B	13	near edge of plume
30-Oct-03	1845	29.17802	91.55490	SB1C	11	near edge of plume
30-Oct-03	1910	29.19063	91.54280	4A	15	
30-Oct-03	1910	29.19063	91.54280	4B	17	
30-Oct-03	1910	29.19063	91.54280	4C	17	
30-Oct-03	1932	29.21700	91.51967	8A	15	
30-Oct-03	1932	29.21700	91.51967	8B	15	

Appendix A: Suspended Sediment Concentration Model Field Data
(Strike-through indicates samples eliminated.)

Date	Time (GMT)	Latitude (N)	Longitude (W)	Sample ID	Suspended Sediment (mg/l)	comments
30-Oct-03	1932	29.21700	91.51967	8C	16	
30-Oct-03	1955	29.24437	91.49920	12A	19	
30-Oct-03	1955	29.24437	91.49920	12B	19	
30-Oct-03	1955	29.24437	91.49920	12C	30	
30-Oct-03	2002	29.27048	91.47250	16A	22	
30-Oct-03	2002	29.27048	91.47250	16B	24	
30-Oct-03	2002	29.27048	91.47250	16C	26	
~~30-Oct-03~~	~~1750~~	~~29.29687~~	~~91.44878~~	~~20A~~	~~103~~	high chlorophyll
~~30-Oct-03~~	~~1750~~	~~29.29687~~	~~91.44878~~	~~20B~~	~~102~~	high chlorophyll
~~30-Oct-03~~	~~1750~~	~~29.29687~~	~~91.44878~~	~~20C~~	~~92~~	high chlorophyll
~~30-Oct-03~~	~~2030~~	~~29.29687~~	~~91.44878~~	~~20+A~~	~~83~~	high chlorophyll
~~30-Oct-03~~	~~2030~~	~~29.29687~~	~~91.44878~~	~~20+B~~	~~82~~	high chlorophyll
~~30-Oct-03~~	~~UNK~~	~~29.35948~~	~~91.39270~~	~~30MIDA~~	~~90~~	high chlorophyll
~~30-Oct-03~~	~~UNK~~	~~29.35948~~	~~91.39270~~	~~30MIDB~~	~~78~~	high chlorophyll
~~30-Oct-03~~	~~UNK~~	~~29.35948~~	~~91.39270~~	~~30MIDC~~	~~92~~	high chlorophyll
~~30-Oct-03~~	~~2115~~	~~29.48315~~	~~91.27555~~	~~AR1~~	~~26~~	land contamination

APPENDIX B: SUSPENDED SEDIMENT MODEL DEVELOPMENT REGRESSION DATA: CHANNEL 1 DARK PIXEL METHOD

$y=2.1273*e^{39.9838x}$

sample ID	suspended sediment (mg/l)	actual reflect ch1-ch1 dk	susp sed if $y=b0*e^{b1x}$	diffs	bias	$diff^2$	RMS error
FLB2A	117	0.0978	107	10	197	100	22.8206
FLB2B	113	0.0978	107	6		36	
FLB3A	168	0.1015	124	44		1936	
FLB3B	175	0.1015	124	51		2601	
FLB5A	169	0.1030	131	38		1444	
FLB5B	169	0.1030	131	38		1444	
FLB7B	151	0.0919	84	67		4489	
C11S	140	0.0955	97	43		1849	
C19S	72	0.0910	81	-9		81	
C23S	155	0.0954	97	58		3364	
R2A	5	0.0221	5	0		0	
R2B	8	0.0221	5	3		9	
R4A	5	0.0260	6	-1		1	
R4B	5	0.0260	6	-1		1	
R6A	6	0.0270	6	0		0	
R6B	4	0.0270	6	-2		4	
R8A	21	0.0546	19	2		4	
R8B	16	0.0546	19	-3		9	
R10A	42	0.0622	26	16		256	
R10B	26	0.0622	26	0		0	
R12A	36	0.0682	33	3		9	
R12B	32	0.0682	33	-1		1	
R14A	31	0.0852	64	-33		1089	
R14B	37	0.0852	64	-27		729	
R16A	55	0.0863	67	-12		144	
R16B	50	0.0863	67	-17		289	
R18A	44	0.0762	45	-1		1	
R18B	43	0.0762	45	-2		4	
R22A	63	0.0960	99	-36		1296	
R22B	56	0.0960	99	-43		1849	
R24A	62	0.0904	79	-17		289	
R24B	64	0.0904	79	-15		225	
R26A	50	0.0856	66	-16		256	
R26B	50	0.0856	66	-16		256	
R28A	84	0.0834	60	24		576	
R28B	86	0.0834	60	26		676	
SB1A	10	0.0550	19	-9		81	
SB1B	13	0.0550	19	-6		36	
SB1C	11	0.0550	19	-8		64	

APPENDIX B: Suspended Sediment Model Development Regression Data: Channel 1 Dark Pixel Method

$y=2.1273*e^{39.9838x}$

sample ID	suspended sediment (mg/l)	actual reflect ch1-ch1 dk	susp sed if $y=b0*e^{b1x}$	diffs	bias	$diff^2$	RMS error
4A	15	0.0502	16	-1		1	
4B	17	0.0502	16	1		1	
4C	17	0.0502	16	1		1	
8A	15	0.0532	18	-3		9	
8B	15	0.0532	18	-3		9	
8C	16	0.0532	18	-2		4	
12A	19	0.0458	13	6		36	
12B	19	0.0458	13	6		36	
12C	30	0.0458	13	17		289	
16A	22	0.0517	17	5		25	
16B	24	0.0517	17	7		49	
16C	26	0.0517	17	9		81	

APPENDIX C: SUSPENDED SEDIMENT MODEL DEVELOPMENT REGRESSION DATA: CHANNEL 2 DARK PIXEL METHOD

$y=1.4857*e^{41.9941x}$

sample ID	suspended sediment (mg/l)	actual reflect ch1-ch1 dk	susp sed if $y=b0*e^{b1x}$	diffs	bias	$diff^2$	RMS error
FLB2A	117	0.1001	99	18	230	324	23.1629
FLB2B	113	0.1001	99	14		196	
FLB3A	168	0.1050	122	46		2116	
FLB3B	175	0.1050	122	53		2809	
FLB5A	169	0.1065	130	39		1521	
FLB5B	169	0.1065	130	39		1521	
FLB7B	151	0.0954	82	69		4761	
C11S	140	0.0996	97	43		1849	
C19S	72	0.0951	81	-9		81	
C23S	155	0.0995	97	58		3364	
R2A	5	0.0258	4	1		1	
R2B	8	0.0258	4	4		16	
R4A	5	0.0297	5	0		0	
R4B	5	0.0297	5	0		0	
R6A	6	0.0319	6	0		0	
R6B	4	0.0319	6	-2		4	
R8A	21	0.0583	17	4		16	
R8B	16	0.0583	17	-1		1	
R10A	42	0.0659	24	18		324	
R10B	26	0.0659	24	2		4	
R12A	36	0.0704	29	7		49	
R12B	32	0.0704	29	3		9	
R14A	31	0.0889	62	-31		961	
R14B	37	0.0889	62	-25		625	
R16A	55	0.0900	65	-10		100	
R16B	50	0.0900	65	-15		225	
R18A	44	0.0799	43	1		1	
R18B	43	0.0799	43	0		0	
R22A	63	0.0997	98	-35		1225	
R22B	56	0.0997	98	-42		1764	
R24A	62	0.0941	77	-15		225	
R24B	64	0.0941	77	-13		169	
R26A	50	0.0893	63	-13		169	
R26B	50	0.0893	63	-13		169	
R28A	84	0.0871	58	26		676	
R28B	86	0.0871	58	28		784	
SB1A	10	0.0647	22	-12		144	
SB1B	13	0.0647	22	-9		81	
SB1C	11	0.0647	22	-11		121	

APPENDIX C: Suspended Sediment Model Development Regression Data: Channel 2 Dark Pixel Method

$y=1.4857*e^{41.9941x}$

sample ID	suspended sediment (mg/l)	actual reflect ch1-ch1 dk	susp sed if $y=b0*e^{b1x}$	diffs	bias	$diff^2$	RMS error
4A	15	0.0599	18	-3		9	
4B	17	0.0599	18	-1		1	
4C	17	0.0599	18	-1		1	
8A	15	0.0629	21	-6		36	
8B	15	0.0629	21	-6		36	
8C	16	0.0629	21	-5		25	
12A	19	0.0555	15	4		16	
12B	19	0.0555	15	4		16	
12C	30	0.0555	15	15		225	
16A	22	0.0614	20	2		4	
16B	24	0.0614	20	4		16	
16C	26	0.0614	20	6		36	

VITA

Renee Terrien Bellotte was born on August 8, 1957, to Charles and Helen Terrien in Worcester, Massachusetts. She was raised in Ashaway, Rhode Island, and graduated from Chariho Regional High School in 1975. After moving to Louisiana in 1978, she worked full-time and attended Louisiana State University. She received her Bachelor of Science degree in physical geography in December of 2001. She enrolled in the Master of Natural Sciences program in January 2002 to pursue an interdisciplinary curriculum which included oceanography, geography and marine geology, and incorporated techniques from remote sensing and geographic information systems. She was a student member of the American Meteorological Society and was awarded full scholarships to attend the 11th Annual Conference on Satellite Meteorology and Oceanography in 2001 and the Annual Meeting in 2003. She is expected to receive her Master of Natural Sciences degree in August of 2007.